Design of a Total Pressure Distortion Generator for Aircraft Engine Testing

by

Kevin B. Cramer

Thesis submitted to the Faculty of the
Virginia Polytechnic Institute and State University
in partial fulfillment of the requirements for the degree of

MASTER OF SCIENCE
in
Mechanical Engineering

APPROVED:

W.F. O'Brien, Committee Co-Chair	P.S. King, Committee Co-Chair

C.L. Dancey, Committee Member

May 2002
Blacksburg, Virginia

Keywords: distortion, HCF, surge margin, stall, generator, jet engine, non-uniform

Design of Total Pressure Distortion Generator for Aircraft Engine Testing

by

Kevin B. Cramer

Committee Co-Chair: W.F. O'Brien

Committee Co-Chair: P.S. King

Mechanical Engineering

(ABSTRACT)

A new method and mechanism for generating non-uniform, or distorted, aircraft engine inlet flow is being developed in order to account for dynamic changes during the creation and propagation of the distortion. Total pressure distortions occur in gas turbine engines when the incoming flow is disturbed. Dynamic total pressure changes may happen slowly, or may occur very rapidly. The disturbance of the incoming flow can change engine operating characteristics, including lowering the surge limit and creating High Cycle Fatigue incidents. In order to create a distorted flow with dynamic characteristics, a mechanism must be developed that when actuated, can change the distortion pattern and intensity with respect to time.

This work covers the initial design of both the distorting and actuating device. The design chosen is a low force design that is practically independent of flow forces. This allows the system to be easily sized for all flow conditions. The study also includes developing the working design into an overall prototype. Testing is also performed to validate the design as the most advantageous choice.

Acknowledgements

I would first like to thank my parents for supporting my studies (and sometimes my wallet) and for always having a encouraging attitude and a patient hand. Without them, I would never have accomplished what I have so far. A thanks to the rest of my family for their encouragement. Also, a large THANK YOU to my girlfriend for her support. Without her here, I would have gone more insane than I already have

I would also like to thank my committee for serving in their capacity. Special thanks to my co-chairmen, first Dr. Walter O'Brien for his vast knowledge, willingness to help and easy going attitude that made working for the department head less stressful than I thought it would be. Thanks to Dr. Peter King, whose friendship, knowledge, PATIENCE and large amounts of guidance enabled me to start and finish my graduate studies.

The project support of Dave Beale and Jim Reed at Sverdrup Technologies was greatly appreciated.

Thanks to those who came before me on this research: Tony, Julien, Grant and Christian. Without their prior work, I would not have known where to start or what to do.

Finally, thanks to all those who endured my senseless rants and overall randomness during my stay in the Turbolab. To those of old, Scott (Dr. Evil) for getting me started, Grant and Christian for providing a never-ending source of entertainment and Maj. Keith Boyer for providing me with someone to model my professional goals after. To those I've met more recent: Mac, Jon, John, Rob, Melissa, Mike, Mono and Matthew I thank for their friendship that made "The Hole" more tolerable. And a special thanks to Joe (Mr. Evil) whose help was appreciated but whose patience, understanding and ability to maintain his sanity in such close proximity to me were a miracle.

Table of Contents

List of Figures.....vi

List of Equations vii

List of Tables ix

1 Introduction..... 1

1.1 Performance Effects of Distortion..... 1
1.2 Aeromechanical Effects of Distortion 2
1.3 Current Testing of Distortion 3

2 Literature Review..... 5

2.1 Swirl Distortion 6
2.2 Total Temperature Distortion 7
2.3 Total Pressure Distortion and Performance Effects..... 9
Early Analysis *9*
Distortion Analysis by the S-16 Committee..... *10*
Modern Analysis *12*
Modeling *13*
2.4 Total Pressure Distortion and Aeromechanical Effects 18
Early Analysis *19*
Modern Analysis *21*
Modeling *21*
2.5 Current Methodologies..... 23
Tests of Distorted Flows *23*
Analysis of Distorted Flows..... *25*
2.6 Motivation for Work 28
2.7 Scope of Current Research 30

3 Design Requirements..... 31

3.1 Size of Wedges..... 31
3.2 Range of Motion..... 32
3.3 Rate of Actuation 34
3.4 Test Cell Conditions..... 36
3.5 Flow Conditions and Forces..... 36
3.6 Boundary Layer Analysis..... 38
3.7 Isolating Individual Forces 42

4 Wedge Design..... 43

4.1 Front Supported Wedge..... 43
4.2 Rear Supported Wedge 45
4.3 Center Supported Wedge..... 46
Standard Configuration..... *47*
Vertical Configuration..... *47*

5 Actuation Design 50
5.1 Actuation Direction 50
5.2 Actuator Placement 52
Inside Placement 52
Outside Placement 53
5.3 Piston-Cylinder 54
Pneumatics and Hydraulics 55
Solenoids 56
5.4 Electromagnetic 57
5.5 Piezo-Ceramic 58
Piezo Stack 59
Piezo Strip 59
5.6 Electric Motor 60
Servo Motors 60
Stepper Motors 61
6 Design Selection 62
6.1 Wedge Selection 62
6.2 Actuator Selection 64
6.3 Overall Design 66
6.4 Concept Model Fabrication 67
7 Design Verification 69
7.1 Wind Tunnel and Test Cell 69
7.2 Distortion Generator 71
7.3 Testing Apparatus 74
7.4 Test Results 75
7.5 Design Prototype 77
8 Conclusions and Recommendations 80
8.1 Review 80
8.2 Conclusions 81
8.3 Recommendations 83
Appendix A: Force Plots for Mach 0.6 Flow 86
Appendix B: Force Plots for Mach 0.1 Flow 87
Appendix C: Free-Body Diagrams for Wedge 89
Appendix D: Free-Body Diagrams for Actuation 91
Appendix E: Measured Actuation Forces 93
Appendix F: Uncertainty Analysis 95
References 96

Vita 101

List of Figures

Figure 1-1: Graph Showing the Factors that Degrade the Surge Line and Distortion Surge Margin, (SAE, 1999) 2
Figure 1-2: Example of a serpentine inlet duct. (Small, 2001) 4
Figure 2-1: Timeline showing the approximate time from design to first flight. (Younghans and Paul, 1989) 5
Figure 2-2: Exhaust Reingestion of a V/STOL Aircraft, (SAE, 1991) 7
Figure 2-3: Typical Types of Distortion Inducing Screens (Eddy, 2001) 11
Figure 2-4: Comparison of Accuracy for Two Volterra Methods and the FRF (Luedke, 2001) 13
Figure 2-5: Pictorial Representation of Parallel Compressor Theory (Reid, 1969) 14
Figure 2-6: Actual Flow's Deviation from Predicted Square Wave Pressure Pattern, (Roberts et al., 1968) 15
Figure 2-7: Multiple Stream-Tube Model Versus Parallel Compressor Theory, (Mazzaway, 1968) 16
Figure 2-8: Comparison of Actuator Disk Predicted Pressures Versus Experimental, (Colpin and Kool, 1978) 17
Figure 2-9: The Different Types of Flutter and Their Placement on a Compressor Map, (Carta, 1989) 19
Figure 2-10: Relationship Between Distortion Intensity and Vibratory Effects, (Danforth, 1975) 20
Figure 2-11: TEACC Methodology, (Davis et al., 1998) 22
Figure 2-12: Example of a Screen that Models Actual Flight Distortions, (Mokelke, 1974) 23
Figure 2-13: One, Two and Three-Per-Rev Screens 24
Figure 2-14: Air-Jet Distortion Generator, (Overall, 1976) 25
Figure 2-15: S-16 Definition of Surge Margin, (ARP-1420, 1999) 26
Figure 2-16: S-16 Correlation Coefficients With Representative Screen Diagrams (Steenken, 1989) 27
Figure 2-17: Typical Campbell Diagram With Critical Speeds Marked, (Manwaring, 1996) 28
Figure 3-1: Comparison of two wedges and their superposition, 3 inches behind wedge, for (a) aspect ratio less than 1 and (b) greater than one. Note that (a) is additive and (b) is not. 32
Figure 3-2: Total pressure drop, in percent of free-stream pressure, caused by 0^o total angle wedge. Distortion due to the support rod is noted with white arrows. 33
Figure 3-3: Total pressure drop, in percent of free-stream pressure, caused by 15^o total angle wedge. Distortion due to the support rod is noted with white arrows. 34
Figure 3-4: Comparison of stability limits for types of distortion. (Adapted from Davis et al., 2001) 35
Figure 3-5: Compressor map showing steady-state distortion stall (large points) and transient distortion stall (small points). Notice that the stall limit for transient approaches that for steady. 36
Figure 3-4: Pressure forces in Mach 0.6 flow for square wedges 38
Figure 3-5: Free-body diagram of ½ wedge with forces resulting from the flow. 40

Figure 3-6: Comparison of resultant force and its components for flow M=0.1 41
Figure 4-1: Drawing of front supported wedge. 43
Figure 4-2: Actuation forces for varying angles of a front-supported hinge. The force makes a large jump from 80^o to 90^o. 44
Figure 4-3: Drawing of rear supported hinge 45
Figure 4-4: Actuation forces for varying angles of a rear-supported wedge. Again, the force makes a large jump from 80^o to 90^o 46
Figure 4-5: Standard configuration, center-supported hinge. 47
Figure 4-6: Vertical configuration, center-supported wedge. 48
Figure 4-7: Actuation force for varying angles of a center-supported wedge. 48
Figure 5.1: Lead screw design for actuation. The nut is (a) fixed and (b) movable. 53
Figure 5.2: Piston-Cylinder design for actuation. 54
Figure 5-3: Electromagnetic design for actuation. 58
Figure 5-4: Piezo-strip design for actuation. 60
Figure 6-1: Overall free body diagram for selected design. 64
Figure 6-2: Diagram of overall distortion generator design 66
Figure 6-3: Model of the selected distortion generator design 68
Figure 7-1: Wind tunnel at Virginia Tech with major components listed. 70
Figure 7-2: Diagram of hinge used in distortion generator model (Adapted from Eddy, 2001). 71
Figure 7-3: Example of two individual wedges, connected together 71
Figure 7-4: Side view of support structure with the sections cut out crosshatched. 73
Figure 7-5: Distortion generator model a) Front view and b) Side view showing the slot. 73
Figure 7-6: Test apparatus with the spring attached and the four test points labeled. 74
Figure 7-7: Non-dimensional graph of predicted flow forces and measured actuation forces. 77
Figure 7-8: Picture of prototype connected to test cell. 79
Figure 8-1: a) Diagram of final design and b) Picture of actual distortion generator. 82
Figure 8-2: Example radial array of split airfoils making up the distortion generator. ... 83
Figure 8-3: Representation of distortion generator as a four-bar linkage. Specifically, a slider-crank mechanism, with 1 being the crank and 4 being the slider. 85
Figure A-1: Drag forces in Mach 0.6 flow for multiple sizes of square wedges. 86
Figure A-2: Lift forces in Mach 0.6 flow for multiples sizes of square wedges. 86
Figure B-1: Pressure forces in Mach 0.1 flow for multiples sizes of square wedges. 87
Figure B-2: Drag forces in Mach 0.1 flow for multiple sizes of square wedges. 87
Figure B-3: Lift forces in Mach 0.1 flow for multiples sizes of square wedges 88
Figure C-1: Free-body diagram for front-supported wedge. 89
Figure C-2: Free-body diagram for rear-supported wedge. 89
Figure C-3: Free-body diagram for center-supported wedge. 90
Figure D-1: Free-body diagram for rotationally actuated wedge. 91
Figure D-2: Free-body diagram for horizontally actuated wedge. 91
Figure D-3: Free-body diagram for vertically actuated wedge. 92
Figure D-4: Free-body diagram for vertically-supported, actuated hinge. 92
Figure E-1: Force comparison for flow of Mach 0.107. 93
Figure E-2: Force comparison for flow of Mach 0.103. 93

Figure E-3: Force comparison for flow of Mach 0.1. 94
Figure E-4: Force comparison for flow of Mach 0.08. 94

List of Equations

Equation 2.1……...25
Equation 2.2……...26
Equation 3.1……...33
Equation 3.2……...37
Equation 3.3……...37
Equation 3.4……...37
Equation 3.5……...37
Equation 3.6……...37
Equation 3.7……...39
Equation 3.8……...40
Equation 3.9……...40
Equation 3.10..……...40
Equation 3.11..……...40
Equation 3.12..……...41
Equation 3.13…….41
Equation 4.1……..……..44,62
Equation 4.2……..45,62
Equation 4.3……..48,62
Equation 5.1……..50,63
Equation 5.2……..51,63
Equation 5.3……..51,63
Equation 5.4……..51,63
Equation 5.5……...55
Equation 5.6……...57
Equation 5.7……...59
Equation 5.8……...59
Equation 7.1……...72
Equation 7.2……...77

List of Tables

Table 3-1……37
Table 7-1……76

1 Introduction

The performance of axial flow turbomachinery is inherently dependent on the mass flow entering the inlet. Therefore, the study of disturbances in this flow is very important and of interest to all involved with these machines. Of primary interest is blockages and distortion of the flow, defined as any type of non-uniformity introduced to a free-stream flow parameter. The flow attributes considered most important and most often studied are total pressure, temperature, and swirl velocity. The most common distortion phenomenon encountered during actual operating conditions is a drop in total pressure. It can be affected by many conditions including physical blockages, time-variant intake parameters and introduction of gases at a lower pressure to the intake air. Distortion introduces many problems, ranging from relatively benign performance reductions to very dangerous structural degradations.

1.1 Performance Effects of Distortion

The most commonly encountered distortion effect, a drop in total pressure, is caused by many methods of external effects causing multiple types of reduced performance. A pressure distortion is most commonly caused by a blockage, or flow effects that mimic a rigid blockage. An obstruction in the flow will consequently reduce the mass flow rate of air transferred to the engine, thus reducing many performance areas including overall thrust, specific fuel consumption and compressor efficiency. These reductions are important to study when determining the design of the engine to meet mission requirements. A more important performance aspect that is affected by distortion is the reduction of surge margin. Surge is defined as the operational line of instability that is associated with violent oscillations in mass flow and can possibly lead to complete flow reversal. The surge margin is the factor of safety between the operation point and the surge line. Engines have a steady-state operating surge margin stated as a function of engine geometry that can be greatly reduced when distortion is introduced. As can be seen in Figure 1.1, the surge line can shift to a lower value because of many different

factors, including distortion (which is shown as the shaded region in the figure). Operating a distorted engine in the same manner as the undistorted situation, the engine could approach or even meet the degraded surge line, causing a dangerous situation to occur that could lead to compressor problems including rotating stall and melted blades.

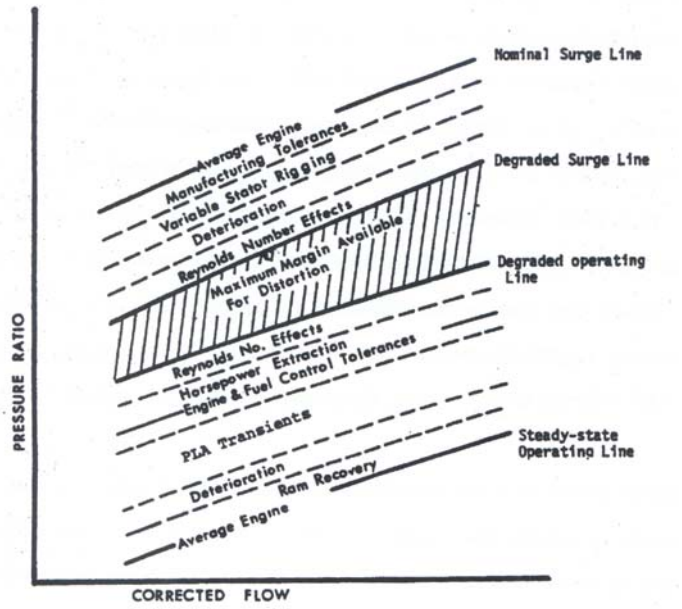

Figure 1-1: Factors that degrade the surge line including distortion surge margin, (SAE, 1999)

Performance effects are based on the aerodynamics of the engine, and are currently considered in the design process of engines during inlet design. The aerodynamic effects of distortion are often considered in a section of design referred to as inlet/engine integration. Aside from these performance degradations, structural problems can also arise from the introduction of distortion to an engine and need to be studied as well.

1.2 Aeromechanical Effects of Distortion

The reduction in mass flow does not affect the physical structure of the compressor blades. The structural problems may arise from the blades passing from areas of high pressure to areas of lower pressure, producing a change in velocity that causes varying forces on the blades themselves. The variant pressure forces produce an

oscillatory excitation source on the blades. The subject of concern is when the oscillations occur at a frequency that approaches the natural frequencies of the blades. If the vibrations occur with high frequency, the integrity of the blade's material can degrade in a phenomenon referred to as High Cycle Fatigue (HCF), and is a very worrisome problem in engines today. The structural deterioration of compressor blades will at best reduce the life of the blades, and at worst causes catastrophic blade failures due to excessive internal stresses. Currently, engine designs assume specific distortion patterns to design and test the engines for operating regions that do not allow the vibratory forces to approach the natural frequencies of the blades.

1.3 Current Testing of Distortion

An early outline of the characterizations and considerations of engine distortion was provided in 1983 by the Aerospace Information Report (AIR) 1419. Because of the ease with which distortion is introduced in actual flight conditions and the importance of its effects, modeling the behavior of distorted machines has become more important. Current modeling procedures include the use of mesh screens and airjets to introduce total pressure distortions to an engine's incoming flow. Screens use a wire grid with small mesh areas to block the flow and create distortion patterns, using the area of flow blockage of the overall screen to control the shape of these patterns. The airjet method uses a momentum exchange between the free stream airflow and a second source of airflow in the reverse direction, and at a higher velocity. Both of these methods create distortion, but they create only one specific pattern of distortion at a time. If successive and differing patterns are desired, the test must be stopped in order to change the screens. Tests involving airjets can only provide test conditions at a steady-state because of the time the momentum exchange takes to occur, and thereby not allowing time-variant testing.

While these methods served as an acceptable modeling method in the past, they remain incomplete, and as new technologies emerge, they become inadequate. Many methods of simulation describe the flow to an engine as uniform and steady. While this is an acceptable assumption for many operating conditions, more situations are arising

where this assumption becomes inaccurate. This is most visible in the world of high-performance aircraft engines, where many new operating conditions have arisen in the past few decades that have developed new patterns of flow distortion. These conditions can include radical maneuvers that can severely distort the inlet airflow in a short amount of time. Other situations include missile exhaust ingestion and formation flying. Newer technologies are also introducing newer distortion conditions. With the introduction of vertical takeoff and landing (VTOL) in the Harrier and continuing in the designs of the Joint Strike Fighter (JSF), ground wash ingestion can introduce distortion patterns. As stealth is becoming more important, the implementation of s-shaped inlets, like the one shown in Figure 1-2, has created new distortion conditions. As the technology and flight conditions that introduce distortion to an engine change, the new flows are becoming more and more time dependent. Currently, there are no acceptable methods of creating transient flows for modeling purposes, but with their growing importance these effects need to be taken into account when modeling the flow.

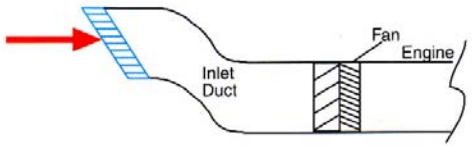

Figure 1-2: Example of a serpentine inlet duct (Small, 2001)

This report discusses the identification of design considerations and the development of a new total pressure distortion generator that will increase test procedure efficiency and allow for transient testing. It includes initial requirements and their effects on the distortion generator design. It also describes the criteria used to select a distortion generator design and the verification development of that selected design.

2 Literature Review

Engineers discovered early in the development of gas turbine engines that including distortion effects into all phases of engine design was necessary for optimum performance and life. Aircraft engine designers have been trying for many years to develop methods of analysis, prediction and testing for these various non-uniform flow situations. In the early era of aircraft engines, distortion tests concentrated on the analysis of observed effects. It was believed that if the problems could be assessed, then methods of correction could be developed. This then led to attempts at predicting distortion effects so that problems could be corrected early on in the design process. Finally, attempts to improve the testing abilities of engineers were studied to better improve testing accuracy and efficiency. All of these aspects could greatly reduce the time an engine requires from initial design to flight certification. A time line is shown in Figure 2-1 outlining the distortion considerations and testing made with respect to inlet/engine integration. This time line represents only the performance effects of distortion; if aeromechanical effects are also included then still longer engine development times are needed. Even with our limited knowledge of distortion effects, engines are still produced in a relatively timely manner. If through prediction and testing, the design process can be shortened then the aircraft engine industry can move forward at a greatly accelerated rate.

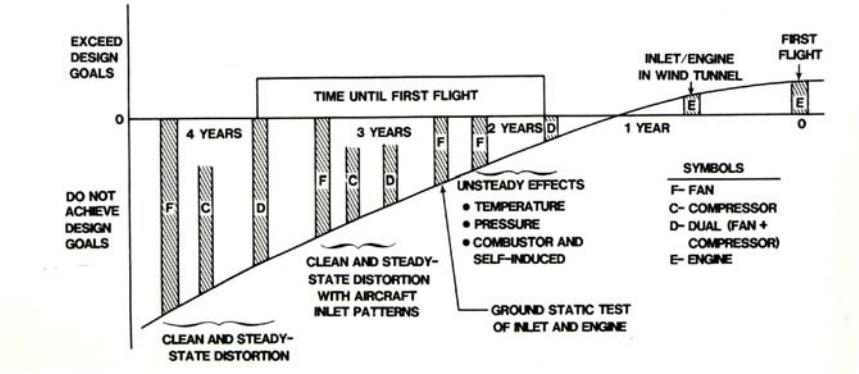

Figure 2-1: Timeline showing the approx. time from design to first flight (Younghans & Paul, 1989)

Many different types of non-uniformity can be introduced to a flow field that will influence the performance and life of turbomachinery. The most commonly studied types are swirl velocity, total temperature and total pressure.

2.1 Swirl Distortion

Swirl distortions are defined as an introduction of flow angularity into the free-stream flow. A non-axial motion of the air can reduce the amount of air flowing through the turbomachinery, thereby affecting performance. One of the largest influencing factors on the studies of swirl effects is the advent of new stealth serpentine inlets. The flow turning done in the curved duct introduces swirl prior to the flow reaching the face of the compressor. This becomes a problem because the swirl increases or decreases the blade aerodynamic loading of the compressor. Blade loading is directly related to stability and surge margin of the engine as well as having vibratory implications that can cause structural degradation.

The Society of Automotive Engineers created the S-16 committee to study distortion effects on engines. This committee is mentioned in more detail later, for their major contribution is in the area of total pressure distortions. But they have also investigated swirl effects and reported on this non-axisymetric flow in an unpublished paper entitled "Intake Flow Annularity: A Current Assessment of the Inlet/Engine Swirl Distortion Problem" (Davis et al., 2001). The S-16 committee characterized various types of swirl distortions and their importance. Another study of swirl distortion, performed at AEDC (Davis et al., 2001), investigated pressure profiles entering and exiting the compressor with induced swirls both in the same direction (co) and opposite direction (counter) of compressor rotation. They performed this study by placing a mesh distortion screen on a rotating ring in front of the compressor face. Their results matched those that were expected, co-rotation produced less loading and counter-rotation produced more blade loading. Other, unexpected results include discovering that "with the presence of swirl combined with total pressure distortion, the compression system may be subjected to a more severe problem than either phenomenon acting by itself" (Davis et al., 2001).

Also, studies of the vibratory effects of inlet swirl have been performed. High Cycle Fatigue caused by excessive vibrations due to inlet swirl distortions were determined to be the cause of failure for the Auxiliary Power Unit (APU) on the Airbus A300 (Lotter, 1982). Also the loading effects of swirl distortion were studied because a cyclical fluctuation in the blade forces can cause blade vibrations to increase. It was found that swirls introduced to the compressor face caused larger blade force fluctuations than pressure distortion (Lecht and Meyer, 1976).

Even with the past and current studies of swirl distortion, it is a less-studied topic because of the greater number of occurrences of the other two types of distortion mentioned, total temperature and total pressure.

2.2 Total Temperature Distortion

Total temperature distortion has long been an area of extreme importance and extensive study. The leading driver in studies of temperature distortion is the ingestion of exhaust gases from missiles (or guns), engine exhaust from other aircraft, and re-ingestion of engine exhaust in vertical takeoff/landing configurations (an example of which is represented in Figure 2-2). In order to perform studies, engineers introduce areas of total temperature distortion to the flow and record the effects on engine performance. The effects of this type of distortion were found to be a lower surge line and an operating point at a lower corrected rotor speed. Recent studies were accomplished by using multiple methods of introducing higher temperature areas of flow to the free-stream.

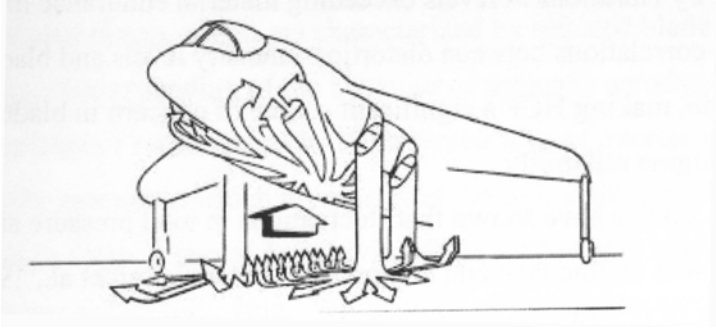

Figure 2-2: Exhaust re-ingestion of a V/STOL aircraft (SAE, 1991)

Studies have concentrated on simulating temperature distortions using many different methods. Wells (1977) constructed a test set-up that generated a temperature distortion comparable to that of exhaust exiting a missile and introduced it to a compressor rig. A problem with his experiment was that the runs were of short duration and the there was poor control of areas of temperature distortion. Wells went on to construct a different type of temperature distortion generator using a segmented hydrogen burner that allowed the test engineers to create controllable patterns of temperature distortion. He later constructed test set-ups that allowed for varying position of the distortion and multiple areas of temperature distortion. Wells used the airjet distortion generator (mentioned in more detail in "Current Methodologies") to introduce areas of higher temperature airflows into the free-stream. These tests were not successful in recreating operational temperature distortions, only determining general effects of temperature distortion. DiPietro (1993) created a temperature distortion generator that provided a method of recreating actual flight conditions. His device generated unsteady temperature distortions, much like those that exist under operational conditions. He also provided data for many types of fuels so that his generator can be used to model multiple situations. Distortion data linked to the type of fuel is important because some devices that produce temperature distortion, such as missile exhaust, involve exotic fuels introduced to the airflow.

Childs et al. (1955) conducted tests with the purpose of creating models of operational temperature distortions. These researchers recreated temperature profiles at the inlet of an aircraft due to missile launches and gun firings and provided data for the operational distortions. They used this data to show how distortion affects the compressor map and combustion stability limits. In providing experimental data from representative temperature distortion cases, these engineers provided data for modeling techniques.

Modeling and prediction of the effects of temperature distortion were investigated by Walter and Shaw (1979) using data collected from test cases of distortion on an F100 engine. This study was one of the first attempts to provide prediction techniques for temperature non-uniformity by correlating theoretical results with experimental data. Another effort to theoretically define the effects of temperature distortions was done by

Braithwaite et al. (1973), where they used the parallel compressor theory (described in detail later) to predict theoretical performance of a J-85 engine subjected to temperature distortions.

As was the case in swirl distortion (and shown later, in pressure distortion) the Society of Automotive Engineer's S-16 committee was also tasked to research temperature distortion. They released the ARD 50015 (1991) to discuss past work and identify causes of temperature distortion, which led to identification of future areas of study and development in the temperature distortion field.

2.3 Total Pressure Distortion and Performance Effects

The most commonly studied type of distortion is the decrease in total pressure, which can cause performance problems that are minor, such as inefficient operation, or more significant and potentially damaging problems, such as surge. Distortion related performance decreases are important to investigate because a main design criterion for aircraft engines is efficient operation, under all operating conditions, including while distorted.

Early Analysis

Early distortion analysis was derived from the study of blunt objects obstructing incoming flow to compressor rotors. Studies were done as early as 1957, when Ashby (1957) examined the wake of a ¼-inch diameter rod and its effect upstream and downstream of a subsonic rotor. Studies such as this one led to the discovery that the performance of turbomachinery was directly affected by the uniformity of the incoming flow. Many of the early attempts at non-uniformity (i.e. distortion) analysis were focused on describing the distortion and not the effects on the engine. Also in 1957, Alford presented a paper that quantified distortion into what he termed the "Inlet Flow Distortion Index." When studies into the effect of distortion on engines began, engineers concentrated on how stall characteristics changed. Early tests based on distortion concentrated on the effects of non-uniform flow on individual engine components (consisting mainly of fans and compressors). Plourde and Brimelow (1970) made a

breakthrough in analysis techniques when they devised a method to predict pressure ratio losses occurring from pressure distortions. They introduced the concept of an average time in order that caused the specific stalling distortion to stand out considerably from other distortion occurrences. Both Cotter (1968) and Reid (1969) presented information that correlated the distortion intensity to the loss of stability pressure ratio (which is directly related to surge margin). Cousins (1979) analyzed surface pressure on compressor blades due to inlet distortions and developed transfer functions that described dynamic blade response. These studies had two primary factors in common. The first was the concentration on component analysis and the second was that all the test conditions studied were steady-state distortions.

In the mid 1960's, the F-111 aircraft (and its corresponding engine, the TF30) were introduced. Problems with this engine developed when unaccounted for engine surges occurred, greatly reducing the operability of the engine. Current techniques of the time were used in accounting for steady state distortions and were not able to describe the encountered surge problems. It was discovered (Plourde and Brimelow, 1970) that "instantaneous" or transient distortions were producing higher than expected reduction in surge margin. This initiated a new area of distortion studies, explored in part by Brimelow et al. in 1974, the ability to predict time-variant distortions and the effect on engines.

Distortion Analysis by the S-16 Committee

A major problem that existed in analyzing distorted flows was the inability to compare separate tests in the same field. Each engine company and test lab had their own methods of quantifying distortion and its effects. This problem was in part solved by the Society of Automotive Engineers (SAE) in establishing the S-16 committee. The committee represented a consortium of engine and airframe manufacturers, civil agencies, and government representatives. Their purpose was to standardize both the testing procedures and analysis of data relating to inlet distortions. Their first publications, Aerospace Recommended Practice (ARP) 1420 and its companion document, the Aerospace Information Report (AIR) 1419, provided guidelines for

consistent methods of testing and the analysis of those tests. The report ARP 1420 offered an outline of the parameters that exist in distortion testing, including the different methods of distortion, with examples shown in Figure 2-3.

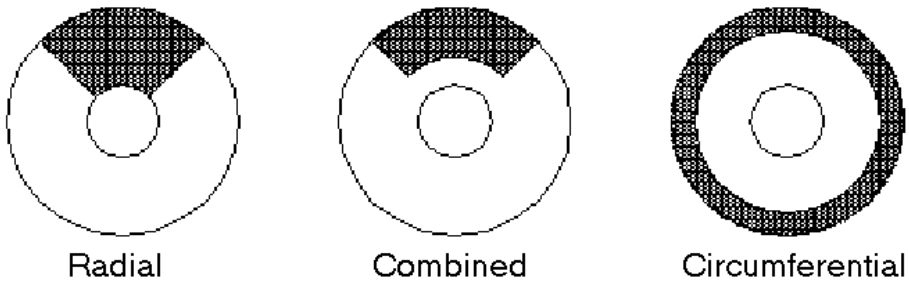

Figure 2-3: Typical types of distortion inducing screens (Eddy, 2001)

The report also includes definitions such as the intensity of the distortion, the extent of distortion, and a parameter termed multiple-per-revolution (MPR) that described several distortions is a short period of time. The definitions provide those who are testing engines a common ground to describe their distortion tests, making communication of results much less complicated. Report ARP 1420 also provides guidelines in the effects of distortion by outlining performance measurements that are directly affected by pressure distortions. This includes definitions for surge margin, surge pressure ratio loss, and factors to be studied that affect engine stability. The ARP also describes testing procedures and data collection, equipping the researcher with guidelines on what test aspects to control and what to look for in test results.

The companion document AIR 1419 was released in conjunction with and as an extension of ARP 1420, providing a more detailed reference with the use of examples as well as distortion analysis guidelines. The use of AIR 1419 enabled the researcher to standardize the analysis of test results so that communicating those same results would be done in a universal manner. The report also contained examples of pressure distortion testing procedures so that gathered data is collected in the same manner allowing for comparisons of tests from multiple sources, such as fans, compressors, or engines. Finally, the report provided examples of data collection methods so that upon comparison, two separate tests are analogous to ensure that any error inherent to the data collection is constant and present throughout all tests.

Modern Analysis

The majority of most recent studies done with respect to inlet total pressure distortion relate to the use of empirical data to develop prediction techniques. Many studies are based on those of Colpin and Kool (1978), where the effects of inlet pressure distortions on inlet flow conditions and wake response were studied. Boller (1998) and Schwartz (1999) both extended this investigation to include dynamic responses of the compressor stage. Schwartz then went on to use correlations, called frequency response functions (FRF), gathered from experimental analysis to devise a method of predicting exit total pressure profiles. Small (2001) then extended Schwartz's work by testing the feasibility of using FRF on modern design compressors. Small also analyzed data in order to develop a method of "tuning" the FRF; so that modeling at different flow conditions than those the data was obtained at could be done accurately. This allowed the tuned FRF concept to be applied to many different compressors and many different flow situations, making it a very powerful technique. The drawback of using either version of FRF is that it is a linear function used to approximate a non-linear phenomenon (which most fluid flows are). This problem is partially solved by Luedke (2001, by using a non-linear function called the Volterra Series to acquire the same result as Small's Tuned FRF, defining the exit pressures from a modern compressor for non-uniform inlet flows. A graph summarizing the accuracy results of two versions of Volterra and the Tuned FRF is shown in Figure 2-4. This graph shows that for most points along the blade (radial immersion) the Volterra series predictions were more accurate (closer to an accuracy of 1) than the tuned FRF. The accuracy was worse as the data was collected near the hubs of the blade because of this flow location's extreme non-linearity, but was still better than the tuned FRF predictions.

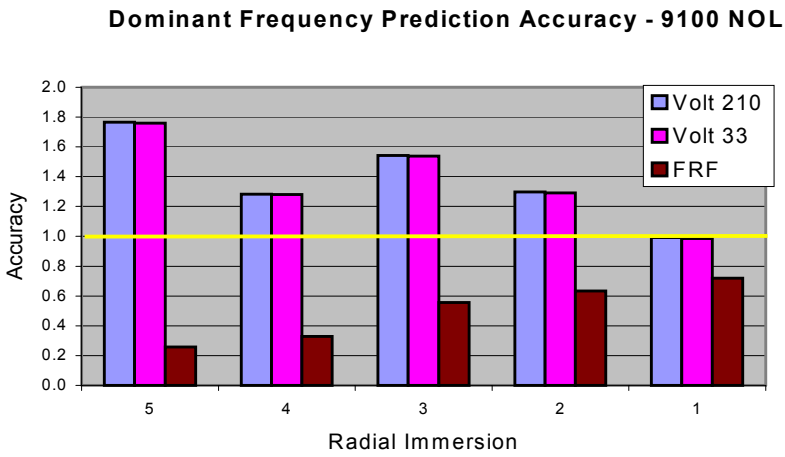

Figure 2-4: Comparison of accuracy for two Volterra methods and the FRF (Luedke, 2001)

As can been seen from the above studies, distortion analysis has moved in the direction of studying many different cases of distortion in order to develop ways of predicting the effects. This approach has been fairly successful and has spawned many methods that predict how distortion will affect an engine's performance.

Modeling

The works of Boller, Schwartz, Small and Luedke led to the developments of prediction methods in order to determine effects of distortion on an engine. This is an important area of study because engine manufacturers and designers are looking for ways to reduce engine development time and costs. If an accurate distortion model could be developed, this would greatly reduce the experimentation now necessary to explore distortion events. Some of the earlier models that were generated are thoroughly discussed by Mokelke (1974), but only the more important methods are discussed here.

In 1959 the first, and still most commonly used, method of predicting the effects of distortion on stall characteristics was introduced, the parallel compressor theory (Pearson and McKenzie, 1959). They modeled a distorted compressor as two separate compressors with each "compressor's" operating point determined separately and averaged to find the overall operating point for the distorted compressor. An example is

shown in Figure 2-5 with the low and high side operating points and their associated average operation point.

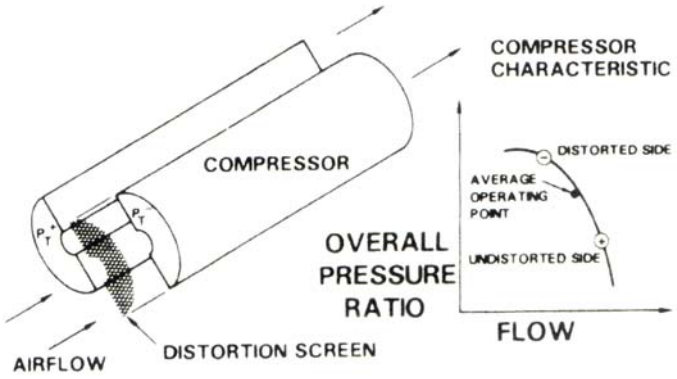

Figure 2-5: Pictorial representation of parallel compressor theory (Reid, 1969)

This method is a simple but powerful modeling technique with a downside of being restricted by five critical assumptions (Pearson and McKenzie, 1959):

1) The distorted compressor consists of two or more independently operating sub-compressors.
2) All sub-compressors have individually uniform inlet conditions and operate on the undistorted compressor characteristic.
3) No circumferential cross-flow exists between sub-compressors.
4) Exit static pressure of all sub-compressors is equal.
5) The entire compressor stalls when an individual compressor reaches the undistorted stall pressure ratio.

Many modeling techniques developed after the parallel compressor model concentrated on improvements or reduction in the number of assumptions made. Roberts et al. (1968) looked into the specific assumptions that caused problems. They found that assumption 3, no circumferential cross-flow, caused the predicted flow to have an unrealistic square-wave shape. The flow in successive stages downstream of the inlet, seen in Figure 2-6, had major deviations from the predicted square-wave pattern.

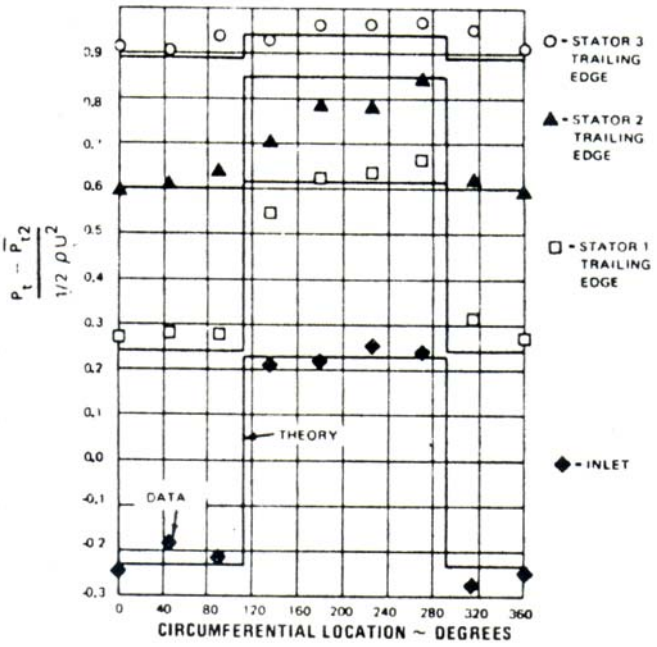

Figure 2-6: Flow's deviation from predicted square-wave pressure pattern, (Roberts et al., 1968)

This work shows that the pressure patterns of the blades (especially in downstream stages) are dependent on time as well as the extent of distortion. Many studies were done in evaluating the time response due to distortion, with Roberts et al. defining this time dependant behavior by employing a reduced frequency parameter. Other explorations of time dependant behavior, including alternate definitions of the reduced frequency parameters, were developed in works by Mikolajczak and Pfeffer (1974), Carta (1972) and Kimzey (1977).

Also accounting for time dependant flows, Adamczyk (1974) developed a model that improved on the original parallel compressor theory. He developed a model that allowed the assumptions of constant static pressure at the exit and no circumferential cross-flow to be discarded. He also allowed for large amplitude distortions in his model (which original parallel compressor theory did not). A problem with Adamczyk's work was that there was a lack of experimental data to verify his model, therefore relegating his improvements to theoretical modeling only.

Mazzawy (1977) made a significant improvement to parallel compressor theory by implementing "multiple pseudo-streamtubes" in place of the sub-compressors described in parallel compressor theory. These streamtubes not only reduced the number

of restrictions to one (the distortion's circumferential extent covers an area of several blade passages), but increased the circumferential resolution of the model. Results of his model are shown in Figure 2-7, where experimental test data is compared with Mazzawy's model and the classical parallel compressor theory.

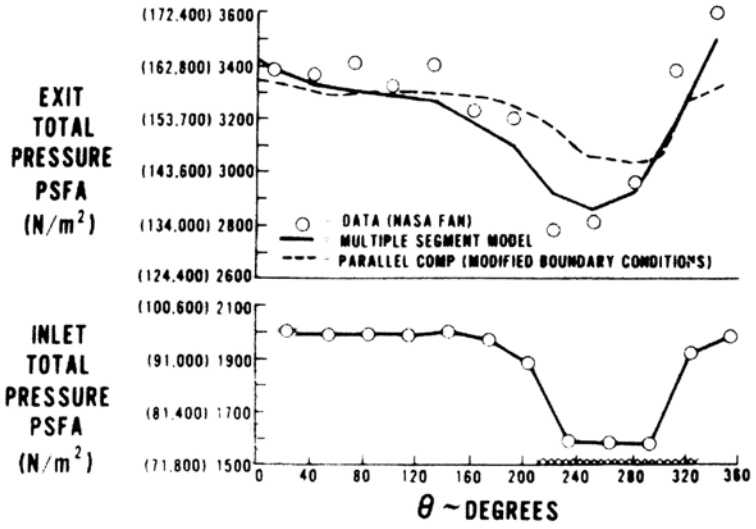

Figure 2-7: Multiple stream-tube model versus parallel compressor theory, (Mazzaway, 1968)

Parallel compressor theory is the backbone of modeling techniques, and is still used (with different modifications) to model distorted flow in turbomachinery. But, as can be seen in Figure 2-7, there is a potential for better accuracy by continual refinement of past and current modeling techniques

Greitzer (1975) introduced another method of modeling, using an actuator disk in place of the compressor. By using an actuator disk, the circumferential velocities and pressure rise done by the compressor blade rows on the flow were included in the evaluation. Greitzer used the actuator disk method to become the first researcher to model compressor rotating stall and surge and in doing he mathematically described what was already experimentally observed as a problem in turbomachinery. Many other engineers expanded upon the actuator disk method, including: Henderson and Shen (1981) who studied unsteady rotor response in their model and Colpin and Kool (1978) who derived transfer functions to model total enthalpy (thereby allowing the exit total pressure to be modeled and compared to experiments, as in Figure 2-8).

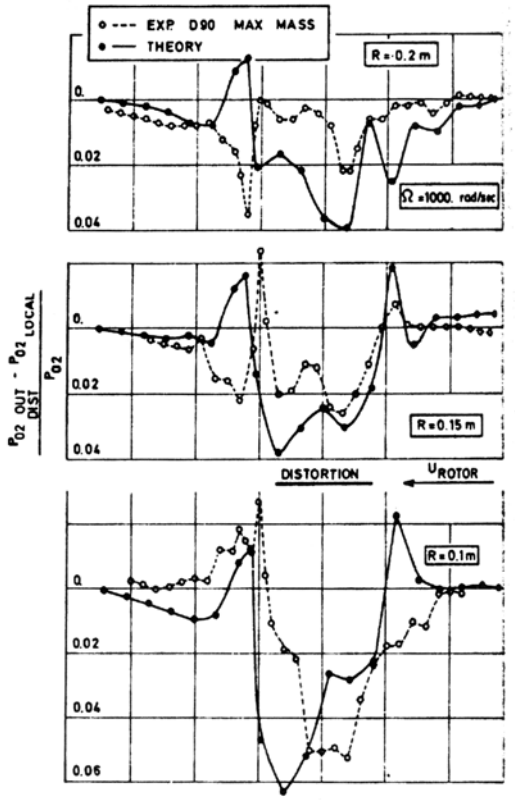

Figure 2-8: Actuator disk predicted pressures versus experimental, (Colpin and Kool, 1978)

While these methods were a basis for studies into the pre-stall behavior of an engine, many times researchers were interested in the effects of a stall downstream of the compressor, leading to studies in post-stall conditions.

Early post-stall modeling attempts were linear models using an actuator disk to introduce blade row work and rotation simultaneously. Nagano and Takata (1970) contributed to post-stall analysis by introducing non-linear equations of motion and first order response functions to model the unsteadiness inherent in compressor flows. In order to improve on the usage of first order response function, Sexton and O'Brien (1980) introduced frequency response functions. They modeled the "quasi-steady total pressure loss" as the forcing function and looked at the dynamic total pressure loss as the response function. This frequency response function was then used by Cousins and O'Brien (1985) to generate a post-stall compressor model. In much the same manner (by

using transfer functions), Hurad (1986) researched modeling unstalled compressor response to a distorted inlet flow.

The current distortion modeling techniques being developed are in the area of Computational Fluid Dynamics (CFD). CFD utilizes the calculation power of computers to solve the complex three-dimensional equations describing a fluid flow. To date, there have not been many CFD methods that account for non-uniform flows. One model generated by Vuillez (1994), uses CFD computer codes to predict surge inception in a single stage compressor. The author himself said that "This method needs further developments before if can be used as a prediction tool in the design procedure, but these are very promising results." A newer CFD modeling method has been developed by Ladd and Norby (1998). Here the researchers use CFD calculations in order to predict peak distortion levels. This method is "shown to be in excellent agreement with the flight test data and validate the accuracy of the Navier-Stokes program for this type of complex three dimensional flow."

As can be seen, many researchers have developed models to help describe the effects of non-uniform flow. They include studies of the distortion itself, studies of the effect distortion has on inlet flow and the effect of flow through a compressor due to distortion. The relationship between all of these studies is that they concentrated on performance effects of distortion, neglecting the problems distortion had on blade vibrations.

2.4 Total Pressure Distortion and Aeromechanical Effects

In addition to performance effects of non-uniform flows, a major concern for engine designers is designing longer lasting machines. One cause of decreased lifespan is fatigue due to blade vibrations. Distortion is known to be a cause of blade vibrations, which can then lead to one of the most worrisome occurrences of blade deterioration, high cycle fatigue (HCF). But even before the current studies of HCF, distortion induced vibrations caused problems for designers.

Early Analysis

Some of the earliest studies of aeromechanical effects of distortion began with the analysis of flutter. Flutter was the term given to any vibratory motion the blades went through due to the airflow. Early flutter studies did not investigate the variety of motions, only how to identify flutter regimes (which can be seen in Figure 2-9) and reduce the vibration. But, in the early 1980's the United States Air Force determined that a specific result of blade vibrations, High Cycle Fatigue (HCF), was of great concern.

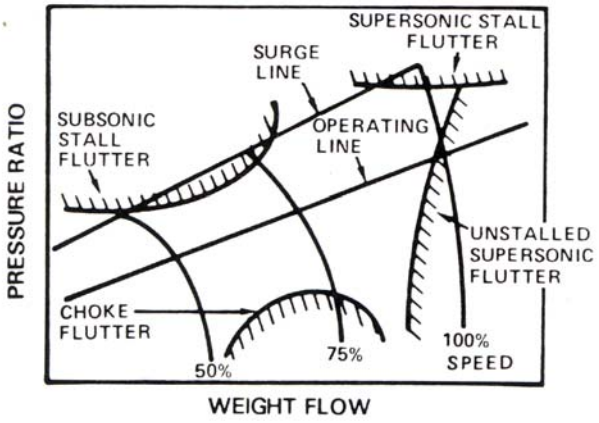

Figure 2-9: The different types of flutter and their placement on a compressor map. (Carta, 1989)

Studies in HCF were undertaken due to discrepancies of expected and actual blade life. Danforth (1975) set forth the idea that blade vibration is caused by an aerodynamic forcing function approaching the natural frequency of the blade and proposed a direct link between distortion intensity and vibratory stresses, as can be seen in Figure 2-10.

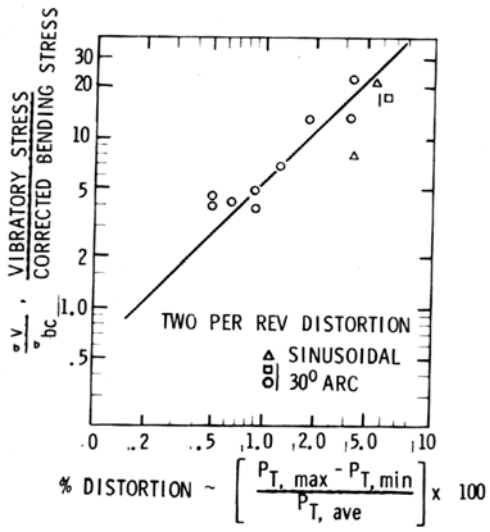

Figure 2-10: Relationship between distortion intensity and vibratory effects. (Danforth, 1975)

Peacock and Overli (1976) investigated the normal force at the blade mid-span based on distortions useing a square and sine wave distortion patterns. They found that the blade reaction was much greater due to the square wave distortion than that of the sine wave distortion. Their studies suggested a correlation between vibratory forces and a change in the flow's incidence angle (due to the reduction in axial velocity associated with distortion). Lecht and Weyer (1976) extended this research by exploring the effects of circumferential distortions on blade force response. They discovered that the peak loads were achieved when the observed blades were completely inside the distorted area, while the minimum loads were found as the blades first encountered the areas if distortion. Both of these studies dealt with the effects of the distortion, but they did not deal with investigating the direct cause of the vibrations, the forcing functions.

Fleeter (1978) studied the blade surface pressures for high engine order forcing functions. He discovered that the effects in the low speed compressor behaved comparably to that of a flat plate analysis. Manwaring and Fleeter (1989) extended the study to lower- order forcing functions by using two 90-degree distortion sectors. They discovered that the two per rev component of distortion dominated the forcing function.

Modern Analysis

Datko and O'Hara (1984) first studied the vibratory responses of newer, integrally bladed disks (commonly referred to as a blisk). They studied the lower order forcing functions in order to compare to the earlier distortion studies of compressors with typical blade to disk connections. Aside from this study, many of the current studies are concentrating on analysis in order to create modeling functions. Rabe et al (1995) studied multiple distortion cases consisting of 2, 3 and 8 per rev distortion tests. Their main result was that they were able to characterize the blade response along the entire length of the chord. Manwaring et al (1996) used the same test results to fully characterize two important aspects of forced response on an airfoil, the forcing function by using the total pressure distortion, and the blade's response by using the surface pressure and strain gauge measurements. The study was compared to numerical models and showed that current modeling techniques held good agreement for conditions away from resonance points. Also using these same tests, Small (2001) and Luedke (2001) generated the models mentioned earlier (see section 2.4) that analyze test data to predict the exit pressures. This data can also be used for HCF applications as well as the performance applications mentioned earlier. Again, it can be seen that the area of analysis has moved away from obtaining data to fix problems to the area of modeling phenomenon to avoid problems.

Modeling

The above-mentioned studies, especially those done by Rabe and Manwaring, were performed with the distinct goal of characterizing aspects of distortion in order to create models to predict its effects. Hah et al (1996) used a numerical solution of the Reynolds-averaged Navier-Stokes equations to model the same experiments of Rabe and Manwaring. Hah compared the numerical procedure to the experimental results and found that his procedure successfully predicted the flow field. Rabe et al. (1999) extended this numerical solution in order to generate a full annular solution. The results were apparently good, except for a problem with the prediction of unsteady blade pressure distributions. It is believed by the researcher that a better computational mesh

will provide better results. Also used for distortion modeling is the Turbine Engine Analysis Compressor Code (TEACC), developed by Hale and O'Brien (1998) and used by the Arnold Engineering Development Center (AEDC). A simple flow chart representation of this method can be seen in Figure 2-11, where a three-dimensional grid (Figure 2-11 a) is needed "on which to resolve the conservation equations," and source terms "representing mass bleed, blade forces and shaft work" (supplied by a streamline curvature code, Figure 2-11 b). TEACC (Figure 2-11 c) then uses these conservation equations to solve the grid and allows both "circumferential and radial control volumes to interact with each other via the three-dimensional Euler equations…" This provides a distortion analysis at many points in time (Figure 2-11 d) that can then be related to transient distortions (Davis et al., 2001). One of the most significant results of this method is the ability to model transient distortion cases, although it is only a steady-state approximation to the dynamic response to distortion.

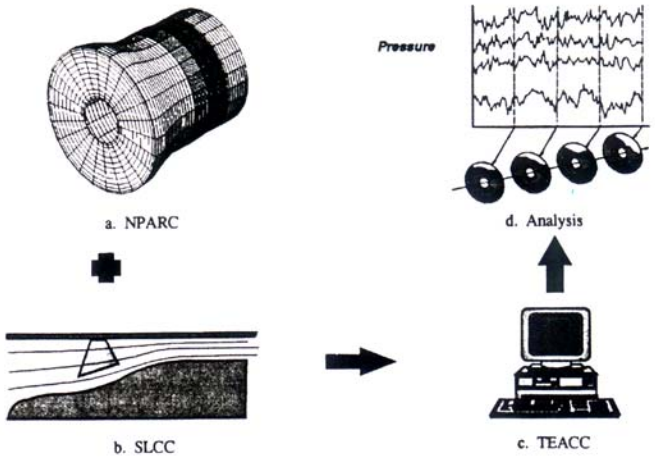

Figure 2-11: TEACC methodology, (Davis et al., 1998)

Although many attempts at fully predicting the effects of distortion that are relevant to HCF studies (forcing functions and response functions) have been done, they are not yet ready to be used as a prediction tool, as is the case in the performance effects of distortion. According to one researcher, "Fully 3-D, unsteady numerical models of full annulus turbomachinery blade rows require further development," (Small, 2001) stating

(but underemphasizing) how far modeling techniques need to be improved before they can be used as reliable predictors.

2.5 Current Methodologies

All of the above mentioned studies performed in analysis and modeling have been done in order to gain better understanding of non-uniform flow phenomenon. Their result has been to develop testing methods and techniques to analyze distorted flows.

Tests of Distorted Flows

Distortion testing has not changed a great deal from when it was determined to be an important flow factor to study. The method most commonly employed (both past and present) to create a distorted flow is that of the direct connect screen. Mesh screens are attached to the front of a fan, compressor or entire engine to create areas of total pressure distortions and variant porosities of the screens are used to create varying intensities of distortions. The shape of the screens can be simple, as is the case of the circumferential, radial and combined screens seen in Figure 2-3, or complicated in order to model actual flow conditions (an example is shown in Figure 2-12).

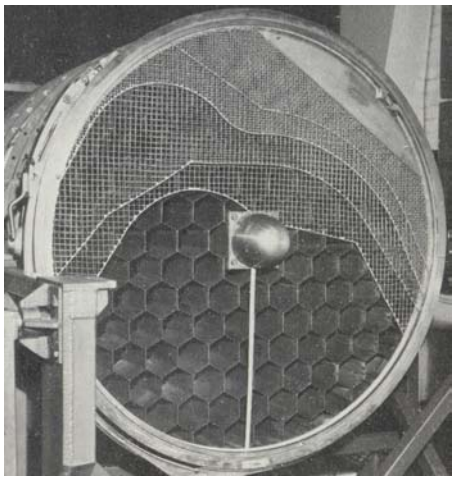

Figure 2-12: Example of a screen that models actual flight distortions, (Mokelke, 1974)

The above configurations are most commonly used for performance tests, while for aeromechanical studies the radial configuration can be employed with multiple, evenly spaced distortion sectors. This creates what is termed a "multiple per rev" distortion condition. A schematic of typical 1,2 and 3 per rev screens is shown in Figure 2-13.

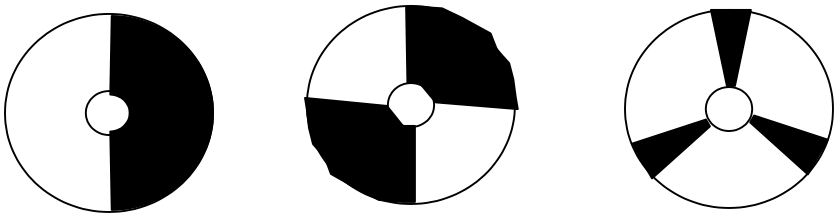

Figure 2-13: One, two and three-per-rev screens

As mentioned at the end of "Early Analysis" in the performance section, a large area of testing interest lies in studies of transient non-uniform flows. Currently, screens do not address this problem. In order to test transient distortion conditions, actual flight data is examined and the maximum distortion level is determined. This representation is acceptable unless the transients are occurring faster than the measurement hardware can record them. Recently, a partial solution has emerged to solve the problems with testing transient flows.

One method developed by Overall (1976) as an attempt to measure time-variant flows is the air-jet distortion generator, as seen in Figure 2-14. The air-jet method introduces a stream of flow opposite the free stream, using the resulting momentum exchange to create areas of lowered total pressure. If short pulsating streams of air are transferred through the system, transient flows can be represented.

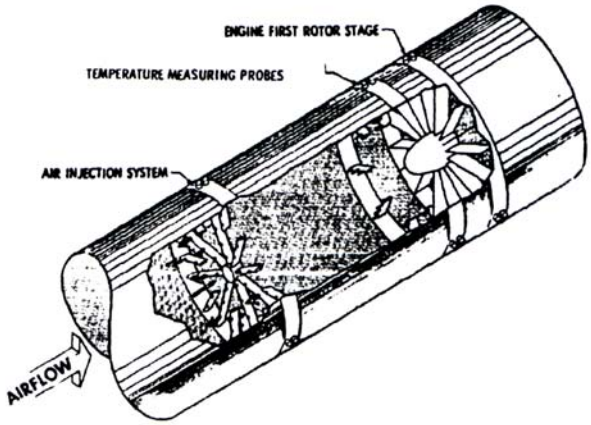

Figure 2-14: Air-Jet distortion generator, (Overall, 1976)

Another advantage of the air-jet method is that the distortion pattern can be altered quickly. As different jets are activated while others are disabled, the distortion pattern can be changed with no new hardware or labor. The major drawback of the air-jet distortion generator is that it introduces physical blockages into the airstream, in the form of support struts. These must be of considerable size so they can house the jets and the transportation hardware for the air that is to be injected into the free-stream.

Analysis of Distorted Flows

Multiple methods are used in the analysis of non-uniform flows to study both performance and aeromechanical effects. When determining the effects of distortion on the performance of turbomachinery, analysis parameters are defined in the ARP-1420 written by the S-16 committee. The definition of surge margin reduction is shown in Figure 2-15 and defined as,

$$\Delta PRS = \frac{(PR1 - PRDS)}{PR1} * 100 \qquad (2.1)$$

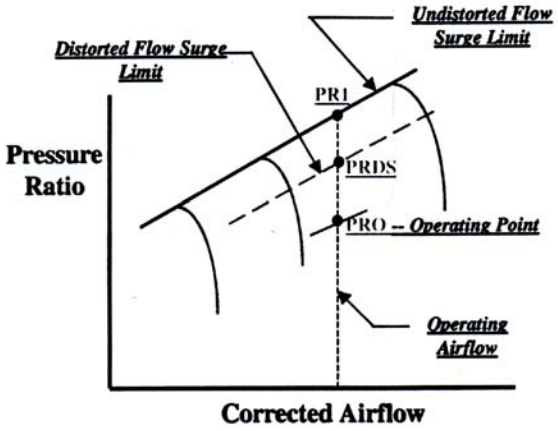

Figure 2-15: S-16 definition of surge margin reduction (ARP-1420, 1999)

The distorted surge margin reduction is used to determine the extent distortion affects performance. In addition, AIR-1419 provides correlation coefficients for the superposition of distortion patterns. This allows for the analysis of simple non-uniform flows to be used to learn about more complicated distortion patterns. A diagram of the different distortion patterns and their correlation coefficients is shown in Figure 2-16. A sample equation using these coefficients and measured pressures to calculate the surge margin reduction is,

$$\Delta PRS = BP * [f(MPR) * EXP * K_c P_c * (\frac{\Delta P_c}{P})_{\max}] + [K_r P_r * (\frac{\Delta P_r}{P})_{\max}] \qquad (2.2)$$

The subscript 'c' refers to circumferential and 'r' to radial. The coefficients BP, MPR, K_c, and K_r are all shown schematically in Figure 2-16.

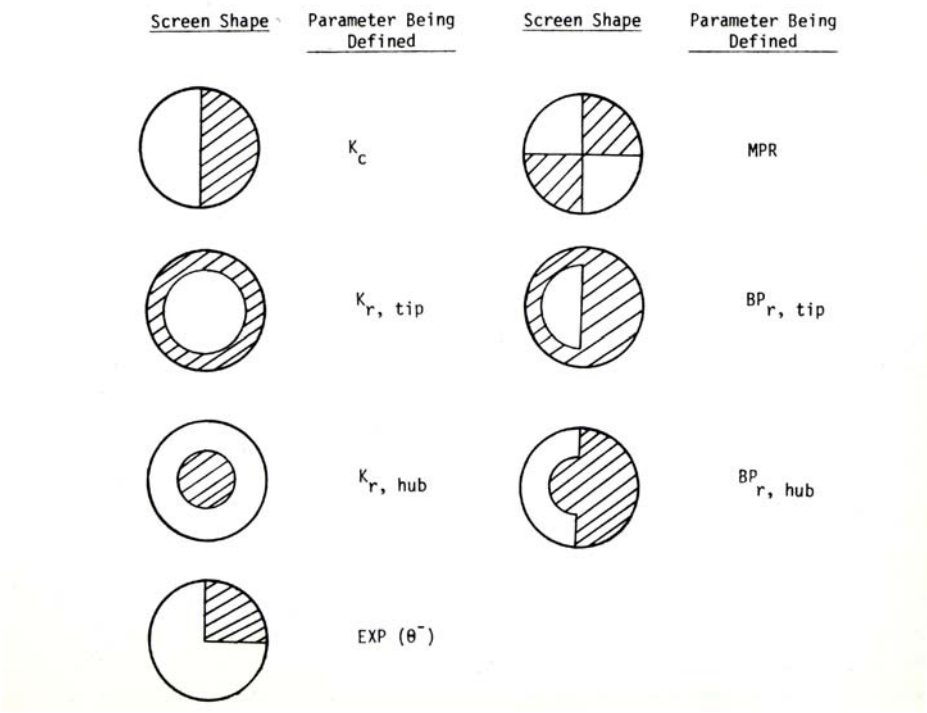

Figure 2-16: S-16 correlation coefficients with representative screen diagrams (Steenken, 1989)

The report, ARP-1420 also describes the data collection hardware and techniques to be used in data collection. These techniques are defined so that the hardware is sufficient to capture the specific information being studied. Also, these testing parameters are defined so that when data is compared between many separate investigations, the collection procedures are constant in order to provide standardization.

When analyzing aeromechanical effects of non-uniform flow, the primary tool used is the Campbell diagram, named for Wilfred Campbell (1924), who was one of the first to study vibrations of a turbine disk due to a flowing fluid. This diagram compares the natural frequency for different modes of the blade's vibration to the rotational speed of the compressor. The speed versus frequency lines for different "per-rev" components are also plotted. The point a natural frequency line crosses a per-rev line indicates a critical speed, which can be seen in the Campbell diagram from Manwaring et al. (1996) shown in Figure 2-17.

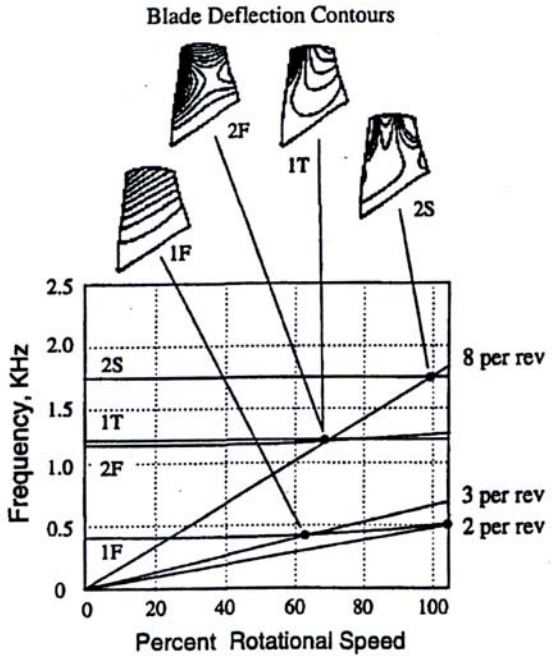

Figure 2-17: Typical Campbell diagram with critical speeds marked, (Manwaring, 1996)

In this graph the first and second bending (flexural) modes, the first torsional mode and the second stripe (combination of bending and torsional) mode are shown with the critical speeds associated with the specific engine tested indicated. This graph helps the engineer to discover if aeromechanical problems exist in their design, because if a natural frequency crosses an occurring per-rev line, and that speed is within the range of operating speeds, a HCF problem will occur.

2.6 Motivation for Work

After reviewing the many different works encompassing the areas of analysis, modeling and testing of distorted flows, it can be seen that there has been placed a great deal of importance and interest on non-uniformities over the years. But one theme was repeated throughout all of the past work, a heavy reliance on experimental data.

Therefore, researchers have explored more effective and efficient methods of conducting tests. Currently, most test engineers use the direct connect screen method to provide the necessary data. While this provides accurate distortion patterns, it does not effectively model all situations, such as transient distortions. Currently transient

distortion phenomena are modeled with screens by simply testing the maximum distortion levels observed in actual transient distortion occurrences. Screens are also very inefficient, because in order to change the distortion pattern new screens must be constructed, which can become very costly. In addition, labor increases because the screens are employed through the direct connect method, meaning that in order to change the distortion pattern engineers need to manually disconnect old screens and connect the new patterned screens. The first method that attempted to fix labor and efficiency problems was the airjet distortion generator. Its greatest drawback is that in introducing air streams that change the total pressure and large support struts that block the flow, the mass flow rate at the engine face can be reduced from that at the inlet.

In studying these current test methods, it is clear that a new method must be developed to generate distortions. This is an opinion shared by many including DiPietro (1996). He researched options for new distortion concepts, beginning with ten ideas utilizing flow blockage (much as a screen does) and momentum exchange (as in an airjet distortion generator). After studying the concepts, he found that because of the ease and lower costs, the flow blockage method was more desirable. Also of advantage is that the physical blockages can cause larger and more controllable distortion patterns. After studying many geometries of blockage, DiPietro decided to implement a "split airfoil" design by using a wedge shape to block the flow. As the angle of the wedge is changed, it produces differing extents of distortion. A large advantage of the wedge flow is that it has fixed separation points. This allows the streamlines of the flow to exist independent of velocity, thereby having no critical Reynolds number. The shape is then the main parameter in producing drag and pressure drops (DiPietro, 1996).

After seeing the advantages of a new wedge shaped distortion apparatus, the idea to develop a testing device utilizing it arose. Jumel (1999) and Eddy (2001) studied the distortions that were produced by a wedge in the airflow. Jumel used a static wedge in order to determine the distance downstream of the wedge the distortion extended. He found that the distortion patterns extended far enough downstream to be used to distort an engine from a safe distance in front of that engine. Also discovered was that the patterns and extents of distortion were easy to predict and therefore easy to accurately generate. Eddy characterized the distortions left by multiple angle combinations for two wedges.

His tests proved that much like the results from Jumel's single wedge tests, the distortion due to multiple wedges was easily characterized. These studies lend credibility to the wedge design. But will it meet the criteria set up in developing a pressure distortion generator? Davis et al. (2001) put forth guidelines and requirements for this development. He hopes to be able to meet seven areas that the next generation of distortion generators must address:

1) Reduction of test cost and cycle time,
2) The evolution of advanced inlet systems,
3) The implementation of super-maneuverability,
4) In-flight weapon launches in aircraft featuring supercruise and stealth capabilities,
5) V/STOL aircraft operation in ground effect,
6) The advent of engines employing light-weight and highly-loaded compressor stages, and
7) Engine performance enhancement through surge margin reduction or active stall control.

In looking at these requirements it was found that the splitting airfoil design that DiPietro proposed should be able to meet the criteria.

2.7 Scope of Current Research

The research performed was the initial design of the distortion generator and the actuation device. The study's purpose was to develop a concept that would be an improvement on current distortion generation techniques. To that end, the driving goals throughout the entire process were: 1) to meet the design requirements and 2) to minimize the necessary actuation forces. Each area provided its own problems and approaches. However, the methods used for selecting the best idea were the same for all aspects. The design requirements were used as initial guidelines for developing many possible versions. Then, the actuation forces were looked at in order to choose the best concept for implementation.

3 Design Requirements

Studies done by DiPietro (1996) and Davis et al. (2001) not only provided general ideas about distortion generator design, but also supplied specific criteria that a distortion generator should have. These were condensed into actual design requirements by Dave Beale of Sverdrup Technologies (Beale, 1997) assigning initial requirements that included specifications for movement rate, size and angular movement. Also included were requirements for maximum operating conditions of the surrounding environment.

As was discussed at the end of the Literature Review, a split airfoil design was selected. To simplify the concept, flat plates were used in place of airfoils creating a simple wedge. The advantages of a wedge design are rooted in its geometry, where the overall moments from each inclined plate making up half of the wedge are canceled by the other, symmetrical half-wedge. Also, if the boundary layer forces are assumed negligible, with this assumption studied later, the distributed pressure force can be modeled as a point force at the center of the half-wedge. The symmetry of the overall wedge allows that each individual half-wedge moment will cancel and contribute nothing to the opening and closing of the wedge. After selecting the underlying design, the criteria for the distortion generator had to be defined in order to form more detailed designs.

3.1 Size of Wedges

In order to gain acceptance of a new distortion generator within the engine testing community, it must take the place of existing generators for all situations. Engines ranging from small turboprops (GE CT-7 diameter of 25 inches) to large commercial hi-bypass turbofans (GE-90 diameter of 158 inches) may require distortion testing and need accommodating distortion generators. Currently, the most versatile method of creating non-uniformities is the direct connect screen, which can be adapted to any type of engine, thereby forcing a new generator to be just as adaptable. This means that a new testing device must be scalable to different sizes. Studies done by the research contractors found

that a size range of 1 inch by 1 inch up to 5 inches by 5 inches overall wedge dimensions would achieve the universality desired. This is an important parameter to define early in the design process, because it will be a factor in determining many other requirements for the device.

3.2 Range of Motion

Early on it was determined a wedge-type distortion generator would be required to move from a fully closed position (0^o) to a fully open position (180^o). When the required size range is considered, this motion requirement could mean as much as a 10-inch travel. But, based on further studies, the range of angles the wedge must go through can be reduced.

The first range restriction can be inferred from the work of Eddy (2001). He studied the pressure distortion patterns of two wedges in both a horizontally aligned and vertically aligned pattern. This study involved multiple angle combinations and found that the overall pressure pattern behaves as a combination of the two individual patterns for aspect ratios less than 1 but not at aspect ratios greater than 1, as seen in Figure 3-1a and Figure 3-1b. The aspect ratio is defined as the ratio of the frontal height to the width of the wedge, and therefore is equal to one at a total angle of 60^o. Following this suggestion in the design of a distortion generator allows the range to be greatly reduced.

a) 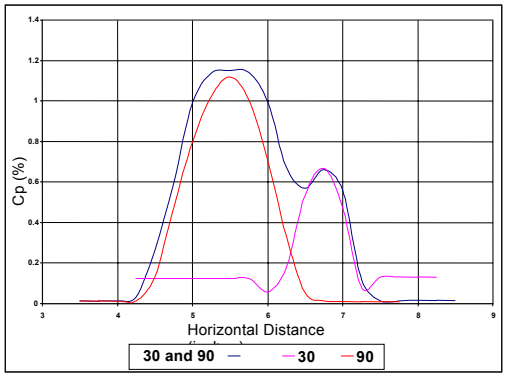

b) 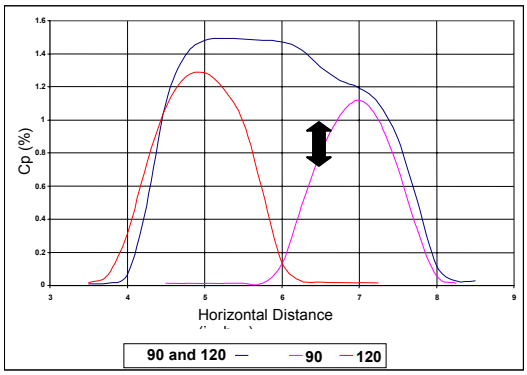

Figure 3-1: Comparison of two wedges and their superposition, 3 inches behind wedge, for (a) aspect ratio less than 1 and (b) greater than one. Note that (a) is additive and (b) is not.

The next study was performed to determine the minimum angle the wedge could be closed to without creating a notable distortion in the flow. Studies into the magnitude

and extent of distortion were performed at wedge total angles of 0^o and 15^o, with the results shown in Figure 3-2. The results observed from the closed wedge were reported as a total pressure coefficient, defined in equation 3.1,

$$C_p = \frac{P_o - P_i}{P_o + P_{amb}} * 100 \qquad (3.1)$$

where, P_o-P_i is the pressure difference measured, P_o is the inlet total pressure and P_{amb} is the ambient pressure. This coefficient had a drop in maximum magnitude of 0.4-0.5 percent and an overall area (neglecting the support rod denoted by the arrows) of pressure distortion measuring 0.8125 square inches. These results were then compared to those of the wedge at an angle of 15^o, and as shown in Figure 3-3, the 15^o wedge results in a maximum drop in total pressure coefficient of 0.4-0.5 percent as well. Differences from the closed wedge appear when the area of pressure drop is considered. From Figure 3-3, it can be seen that the distorted area of the 15^o wedge is 1 square inch. This is an approximately 20% increase in distorted area and mandates that the wedge must be closed to 0^o in order to maintain a minimal disturbance to the flow.

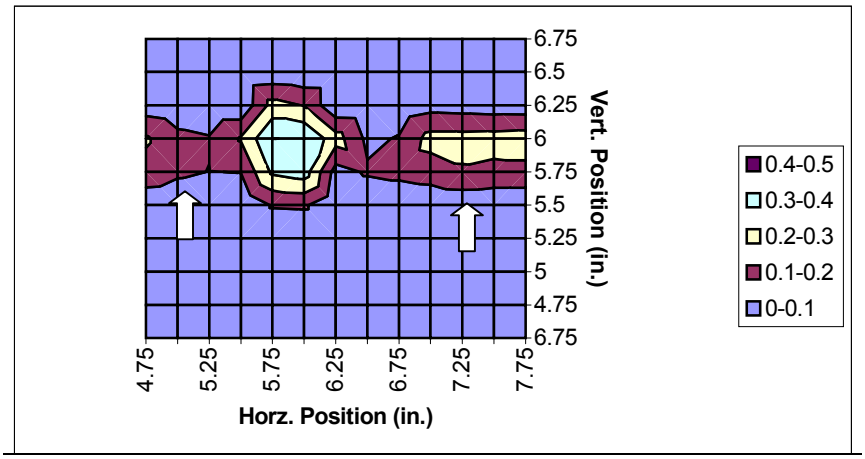

Figure 3-2: Total pressure drop, in percent of free-stream pressure, caused by 0^o total angle wedge. Distortion due to the support rod is noted with white arrows.

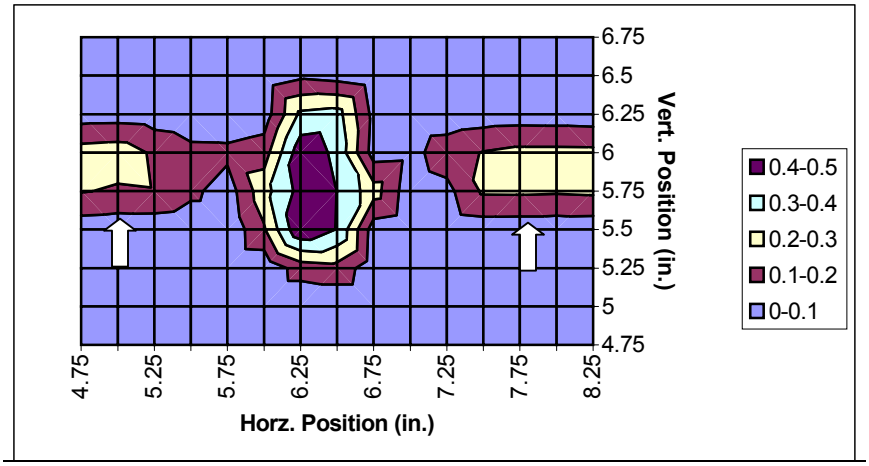

Figure 3-3: Total pressure drop, in percent of free-stream pressure, caused by 15° total angle wedge. Distortion due to the support rod is noted with white arrows.

From the above studies, the operating range of motion for the wedge is a minimum angle of 0° and a maximum opening angle of 60°. These studies greatly reduce the amount of travel necessary for the actuation mechanism, which can lead to smaller and less expensive actuators to meet the requirements.

3.3 Rate of Actuation

Transient effects of distortion have been a growing area of importance, starting with the experiments performed on the F-111 aircraft mentioned in the section entitled "Total Pressure Distortion and Performance Effects." A new distortion generator will need to not only replace existing methods, but improve on them as well. To this end, a new distortion generator will include the capability to model time-dependant distortion effects as well as steady-state effects.

Currently, test engineers use the peak distortion level over a representative period of time to model transient effects, such as turbulence. This method results in over-design, by creating an engine that can operate under the worst distortion levels all of the time. But this does not take into account the time spent at peak levels or the vibratory effects of constantly changing pressure levels. Other problems with the representative peak level method include the limitation that this test only accounts for transient magnitudes, and not positions.

The most common problem involving transient positions is inlet swirl. Directional transients such as swirl can reduce the stability limit of an engine. An example of this is shown in Figure 3.4, where stability limits are shown for a clean inlet, stationary distortion and swirl distortion (both co and counter rotation). Also involved with swirl distortion is the inherent vibratory problems with a single blade being subjected to the cyclic nature of swirling flows.

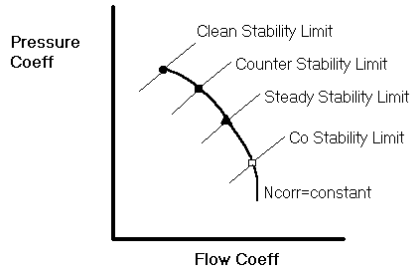

Figure 3-4: Comparison of stability limits for types of distortion. (Adapted from Davis et al., 2001)

Distortion position and magnitude transients can be modeled by changing the intensity and extent of distortion, and then measuring pressures over this entire process. The most pressing problem with modeling transient processes is how to achieve realistic patterns and changing flows. This problem creates a question of how fast a modeling device should change the distortion in order to accurately model distortion occurrences.

The frequency of transient variations that should be studied is not known, but the current contract requires full travel in 0.5 seconds. If the maximum travel is considered (10 inches, 180^{o}), the requirement becomes a 20-inch per second (360 degree per second) rate. But, if the range restrictions evaluated earlier are imposed on the design, the maximum rate reduces to 5-inches per second (120 degrees per second). It is important to note that lower rates (1.5 degrees per second) do not introduce performance problems seen elsewhere, as can be seen in Figure 3-5. Therefore, studies involving transient distortion should test at higher rates, with the current design having a rate requirement of 120 degrees per second, used in order to meet the contractor's requirements after assessing restrictions on the total travel.

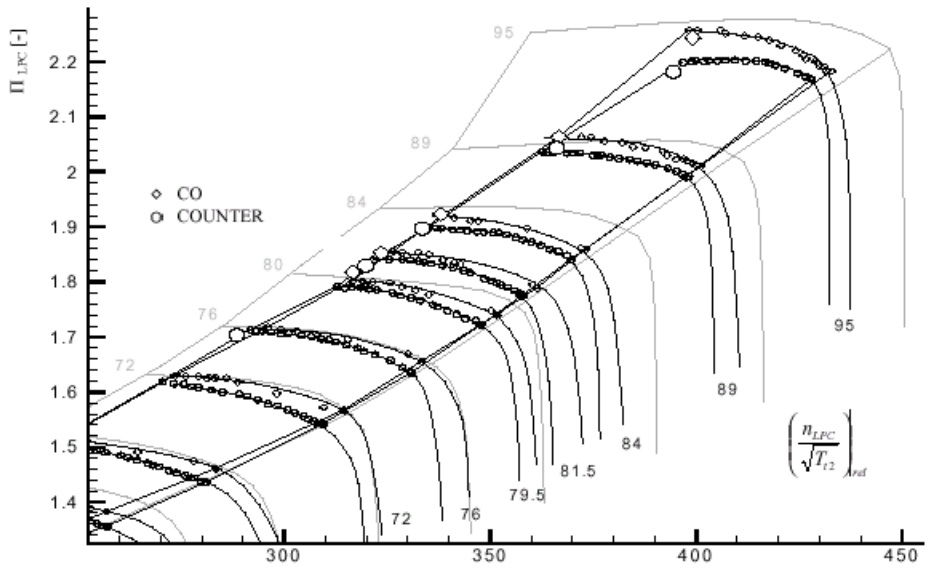

Figure 3-5: Compressor map showing steady-state distortion stall (large points) and transient distortion stall (small points). Notice that the stall limit for transient approaches that for steady.

3.4 Test Cell Conditions

An important factor in any design process is defining the operation conditions. The volatile nature of turbomachinery introduces uncommonly high conditions. In order to develop a test device that will be used in many different situations, the operating conditions must cover a large range. Given as the upper conditions by the contractors are a Mach number of 0.6, a free-stream total pressure of 40 psia, and a free-stream total temperature of 300^{o}F. These conditions are important in material selection and device structure, because the materials must not degrade under the high pressures and temperatures and the device must be able to withstand the drag forces placed on it by the high air speeds.

3.5 Flow Conditions and Forces

In order to properly size the support structure as well as the actuation system, the forces acting on the system need to be determined. To assure that the distortion generator will operate correctly under the range of operating conditions given above, the forces were calculated for the largest values of test cell conditions for a range of wedge sizes.

Forces on the airfoil are generated by a pressure difference between the upper and lower surface. The resulting pressure force, F_{press}, acts perpendicular to the plate. The pressure force can be calculated using,

$$F_{press} = C_N \frac{\rho U^2 A}{2} \tag{3.2}$$

where, C_N is the normal coefficient, ρ is the density, U is the free stream velocity and A is the reference area. The normal force coefficient is a function of the angle of the plate, and is given for multiple angles in Table 3.1. These values were determined from experimental data on a three-dimensional inclined plate representing half of the wedge design, found in Blevins (1984).

Table 3-1: Normal force coefficients for varying angles (adapted from Blevins, 1984)

Angle	**0°**	**10°**	**20°**	**30°**	**40°**	**50°**	**60°**	**70°**	**80°**	**90°**
C_N	0.000	0.399	0.872	1.281	1.470	1.103	1.082	1.071	1.061	1.050

This force is normally transformed to an x-component, the drag force (F_{drag}), and a y-component, the lift force (F_{lift}), with the drag force always acting parallel to the flow and the lift force always acting perpendicular to the flow. Therefore the normal coefficients can be split into a drag and lift coefficient by the method shown in Equations 3.3 and 3.4.

$$C_D = C_N \sin(\theta) \tag{3.3}$$

$$C_L = C_N \cos(\theta) \tag{3.4}$$

The drag and lift for a flow over a bluff body can then be calculated from equations 3.5 and 3.6,

$$F_{drag} = C_D \frac{\rho U^2 A}{2} \tag{3.5}$$

$$F_{lift} = C_L \frac{\rho U^2 A}{2} \tag{3.6}$$

where, C_D and C_L are the drag and lift coefficients, respectively, ρ is the density, U is the free stream velocity and A is the reference area. The reference area was used because, as the angle of the wedge is increased, the area exposed to the flow is increased as well, and subsequently increases the force acting on the wedge. In the case of a three-dimensional

inclined plate model, the surface area (the length multiplied by the width of the wedge) was used. This area remains constant for all angles, therefore the variation of the forces is accounted for in the force coefficients. In a later, two-dimensional analysis, the reference area will be the frontal area (height of wedge multiplied by the width) and will therefore change with the angle. The pressure forces for different area wedges (all within our design range) are shown in Figure 3.4 for a flow of Mach 0.6. This force is broken into lift and drag components in Appendices A and B for flows of Mach 0.6 and Mach 0.1, respectively. It is important to note that these forces were calculated assuming the flow to be inviscid which negates the effect of boundary layer forces that act on the wedge.

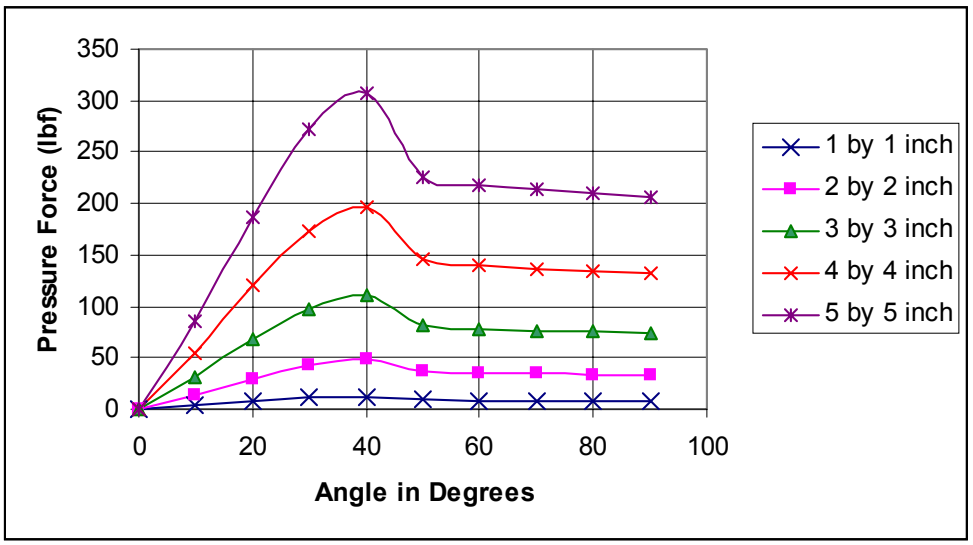

Figure 3-4: Pressure forces in Mach 0.6 flow for square wedges

3.6 Boundary Layer Analysis

When looking at real flows over immersed bodies, the contribution of boundary layer forces (viscous drag) must be included in any analysis. If these forces are significantly smaller than the other forces, the viscous forces can be neglected. Having no boundary layer drag allows the distributed force on the surface of the wedge to be assumed constant. If this force is constant, then it can be combined into a point force at

the center of gravity and by describing the force at a point later analysis of wedge designs will be simplified. In order to determine if the boundary layer is negligible, the flow conditions and the forces themselves were examined.

To begin analyzing a boundary layer the fluid and its viscous forces were evaluated by calculating the Reynolds number, using equation 3.7,

$$\mathrm{Re} = \frac{Ul}{\nu} \qquad (3.7)$$

where, U is the free stream velocity, l is the length of the body and ν is the kinematic viscosity of the fluid. The definition of the Reynolds number is the ratio of inertial forces to viscous forces. Therefore, a high Reynolds number would lend validity to he assumption that boundary layer forces are negligible. The test conditions of the flow to be used have the following properties: free stream velocity of 41.1 ft/s (Mach 0.1), a kinematic viscosity of $1.57*10^{-4}$ ft/s^2, and a wedge length of 0.0833 ft. This corresponds to a Reynolds number of approximately 72,000. A typical convention used in fluid flow analysis is that any flow with a Reynolds number above 100 is dominated by inertial effects (Munson et al., 1998). If the same analysis is performed for the worst-case flow (Mach 0.6), the resulting Reynolds number is approximately 126,000. This allows for the conclusion that under the intended operating conditions, the boundary layer forces can be neglected. But this is only a method of assessing the significance of the boundary layer. In order to determine if the boundary layer is actually an important factor in the force analysis, a quantitative study had to be performed.

The first analysis done was a study of forces to create a free-body diagram, as seen in Figure 3.5 with all relevant forces listed. The symmetry of a wedge allowed the system to be modeled by doubling a ½ wedge, represented as an inclined plate. In addition to the lift, drag and pressure forces, the boundary layer viscous force (τ) is included. The resultant force is the actual force due to the pressure and boundary layer forces combined. An important note is that the lift and drag forces shown in Figure 3.5 are the components that make up the resultant force, not the pressure force.

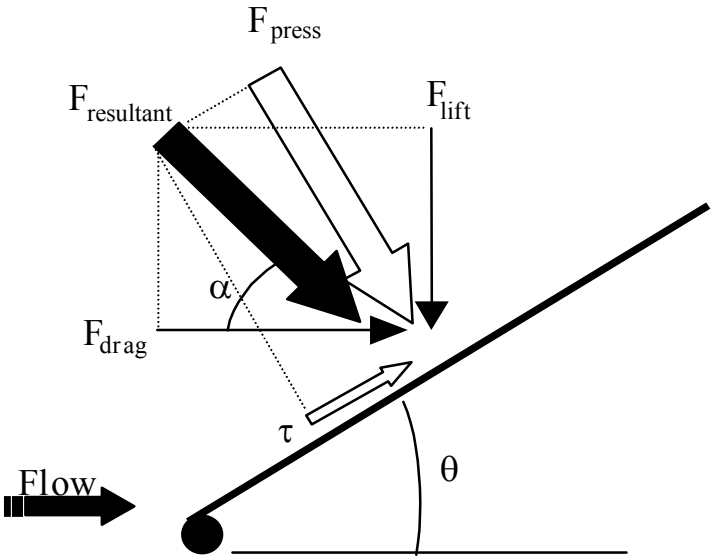

Figure 3-5: Free-body diagram of ½ wedge with forces resulting from the flow.

In order to find the resultant force, two sets of experimental data were used. The first data set contained drag coefficients for various angles of a wedge. This drag coefficient (C_D) was obtained from tables where the researcher, Blevins, measured the drag force directly of a wedge, which includes the effects of boundary layer forces. The second set of data was a list of pressure force coefficients (C_N) measured, by Blevins, on an inclined plate at various angles. Any drag or lift forces generated from this pressure force will be ideal and not contain boundary layer forces. The drag forces and pressure forces can be calculated from these two sets of coefficients using equations 3.8 and 3.9,

$$F_D = C_D \frac{\rho U^2 A}{2} \tag{3.8}$$

$$F_{press} = C_N \frac{\rho U^2 A}{2} \tag{3.9}$$

Using these results simultaneously in equations 3.10 and 3.11 gave the resultant force after using equation 3.12 to calculate the angle α.

$$F_{\text{resultant}} = \frac{F_{press}}{\cos[90 - (\alpha + \theta)]} \tag{3.10}$$

$$F_{\text{resultant}} = \frac{F_{drag}}{\cos(\alpha)} \tag{3.11}$$

$$\alpha = \tan^{-1}\left[\frac{F_{press}}{F_{drag}\cos(\theta)} - \tan(\theta)\right] \qquad (3.12)$$

Finally, the boundary layer force was calculated using equation 3.13,

$$\tau = F_{\text{resultant}*}\cos(\alpha + \theta) \qquad (3.13)$$

and was then compared to the resultant force. In this comparison, the two components of the resultant force, the normal and boundary layer forces, were investigated to determine their relative importance. This was done by determining their percent contribution to the resultant force. The results are shown in Figure 3.6, where it can be seen that the worst-case is around a total wedge angle of 40°, where the viscous force is 0.2 lbf, but only contributes 17% to the resultant force. At this same angle, the normal force contributes the remaining 83% of the resultant force. Although the viscous contribution is not negligible, the forces are relatively small compared to the other flow forces. The boundary layer dominates the overall force at smaller angles, but the magnitudes are very small. The same tests were performed for the Mach 0.6 test conditions, and the results were the same.

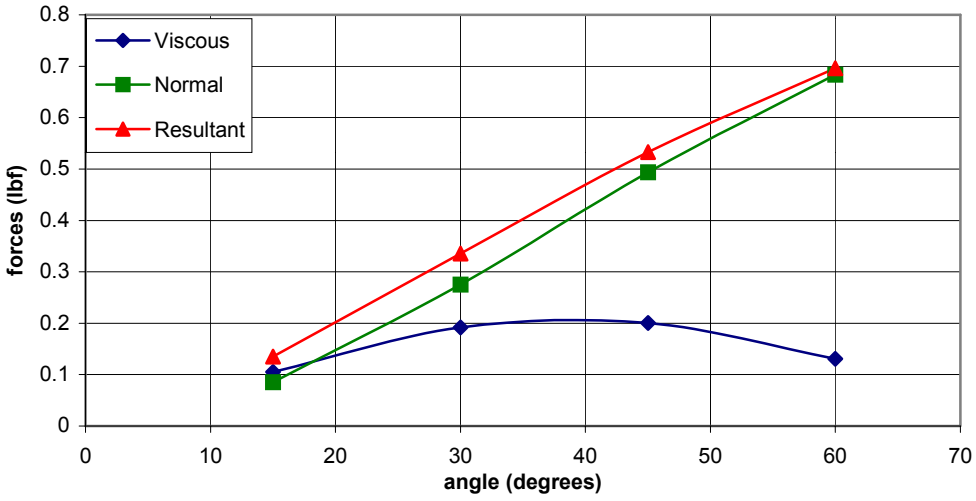

Figure 3-6: Comparison of resultant force and its components for flow M=0.1

From this analysis, it was concluded that at angles where the boundary layer is the dominant force, the magnitude is still not small enough to neglect. At larger angles, where the magnitude of the boundary layer force becomes large, it is overshadowed by the pressure force, but still not negligible. But, by looking at the symmetry of the wedge the boundary layer forces can be assumed neglected. This is because when evaluating the actuation force only, the boundary layer forces on the two halves of the wedge counteract each other. This method of force cancellation is explained in more detail in the "Wedge Selection" section where it is used to cancel out other flow forces.

3.7 Isolating Individual Forces

Once the boundary layer force was determined to be negligible, the design could begin to be refined. The first design aspect looked at was the reduction of forces. In order to achieve this, the pressure force was again split into lift and drag components. This was done with the intentions of designing the wedge and support structure to cancel out all or part of each component. This would provide large advantages in actuator selection. Therefore, in all of the cases of wedge designs, the pressure force was not directly considered, only the lift and drag components.

4 Wedge Design

Based on the studies of DiPietro (1996), Jumel (1999) and Eddy (2001), a wedge configuration was selected for the distortion generator, but other criteria still needed to be identified in order to refine the design. One area of concern was the possibility of foreign object damage (FOD). This is of great concern whenever any test is conducted in front of an engine, and therefore the minimization of FOD possibilities was a factor in considering the design of the wedge. Another criterion identified was simplicity, because the overriding goal of this project is to introduce a design that will replace screens and be accepted by the engine testing community. Screens are a very simple, but inefficient, method of creating distortion and therefore, if a new test apparatus is to gain acceptance, it will have to maintain the simplicity of screens while increasing the overall test process efficiency. The most important design criterion identified was the reduction of forces. Support to the wedge can be provided so that the flow forces are partially negated. Different magnitudes and directions of support can be provided based on the wedge design, providing numerous advantages in selecting an actuation device.

4.1 Front Supported Wedge

The simplest method of supporting the wedge was by using the pin through the rotational hinge. Using a rod as the pin, it was extended out both sides to the extents of the test cell, supporting the wedge. This created a configuration as seen in Figure 4-1, where the rod at the front of the wedge extends outwards in both directions.

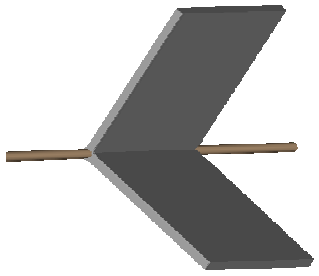

Figure 4-1: Drawing of front supported wedge.

With the distributed pressure forces on one half of the wedge modeled as a point force at the center of an inclined plate, a free-body diagram showing all relevant forces was produced, as seen in Appendix C, Figure 1. The pressure force (F_p) was separated into lift and drag components (F_L and F_D, respectively) in order to solve for the arbitrarily placed, wedge actuation force (F_{act}) needed to move the wedge. This actuation force is a representative force used to show how wedge design affects the required forces. The type of actuation force chosen was two vertical forces applied independently to each side of the wedge, and is discussed in detail in the "Actuation Selection" section. The symmetry of this method of actuation allows the FBD to be represented by half of the overall system, making evaluation and comparison easier. The overall actuation force, $F_{overall}$, is later defined and evaluated in the "Design Selection" section. The wedge actuation force was solved by summing the moments about point A. Knowing that if the wedge is not to move, the moments must sum to zero, the actuation force can then be calculated using equation 4.1

$$F_{act} = \frac{(F_L * x) - (F_D * y)}{x} \quad . \tag{4.1}$$

The actuation force needed for this wedge design was then calculated for varying flow conditions and sizes. Figure 4-2 shows the actuation force needed for a front-supported wedge within the design range of sizes, over a full range of motion, for a flow of Mach 0.6. The most important information for this wedge came later with the comparison of equation 4.1 to other actuation forces.

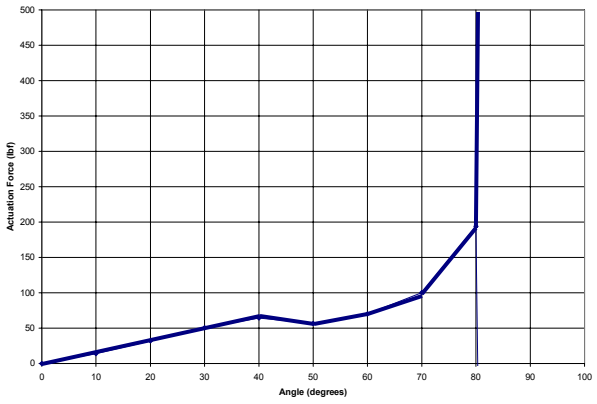

Figure 4-2: Actuation forces for varying angles of a front-supported hinge. The force makes a large jump from 80° to 90°.

4.2 Rear Supported Wedge

The next wedge design was the first developed with the idea of using the support structure to counteract portions of the flow forces. The support rod was moved from the front hinge point to behind the wedge. Struts connect the wedge to the rod, transferring the flow forces to the support. To allow the hinge to move through its' full range of motion, the struts must hinge around both the support and wedge. To this end, slots were manufactured along the length of the wedge and the struts secured inside the slots with pins. The slots need to be large enough to allow for an increasing part of the strut to rotate through the opening as the angles become smaller. This design can be seen in Figure 4-3, where there are two struts on each half-wedge for added structural support and redundancy.

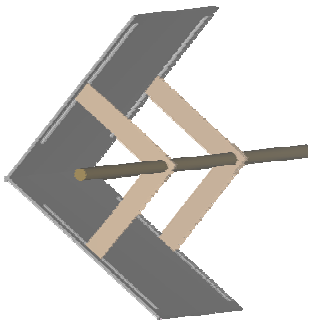

Figure 4-3: Drawing of rear supported hinge

As was done before, a free body diagram was generated (Appendix C, Figure 2) and the arbitrary actuation force found by again summing the moments about point A. The actuation force found was,

$$F_{act} = \frac{[(F_L * x) - (F_{SY} * x)] + [(F_D * y) - (F_{SX} * y)]}{x} \qquad (4.2)$$

where, F_{SY} and F_{SX} are the components of the support force (F_{sup}) from the struts. These forces are dependent on the half-angle of the wedge, θ, represented in the free-body diagram as f(θ). Therefore, the struts support varying amounts of the flow forces, with

the extent of support depending on the wedge angle. Figure 4-4 shows the actuation forces necessary to open the rear-supported wedge over a range of half-angles.

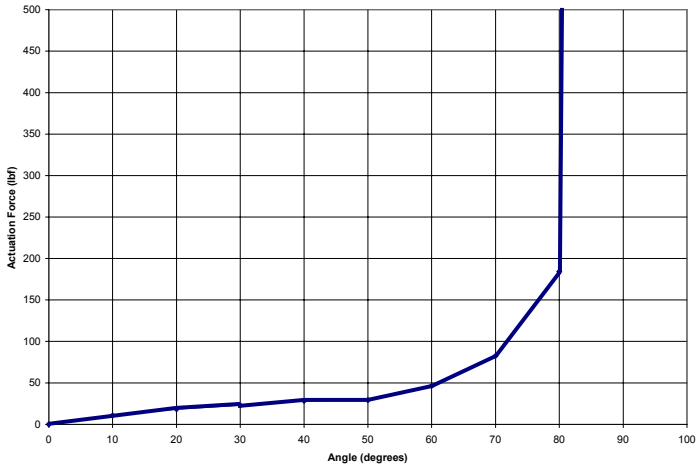

Figure 4-4: Actuation forces for varying angles of a rear-supported wedge. Again, the force makes a large jump from 80^{o} to 90^{o}.

A large disadvantage of this wedge configuration is that when the support is behind the wedge, an added structural member will have to be added to secure the front of the wedge and maintain its orientation to the flow. Additionally, if the wedge and strut have fixed dimensions, either the front of the hinge or the support rod has to be allowed to move horizontally.

4.3 Center Supported Wedge

The dominant problem encountered with the rear-supported wedge was that the amount of force counteraction varied with the angle. Therefore, in certain configurations, the positioning of the support only provided a minimal amount of assistance in reducing the necessary actuation force. Devising a method of decreasing the actuation force at all angles would be very helpful in the wedge design. It was found that by placing the support rod in alignment with the center of the wedge, the support force acted in the horizontal direction at all angles, thereby counteracting the entire drag force. But, there were difficulties maintaining the support rod at its center location for all angles that had to be overcome.

Standard Configuration

Consistent with the design and support orientation of the rear-supported hinge, a scissor system around the hinge, as shown in Figure 4-5 was created. This arrangement allowed the hinge to close around the support without the rod moving. Moving the hinge to the center does not eliminate the requirement of a front-horizontal support, like the rear-supported wedge, because at lower angles the wedge would not stay oriented to the flow. A free-body analysis was again performed, and is shown in Appendix C, Figure 3.

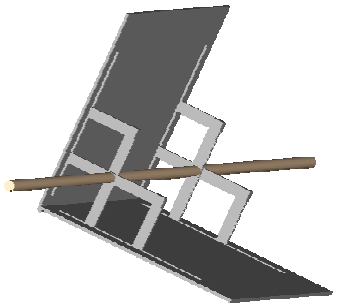

Figure 4-5: Standard configuration, center-supported hinge.

Vertical Configuration

Using the same idea of a center placed support structure, a new variation was developed. The support structure was rotated to the vertical position, placing it in the same direction as the motion of actuation. This design can be seen in Figure 4-6, noting that this picture has an airfoil support structure in place of the round one previously pictured. This was decided upon at the same time as rotating the support, and therefore is included in the picture and discussed later in the "Design Selection" section. As was done with the other designs, a free-body diagram was performed on this design, but it was the same as the standard configuration, center-supported wedge (Appendix C, Figure 3). Both the standard and vertical configuration possess the same motion, therefore having the same force analysis. The support force for this design, F_{sup}, is in the horizontal, x, direction. This support force cancels out the drag force on the wedge, making the necessary actuation force, F_{act}, equal to only the lift force.

$$F_{act} = F_L \tag{4.3}$$

The arbitrary actuation forces over a range of half-angles are shown in Figure 4-7, but are the same as the lift force graph included earlier.

Figure 4-6: Vertical configuration, center-supported wedge.

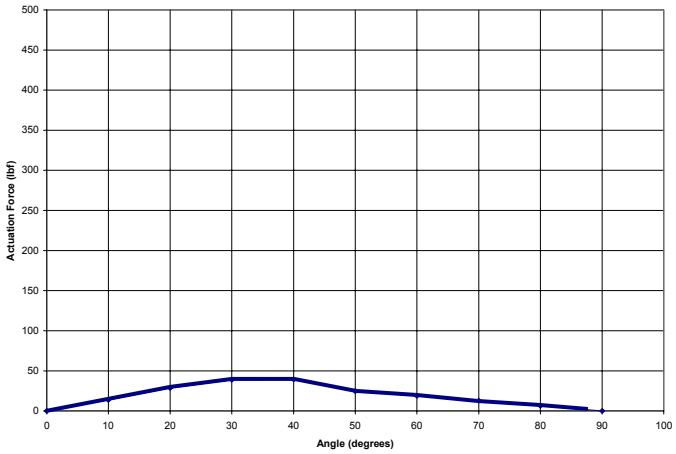

Figure 4-7: Actuation force for varying angles of a center-supported wedge.

An advantage of this design is that the configuration requires small actuation forces throughout the entire range of motion. Also, orienting the actuation motion in the direction of wedge motion allows the connection between actuator and wedge to be simplified. Also discovered was that a parallel motion-orientation allowed the link between wedge and actuator to be placed inside of the support structure, thus reducing the FOD hazard introduced by this connection. Placing the transmission device inside of

the support also allows for less flow disruption than separate support structures and transmission devices.

5 Actuation Design

When considering ideas for introducing movement to the wedge, two parameters were of primary concern. First was the ability of the actuator to provide the necessary travel to move fully through the determined range of motion. The other consideration was that the actuator needed to provide enough force to move the wedge under the worst conditions set forth in the "Design Requirements" section. The mechanism must meet both requirements in order to be considered for use in the overall design. Another, secondary, consideration was the time required to achieve the desired travel. The inability of the actuator to meet the time requirements may disqualify an actuator design from selection because of its intended future use in transient studies. The force and travel requirements are both dependant on the wedge design, and therefore actuation assessment was performed after the wedge concepts were evaluated.

5.1 Actuation Direction

The determining factor of the force needed to move the wedge was the direction of actuation. Different orientations have the possibility of drastically reducing the effect of flow forces on the system. Four set-ups were studied to find the direction that encountered the least number and magnitude of resistance forces.

The first actuation direction was developed to work with the rotational motion of the splitting wedge, using a torsional actuation force about the front hinge. In order to move both sides of the wedge, two oppositely rotating forces had to be applied. A free-body diagram (FBD) of this configuration is shown in Appendix D, Figure 1. Because the two sides are symmetrical and have opposing forces, this FBD was separated into two, identical FBDs. Therefore, the directional actuation force (T_{dir}) found for one half of the wedge could be doubled to find the overall directional actuation force. Summing the moments about the hinge point and then doubling it gives the necessary directional actuation torsional force of the wedge, given in equation 5.1.

$$T_{dir} = 2\left[(F_L * x) + (F_D * y)\right] \tag{5.1}$$

The second direction of movement considered was the horizontal direction. The front hinge was allowed to move in the horizontal direction with the remainder of the wedge held stationary, using the travel of the entire hinge to open and close the wedge. A FBD of this design is shown in Appendix D, Figure 2. Summing the forces in the horizontal direction gives the actuation force (F_{dir}) as,

$$F_{dir} = 2F_D \tag{5.2}$$

This design was an improvement over the torsional design because it depended on the drag forces only, not the drag, lift, and distance the forces acted over; as was the case for the torsional actuation.

The next two designs involved rotating the actuation direction to the vertical direction. The first vertical configuration involved a force pushing up on the wedge to rotate it about the hinge. A FBD of this is shown in Appendix D, Figure 3. Because each inclined plate that makes up the wedge requires a movement force, two directional actuation forces were needed. To solve for the directional actuation force's dependence on the flow, the symmetry again allowed the FBD to be cut in half. The final force was found by doubling the directional actuation force calculated. Therefore, summing the forces in the vertical direction produced the overall directional actuation force (F_{dir}) as,

$$F_{dir} = 2\ F_L \tag{5.3}$$

This design was an advantage over the horizontal actuation because, as is shown in Appendices A and B, the lift force was lower than the drag force when evaluated over the entire range of motion.

The final actuation direction was a modification on the purely vertical motion. One half of the wedge was held stationary, while the other half was permitted to move in the vertical direction only. This configuration's FBD can be seen in Appendix D, Figure 4. Using the same methods as before, the single directional actuation force was found to be independent of all flow forces, and only dependent on the vertical support force (F_{supy}), as seen in equation 5.4.

$$F_{dir} = F_{supy} \tag{5.4}$$

This support force relied on the actuation force applied, meaning its value was coupled to the force applied by the actuator. Because the support force is not dependant on any flow

forces, for any flow speed or wedge size the necessary directional actuation force would still only be dependant on the support force. This was determined to be a large advantage for conducting successive tests having varying flow conditions.

An important note for all of these designs is that the weights of the wedge and hinge pin were neglected. This did not quantitatively change the evaluations, because the weights contributed to certain directional actuation forces and detracted from others. Also, the moments about the upper and lower plates either increased or decreased, dependent on the direction the weight acted in. But, being evaluated here were methods to minimize the dependence of the direction of movement on flow forces. Therefore, the weights should be neglected in order to find the best actuation direction based on configuration and not material properties or construction methods.

Other factors in actuator selection exist which are independent of the actuator's operation, including those that are correlated to the entire system (e.g. complexity), and others dependent on system interaction (e.g. actuator with the wedge).

5.2 Actuator Placement

Another important design criterion that related to the wedge design was the placement of the actuator. Considerations for this requirement included transmission of power, complexity, length of travel, and flow disruption. All of these considerations depended on the design of the wedge, as well as the direction of actuation. However, for the current study the placement of the actuator was considered independent of these two factors to allow for a direct comparison of ideas. The two designs considered were placing the actuator inside or outside of the test section.

Inside Placement

Placing the actuator inside the test section, adjacent to or even integrated into the wedge, would guarantee additional disruption of the flow. This disturbance could be caused by the actuator itself being in the flow or, from restrictions on how far the wedge could close due to the size of the actuator. As was shown in the "Range of Motion" sub-section of "Design Requirements", the wedges must close to as close to 0^o, in order to

minimize the amount of undesired flow distortions. The overall feasibility of inside placement was ultimately determined by the motion of the wedge and the actuator selected.

Outside Placement

If the actuation device was located outside of the test section, the wedge would be able to close farther and approach an angle of zero. The size constraints of an actuator associated with locating it inside the test section would also be largely eliminated. In addition, maintenance and replacement of the actuators became much easier if they were located outside the test section. Finally, if devices were located outside of the test section, the FOD hazard reduced because of the fewer moving parts located inside of the flow. A disadvantage of moving the actuator outside of the test section was that the force generated by the actuator must be transferred over a longer distance. Two methods studied for transferring the force into the test cell were lead screws and cables/rods.

A lead screw draws a nut along its threads, with the nut being fixed (as shown in Figure 5.1 a) or movable (as in Figure 5.1 b). In the fixed nut configuration, the screw is the traveling element. If the screw was connected to the front of the wedge, it moved the wedge in or out with the screw. In the movable nut configuration, the nut was connected to the wedge. Then, as it moved along the screw, it would open or close the wedge. One problem with either implementation of lead screws was the introduction of a rotational motion, adding complexity to the system.

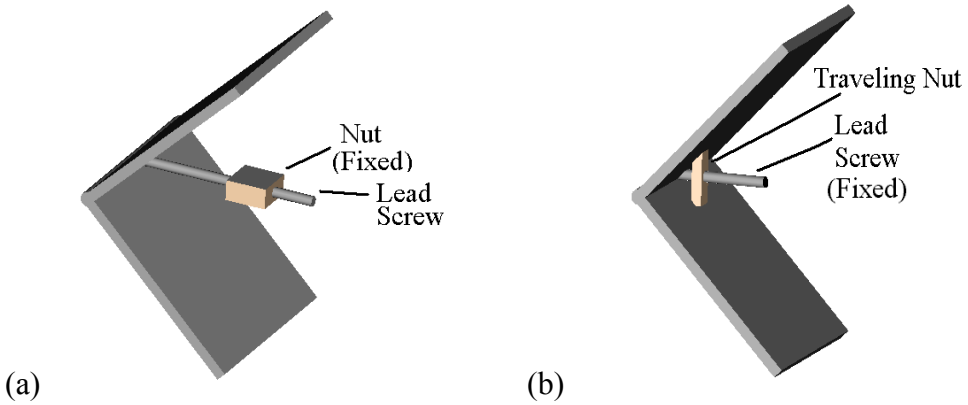

Figure 5.1: Lead screw design for actuation. The nut is (a) fixed and (b) movable.

Cables are a simple way of transferring the motion of the actuator from the outside of the test cell to the wedge on the inside. If cables or rods were used, 100 percent of the power would be transferred to the wedge. Additionally, cables are bendable, allowing them to conform to the structure of the wedge. But, this flexibility can cause problems, especially if multiple cables were used because they could interfere with each other. Also, they are rigid only when force is acting on then, and therefore do not adapt to changes in the direction of flow forces (as was the case in the lift force at angles over 45 degrees). This problem was solved by using rods. Their rigidity almost eliminated interference problems and allowed them to continue working if the direction of force changed.

The placement of the actuator depended on the concept selected. Some concepts could only be placed inside, some only outside and some were operable in either position.

5.3 Piston-Cylinder

These types of devices rely on a force generated inside a cylinder to expand and contract the piston. The downside of piston-cylinders is that in order to generate large enough forces, the cross-sectional area of the piston needs to be large. The inherent linear motion of this type of device lends itself to either inside or outside positioning. The actuator can be connected directly to the wedge or the linear force can be transmitted quite easily into the test cell. A picture of the inside placement of a piston-cylinder design is shown in Figure 5.2.

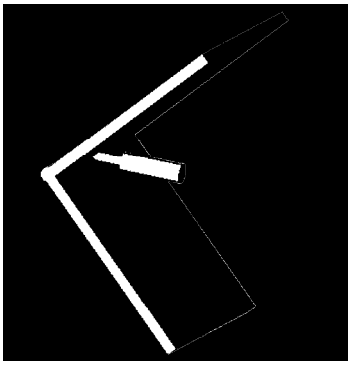

Figure 5.2: Piston-Cylinder design for actuation.

Pneumatics and Hydraulics

These two separate actuation ideas rely on the same principle for actuation, extracting work from a fluid. In pneumatics the fluid is pressurized air, while in hydraulics it is a specialized liquid. Both concepts use a piston that is extended or contracted by the flow of either the air or liquid. A valve is used to release the fluid's pressure, creating a vacuum behind the piston and drawing it back to fill the void. Or, alternately, a spring may be attached to the piston to create the retraction motion. In the latter situation, the fluid is pumped into the cylinder, overcoming the spring force, and moveing the piston. A hydraulic cylinder uses added pressure at one end to move the piston at the other end. This applied force can be multiplied if the pistons are of different sizes. Pascal's Law, as shown in equation 5.5, defines the force differences,

$$F_2 = \frac{A_2}{A_1} F_1 \tag{5.5}$$

where: F_2 = force on the acting piston

F_1 = force on the applied piston

A_2 = area of acting piston

A_1 = area of applied piston

From this equation, it was seen that a force increase directly corresponds to area increase. Thus, in order to obtain a force of any considerable size, the area must also increase a considerable amount, or higher pressures must be used (Munson et al, p. 48). Another drawback of these two systems is that a fluid must be carried over a distance. With inside actuator placement, the fluid must be transported a sizeable distance to the actuator. This means that added support structure (tubes for the fluids) must be used. Also, added complexity is introduced because aside from the pistons, valves must be installed to release pressure in the system to allow the piston to move. Valves also require control mechanisms (usually electrical) that increase the number of necessary components. Additional problems arise with the size limitations of inside placement. The necessary piston-cylinders to provide the forces needed would be in the range of half the wedge size (Festo-USA). Another problem exists with the pneumatic version of a piston-cylinder device, because the system lowers the pressure in the cylinder by exhausting pressurized

air, possibly to the flow field. This can be a problem when the goal is to produce a distortion that is measured by the total pressure drop.

An advantage of this concept is that the fluid support structure can be flexible, allowing it to comply with the shape of the distortion device. Also, in the case of pneumatics, the wedge's support structure could be used to carry the pressurized air without another source of encasement.

Solenoids

Another actuation device utilizing the piston-cylinder design is the solenoid. A solenoid is an electromagnetic device, where the theories behind electromagnetism are discussed in the next section. But this theory can be implemented to create a device that acts in a linear motion in the same manner as the other piston-cylinder devices. This is done by coiling electrical wires in a cylindrical fashion. When an electrical current is passed through the wire, a magnetic field is generated inside the coils. If an iron core is introduced, the magnetic field is intensified. The theory behind a solenoid is based on the fact that a magnetic field has a tendency to maximize itself. Therefore, if a moveable iron core is nearby, the magnetic field will draw it in to fill up the air spaces, maximizing the magnetic field and moving the iron core in a linear direction.

Advantages of solenoids are their large travel distance to size ratio. Some solenoids have travels twice their overall size. This is an excellent attribute, except that the overall sizes are not large enough to provide enough travel for the upper bound of the necessary wedge-size range.

Disadvantages of solenoids include a limited stroke and low forces. The overall stroke of solenoids is usually smaller than other actuation devices (around 1 inch maximum) (Newark Electronics). This will not allow for the full actuation of wedges at the upper end of the size range. The second problem is that most solenoids cannot produce enough actuation force to overcome the pressure forces acting on the wedge. Although a solenoid has disadvantages in its design, the overall theory of electromagnetism may be a good method of actuation in a different implementation.

5.4 Electromagnetic

Using electromagnetism for actuation involves exploiting the magnetic field created when electricity is passed through a wire. The magnetic field can be useful for actuation purposes because of its properties of attraction to oppositely charged magnetic fields and repulsion to equivalently charged magnetic fields. Electromagnets are made by wrapping many coils of wire around a solid core. Electricity is then passed through the wire, where the motion of the electrons creates a magnetic field. By adding current to the wire or tighter coiling of the wire, the magnetic filed can be increased to a point where it is powerful enough to achieve practical mechanical applications. If electromagnets are attached to the two sides of the wedge, the repulsion and attraction of their magnetic fields could move the wedge. Alternatively, a permanent magnet could be placed on the wedge, providing a constant source of repulsion/attraction for electromagnets on the sides of the wedge.

An inherent problem with electromagnetism as a driving force is its dependence on the distance between the magnetic field and repulsion/attraction surface. The force between an electromagnet and a larger magnetic field (such as a permanent magnet) is given in equation 5.6 as,

$$f = -\frac{\mu_0 p_{m1}(M_2 A_2)}{2\pi d^3} \tag{5.6}$$

where, f is the force, d is the distance between the coil and magnetic field, A_2 is the area of the magnetic field and the other variables are material and magnetic properties. This equation shows that the force decreases by the cube of the distance. If two electromagnets are used in direct repulsion/attraction, the force decreases by the distance to the fourth power (Slemon, 1966). These two equations lead to the conclusion that as the distance increases between any source of repulsion/attraction and the electromagnet, the force would become drastically smaller.

One idea of overcoming the force problems associated with increased distances is to introduce a magnetic track for the electromagnets to follow, an example of which is shown in Figure 5.3. This would provide a small distance that the force would have to be generated over. The track is arced so that if an electromagnet were attached to the wedge, the magnetic track would have the proper orientation of the magnetic fields at all

angles. The problem with a track solution is that if a constant magnetic field was present in the track, no motion would occur. Therefore, a movable area of magnetism would have to be introduced to induce motion of the electromagnet (and the wedge it was connected to) in the desired direction.

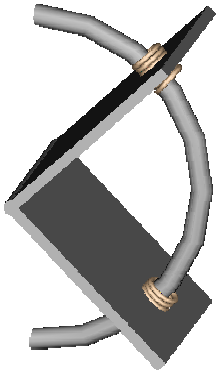

Figure 5-3: Electromagnetic design for actuation.

5.5 Piezo-Ceramic

Piezo-Ceramic materials change dimensions when an electric field is applied to the material. They have many advantages that make them a desirable solution. The most important advantage is that they provide large forces that would aid in overcoming possible forces on the wedge for any flow situation. Other advantages of piezos include a very fast response time, ease of control by using electrical signals, and a very flexible array of possible geometries. Piezos also have disadvantages that would make them a poor choice to meet the actuator requirements. The largest disadvantage is restricted travel. In a product search, one of the longest travels found was approximately 0.8 inches (Physik Instrumente). This actuator had an overall, unexcited length of 7.1 inches, making the actuator too long for smaller sized wedges and its travel too small for the upper bounds of the wedge sizes. Because the motion of a piezo is associated with its change in physical geometry, the only practical placement option is inside the test section. However, this still provides multiple options for the implementation of piezos for actuation purposes.

Piezo Stack

A stack of piezoelectric material could be used to make a push/pull mechanism much like the one shown in Figure 5.2 for the piston-cylinder designs. The problem with this design is that a reasonable sized actuator would not have the travel necessary. An actuator consisting of discs of piezo-ceramic material has a length change given by:

$$\Delta L \approx d_{33} * n * V \qquad (5.7)$$

where: ΔL = change in length
d_{33} = dielectric constant
n = the number of discs
V = the voltage supplied

The dielectric constant used in equation 5.3 is on the order of 10^{-11} inches per volt. Assuming a voltage in the kilovolt range, the number of ceramic discs required to achieve a necessary travel is in the hundreds of thousands. This would result in a piezo-stack outside of normal production and of too great a length to be practical (Physik Instrumente).

Piezo Strip

Another method developed for piezo-ceramic actuation was placing a thin strip of piezoelectric material on the outside of the wedge, as seen in Figure 5-4. When this material contracts, it would open the wedge, and when expanded, the wedge would close. This solution requires thin materials but contains no internal mechanisms, making it a clean solution. Again, the problem with this proposed solution is the lack of travel. The length change of a strip of piezoelectric material is given by:

$$\Delta L \approx d_{31} * E * L_o \qquad (5.8)$$

where: ΔL = change in length
d_{31} = dielectric constant
E = electric field strength
L_o = original length

Again, the dielectric constant is on the order off 10^{-11} inches per volt and the electric field strength has a maximum value of 50,000 volts per inch. The travel needed is much smaller, 0.4 inches (half the circumference of the hinge pin), because of the direct connection of the material to the wedge. This gives a necessary original length of the

piezo strip of approximately 660 inches, which is impossible to implement for wedges within the range of sizes to be used.

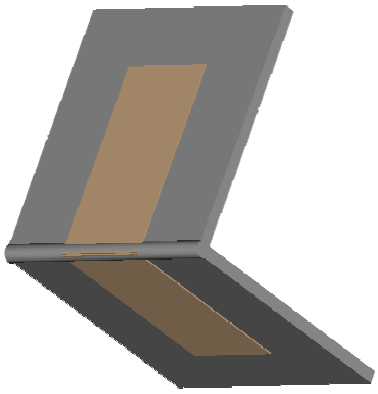

Figure 5-4: Piezo-strip design for actuation.

5.6 Electric Motor

A motor uses electric energy to move an extension either linearly or in rotation. Their actuation advantages include an overall small size and the possibilities of large travel. In addition, a motor can be placed inside the test cell or outside, depending on the overall distortion generator design. The key problem in using motors for an actuator is that a small motor produces a small force. Therefore, larger motors would have to be implemented in order to produce the higher forces that may be necessary. Electric motors are classified by their control schemes, with their construction and application designed around how the motor is controlled under the planned operating conditions.

Servo Motors

Servo motors are AC/DC motors that use electrical inputs from the user to create motion. The most important disadvantage of this motor type is the complex control system. As the load on the wedge increases, the travel of the motor's extension arm is lessened, creating situations where the control cannot be achieved by simple linear, timing methods. A feedback mechanism is needed to output the position of the object

being moved to the controller at all times. Therefore, complicated control mechanisms need to be implemented in order to actuate the wedge from any given angle to any other, final angle. Complicated control of a servo motor necessitates multiple powered systems (motor and controller), adding unwanted complexity to the design.

Stepper Motors

A stepper motor can be substituted for a servo motor, and create a system without the control problems associated with servo motors. A stepper motor moves one mechanically pre-selected increment (step) for every pulse of electricity passed to the motor. It will move the step no matter the force placed on it, provided the force does not exceed the maximum output force. Stepper motors provide a simple, open loop solution to using motors to actuate the wedge. Problems with steppers are similar to the problems associated with servo motors, the most important being the small torque output for small motors. But this problem may be overcome by placing the motor on the outside of the test cell, as described as a design option earlier.

A motor may solve a number of actuation problems, but it must be compared to the other designs in order for the best method for the overall distortion generator design to be selected. Selection criteria must be developed based on what actuation features are most desired. Some have already been laid out, such as force and travel distance. But other, more selective, criteria must be decided upon in order to select the best actuation design.

6 Design Selection

The main factor in choosing a wedge design was the minimization of the necessary actuation force. There were two primary factors in achieving lower forces, orientation of support forces and direction of actuation. Combining the best methods from both of these areas provided the optimum design. While these factors are not independent of each other, there were enough individual advantages within each design aspect to allow them to be looked at separately and combined into the final design.

6.1 Wedge Selection

The first aspect studied was the orientation of the support forces. As was shown in the "Wedge Design" section, three methods of support were looked at: front, rear and center. As was mentioned in the earlier section, in order to compare these three designs an arbitrary actuation force was added to the free-body diagram (FBD). This force was the double vertical orientation, mentioned in the "Actuation Design" section. The actuation direction was chosen for its symmetry, allowing half-wedge FBDs to be created, which can be seen in Appendix C. The actuation forces from these FBDs were calculated and are shown again, below.

Front Support: $$F_{act} = \frac{(F_L * x) - (F_D * y)}{x} \quad (4.1)$$

Rear-Support: $$F_{act} = \frac{[(F_L * x) - (F_{SY} * x)] + [(F_D * y) - (F_{SX} * y)]}{x} \quad (4.2)$$

Center Support: $$F_{act} = F_L \quad (4.3)$$

The center support design had the least required actuation force, for all angles. Using the force comparisons to select the center-supported design, the best configuration then had to be determined by looking at the actuation direction.

The four different actuation directions were compared to find the solution that, again, provided the minimum actuation force, with the FBDs located in Appendix D.

The actuation forces were found by summing forces in the direction of the actuation force, and evaluating the actuation force necessary for equilibrium. These equations are:

Rotational: $$T_{dir} = 2\left[(F_L * x) + (F_D * y)\right] \quad (5.1)$$

Horizontal: $$F_{dir} = 2F_D \quad (5.2)$$

Double-Vertical: $$F_{dir} = 2\ F_L \quad (5.3)$$

Vertical-Supported: $$F_{dir} = F_{supy} \quad (5.4)$$

where, the variables are defined in the "Actuation Design" section. The rotational direction remained a torque because, the aspect being compared was the dependence on the flow and not the computational values that would require a conversion to force. As can be seen from these equations, the vertical-supported direction is independent of the flow forces and was, therefore, selected. Actuation forces that are independent of the flow are important in the design because it allows the same force to be used at all flow speeds and all wedge sizes. The support force seen in equation 5.4 is directly related to the actuation force, meaning that this value is a function of the magnitude of force applied to the wedge for actuation. This is a complicated problem, but it is not important for design selection. The important conclusion from this comparison is that the vertically-supported structure has an actuation force independent of the flow.

Also, when comparing the two center supported designs to each other, the vertically configured method is simpler. The support structure running in the same direction as the actuation travel allows easier transmission of motion to the outside, if that becomes necessary. The standard configuration would require a 90-degree change of direction, assuming the actuation motion enters parallel to the support structure. Another advantage of the vertical configuration is that any linear actuation can be contained inside the support structure, reducing the FOD hazard. This design configuration will also not require a support to maintain its orientation to the flow, as others would.

Implementing these selection criteria allowed us to choose the wedge design: a center supported, vertical orientation wedge with vertically supported actuation direction. This overall selection will provide the lowest overall needed actuation force. The necessary overall force is only the support force, F_{supy} . The FBD for the combined support forces and actuation direction is shown in Figure 6-1. The weights are included here in order to calculate the overall actuation force necessary ($F_{overall}$). This also was

chosen as the best concept because of the many other advantages found with the individual evaluations of wedge design and actuation direction.

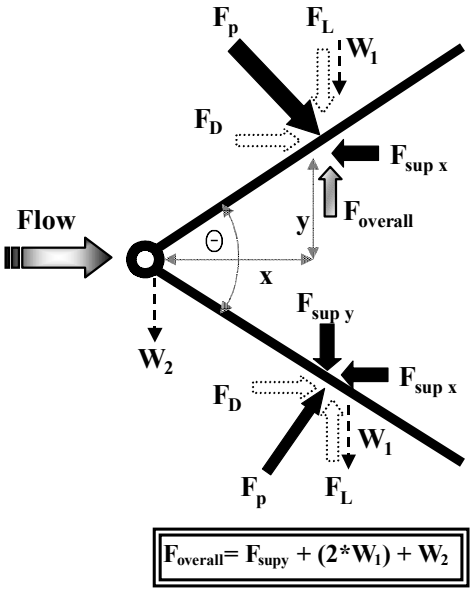

Figure 6-1: Overall free body diagram for selected design.

6.2 Actuator Selection

As was the case with the wedge selection, actuation selection was done by looking at multiple characteristics independently. After determining the best design for each aspect of actuation, they were combined to form the final actuation design. The aspects looked at were actuation direction, type of actuation and actuation placement. Some of these features also had additional characteristics that had to be decided upon.

The direction of actuation was already chosen during wedge selection. Therefore, the selection process will not be repeated, only the result. The vertically supported direction was decided upon for its low necessary actuation forces.

Next, the type of actuation was studied, with the initial concepts for moving the wedge presented in the "Actuation Design" section. Before comparing the designs, selection criteria were developed. These criteria were applied to the designs in order of importance. The first design condition was the necessary size to force ratio. This determined if the actuator generated the force needed for actuation while maintaining a small size. The concepts that passed this standard were the motor, pneumatic cylinder

and hydraulic cylinder. The next criterion was a comparison the overall number and complexity of the system's components. This was important to provide the actuator with an ease of operation. The complexity of hydraulics proved it a poor choice for passing this standard. A hydraulic system has many components including a pump, accumulator, and specialized hoses. Finally, the selection process for the type of actuation investigated the simplicity of the overall system and the FOD hazard. These are included together because with a structurally simple design comes a low FOD hazard. Here, the motor passed on because of the method of force generation a pneumatic device uses. The air required to move a pneumatic piston must be pressurized. With this added pressure comes the hazard of rupturing the containment structure. Also, as was mentioned in the "Actuation Design" section, a pneumatic piston requires a valve close to the movement point. This could introduce a FOD hazard if an inside positioning scheme were used.

The final actuation design aspect investigated was the placement of the actuator. For the requirements set forth, an outside placement was chosen. This was done because of the low flow disruption, lack of size restrictions, lack of operating condition restrictions and low FOD hazard associated with placing the actuator outside of the test section. Additionally, the overall effectiveness of the distortion generator will improve with the ability of the wedge to completely close, which can only be accomplished by placing the actuator outside of the test cell. Also, ease of both operation and maintenance are increased with the lack of size and operating condition restrictions. Less hardware restrictions can also prove to be a more cost effective scheme by allowing more choices in the models of actuator to be used. Finally, with fewer moving parts inside the test section, the risk of a FOD incident is drastically reduced.

Based on the assessments of the three most important aspects of the actuator, the final design chosen was a motor actuating in the vertically supported configuration, placed outside of the test cell. With this decided, specifics of the design had to be decided upon, with the first to be the type of motor that would be used. A stepper motor was chosen because of the simplicity of its open loop control scheme and positive positioning aspect. This will make the design of a control system as well as the operation of the distortion generator less complicated for those in the future. Also, it was decided to use a combination of a lead screw and rods to transfer the force to the wedge inside the

test section. A lead screw would be used to convert the rotational motion of the motor to a linear motion. The rod would be used to then transfer this linear motion from outside the test section to the wedge. This configuration would eliminate the potential problems associated with adding a rotational movement to the linearly moving components necessary inside the test section. A lead screw was chosen over a rack and pinion set-up because of the lead screw's ability to be used in any orientation. A rack and pinion can only be used in horizontal configurations without any added support.

6.3 Overall Design

Based on the above two selections, the overall design chosen was a vertical wedge, supported in the center and actuated by a motor driving a lead screw. A diagram of this configuration is shown in Figure 6-2. This design will provide the optimum minimization of the necessary actuation force and a method of actuation that will work under all of the design requirements. The next step was to work out the design specifics of the distortion generator. This was done by constructing a concept model for design, as opposed to operational, purposes.

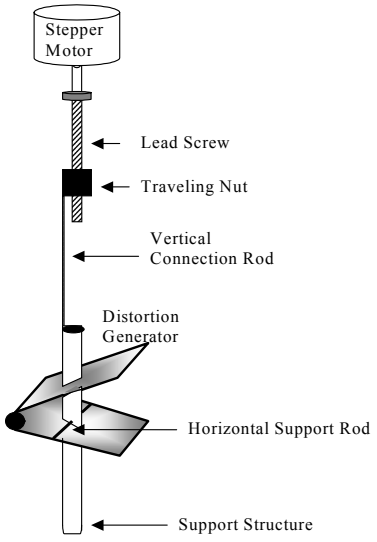

Figure 6-2: Diagram of overall distortion generator design

6.4 Concept Model Fabrication

A model, seen in Figure 6-3, was built of the selected distortion generator in order to identify methods of construction and problems that may occur. This model was a movable representation of a three-part array using the selected design. The first information gathered in the construction of the model was that the linking of the vertical connection rod and the horizontal support rod required a 90^{o} connection. This was solved by using a small eyebolt on the end of the vertical connection rod to move the horizontal support rod. Also, the slot that was cut into the wedge to accommodate the support structure needed to be larger than originally thought. In order to allow for a fully open position, the slot had to extend the full length of the wedge. This was solved by deciding that two individual wedges would be connected together by the horizontal support rod. This would allow the length of the slot to extend to the ends of the wedge, and the width of the slot to be determined during construction so it would allow enough room for the support structure to not interfere with movement. Another problem discovered during construction of the model was one that cannot be fixed, but was inherent to the design. Because one side of the wedge was fixed and the other could move in the vertical direction, the center of the wedge moved vertically as the angle of the wedge changed. The area of lower pressure will also shift as the distortion is created, causing patterns of distortion that vary from the predicted. It is believed that this can be overcome by compensating for the shift in a computerized control scheme. Constructing the model also helped in the discovery of a design improvement. The support structure, originally intended to be circular, was chosen as an airfoil shape. This improvement allowed less flow disruption and more internal area for the vertical connection rods. This model was very helpful as a first step in constructing the distortion generator. It allowed the layout to be determined using materials that were inexpensive and easy to shape. Creating a model was very beneficial as a precursor to the actual construction of prototype.

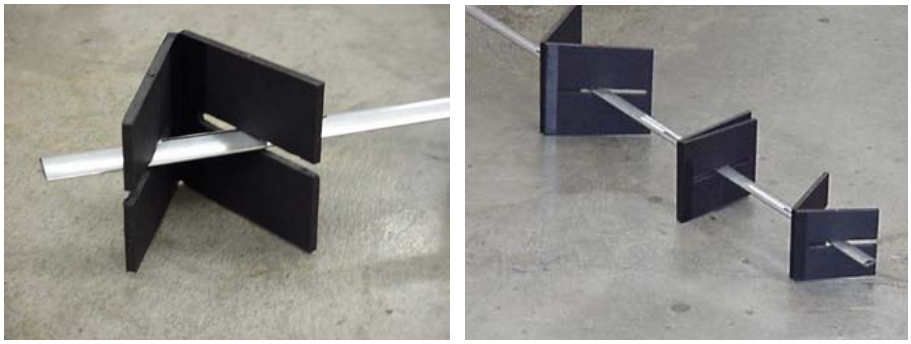

Figure 6-3: Model of the selected distortion generator design

7 Design Verification

After the design was selected, a method had to be developed to verify the assertions made. The main focus of the testing was to show that the actuation forces were low enough for practical purposes and were independent of the flow. In order for this to be accomplished, a testing set-up had to be created that would allow the linear actuation force outside of the test section to be measured.

7.1 Wind Tunnel and Test Cell

In order to measure the actuation forces necessary, the first task was to find an acceptable wind tunnel for the testing. A tunnel built by a Virginia Tech student, Tkacik, for his work on stalled flows was found to be a suitable choice, and is shown in Figure 7-1 (Tkacik, 1982). The main reason this tunnel was selected was because of its prior use in both Jumel's and Eddy's studies. In order to maintain a commonality with these earlier studies, the same wind tunnel was selected for the testing. This wind tunnel uses a model BIA, size 630 class II centrifugal blower built by Aerovent Corporation. The fan is driven by a 15 horsepower electric motor and has an adjustable inlet area for altering the flow speed. This is accomplished by variable inlet guide vanes on the fan's inlet. Original design speeds of 49.2 ft/s to 157.5 ft/s were reported, but for the testing of this experiment, one speed was used, 114.4 ft/s. A honeycomb and 3 screens are located inside the settling section in order to reduce free stream turbulence before entering the nozzle. The flow speed is increased by a nozzle constriction from 9 ft^2 to 1 ft^2, which is the exit area of the tunnel.

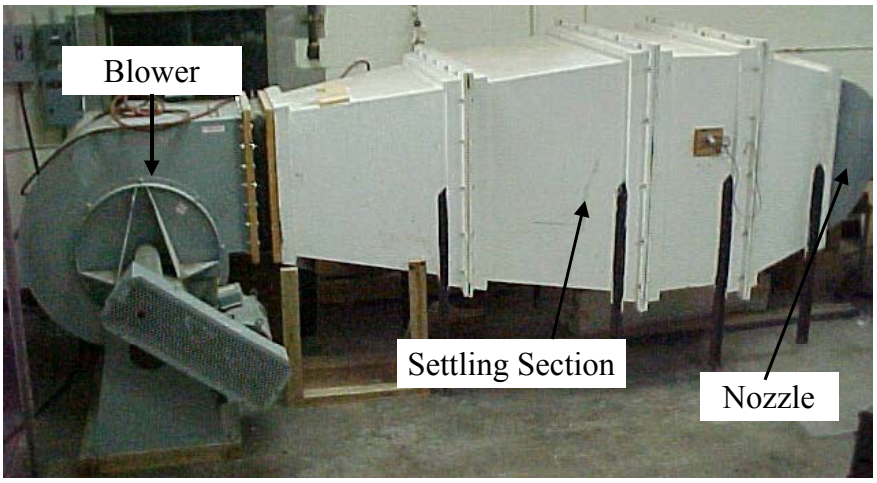

Figure 7-1: Wind tunnel at Virginia Tech with major components listed.

A test section was constructed that would match this tunnel exit area. Eddy constructed a 1 ft^2, ½-inch thick Lexan™ test section. This test section was 3 $^1/_3$ feet long, and had a mounting flange on one side in order to mate with the tunnel. This test section, with some modifications, was determined suitable for the proposed test forces. These modifications included cutting airfoil-shaped holes ½-inch long and ¼-inch wide, aligned on both the top and bottom of the test section. These holes were made so the support structure could protrude from the test section, allowing it to be fixed in place. Adjacent to the airfoil shaped holes, slots were cut to allow for protruding supports from the support strut that would hold the entire distortion generator in place during testing. Also, a 4 in^2 access hatch was cut into the top of the test section so that the distortion generator could be constructed outside of the test section, and placed inside after it's completion. Finally, a $^2/_5$-inch hole was drilled 4 inches in front of where the distortion generator was placed. This hole allowed access to the free-stream flow for the pitot-static probe in order to make velocity measurements. These modifications allowed the distortion generator to be incorporated into the test cell for the force testing.

7.2 Distortion Generator

Although the design and layout of the distortion generator were defined in the "Design Selection" section, some construction requirements were still needed. The most important of these was the size of the wedge to be used. The "Design Requirements" section lists the size range as 1 in^2 to 25 in^2. In order to closely model the tests of Jumel and Eddy and generate forces significant enough to be measured, a wedge size of 2 inches by 2 inches was chosen. This was constructed from two, 2 inches tall by 1 inch wide hinges. These were modified versions of the same model used by Eddy, McMaster-Carr model 1624A51, as shown in Figure 7-2. Although the design called for a single wedge with a slot cut down the middle for the support structure, two of the 2 by 1 inch wedges were used and connected by horizontal support bars. A picture of this completed generator element is shown in Figure 7-3.

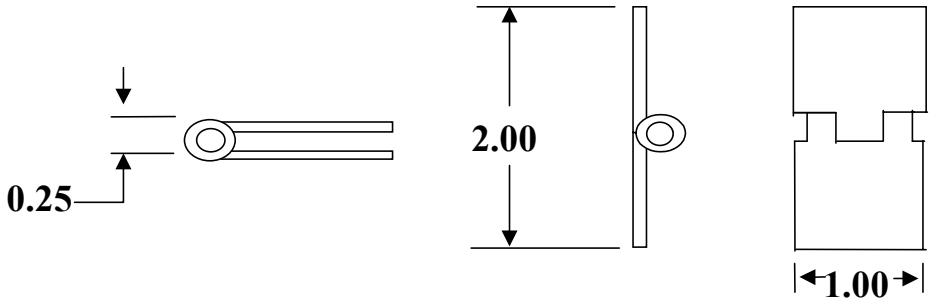

Figure 7-2: Diagram of hinge used in distortion generator model (Adapted from Eddy, 2001).

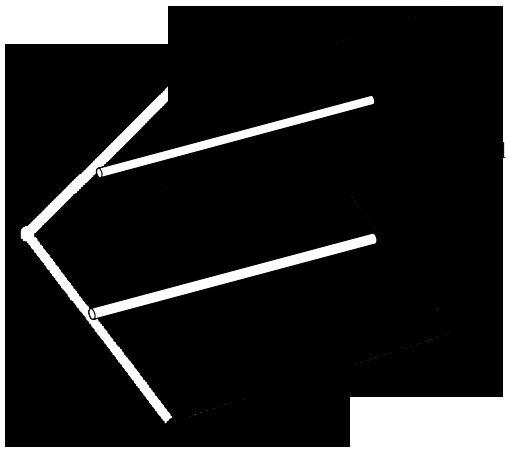

Figure 7-3: Example of two individual wedges, connected together.

These size of these support bars, as well as the other supports, had to be selected. The supports examined were the horizontal support rods, the vertical connection rod and

the overall support structure. The horizontal rods had to be able to withstand the bending forces placed on them, which was the drag force generated by the wedge. The maximum drag force that would be encountered would be 1 lbf, for a 4 in^2 wedge in a Mach 0.1 flow. The horizontal support rod was modeled as a simply supported beam, where the maximum deflection was given in Beer and Johnston (1992) as,

$$\delta = \frac{FL^3}{48EI} \tag{7-1}$$

where: δ = deflection
F = force on beam
L = length of beam
E = modulus of elasticity
I = moment of inertia

A $^1/_{16}$-inch diameter, 2-inch-long piece of steel music wire was chosen for its size relationship to the overall generator. This would experience a maximum deflection, under the above-mentioned conditions, of 75 mils. This is more than acceptable for the tests to be conducted.

The next support studied was the overall support structure (airfoil). Again it was modeled as a simply supported beam, but this time the shape was approximated as a hollow, aluminum rectangle. The calculated deflection for this support was found to be small and definitely not of concern.

Finally, the vertical connection rod was not examined for bending. The only forces acting on this support are axial ones, since it is not exposed to the flow. The steel music wire used ($^3/_{32}$-inch diameter) was assumed to be strong enough for the axial forces being used.

The next step in constructing the distortion generator was to cut holes into the support structure for the horizontal support rods. The selected support was a 16 inches long by ¼-inch wide, ½-inch chord, $^1/_{100}$-inch thick aluminum airfoil. The upper pin had a slot manufactured instead of a hole so that when the vertical support rod was connected to the horizontal support rod, the horizontal one could move through the range of motion of the wedge. The drawing used for modifying the support structure is shown in Figure 7-4. The clearances between the cuts and the horizontal support rods were kept small ($^1/_{64}$-inch) in order to minimize the horizontal vibrational motion of the overall wedge in the airflow.

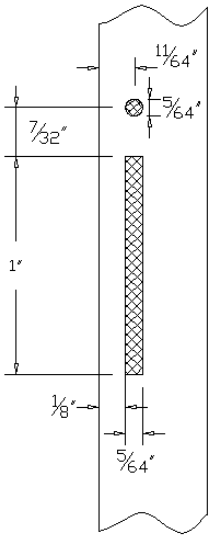

Figure 7-4: Side view of support structure with the sections cut out crosshatched.

The final step in construction of the distortion generator was the assembly. The vertical support rod is connected to the top horizontal support rod by using an eyelet connector. This piece of hardware has a connection end diameter of $^{3}/_{32}$-inch and an eye diameter of $^{1}/_{16}$-inch. The horizontal supports were connected to the wedges using a quick drying, metal epoxy. Graphite powder was spread on the slot and hole to reduce the friction generated during movement. The assembled generator can be seen in Figure 7-5, where it is important to note that it is assembled upside down from Figure 7-4. This was done so that if a failure occurred, the wedge would close to the 0^{o} position.

a) 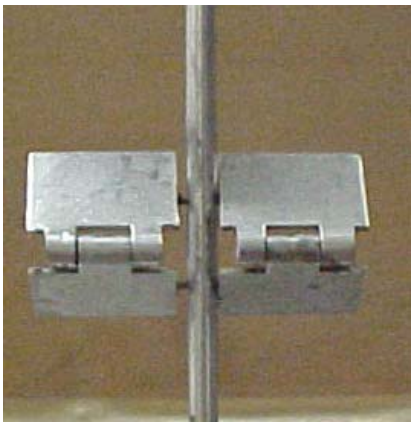 b) 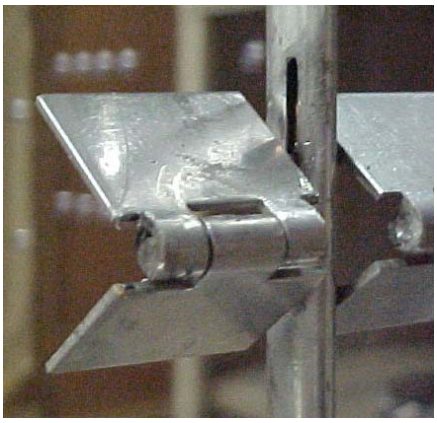

Figure 7-5: Distortion generator model a) Front view and b) Side view showing the slot.

7.3 Testing Apparatus

In order for the design of the newly created distortion generator to be acceptable, its must act in a method very close to the predicted manner. A device needed to be created so that it could be determined if the actual device was following the predicted behavior. The primary behavior that was studied in order to validate the distortion generator's performance was the actuation force. This was the main driving factor in the design and remained the main driving factor in testing as well. Therefore, a test mechanism had to be developed to measure the actuation force at pre-determined operating conditions.

It was decided that the simplest method of measuring the actuation forces for different conditions was by using a spring. A spring will move a specified distance for a given force, with this distance dependant on the spring constant, being 0.2 pounds per inch for this specific spring. Therefore, a test stand was constructed to provide a stationary attachment point for one end of the spring, while the other end was connected to the vertical support rod. In this design, as more force was applied to the wedge from the flow, the spring stretched to a larger distance. If this distance was measured, the force applied could be calculated. The test apparatus can be seen in Figure 7-6 with a ruler attached for measuring the change in spring length.

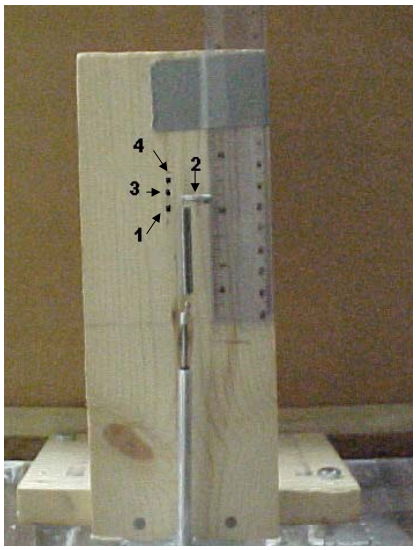

Figure 7-6: Test apparatus with the spring attached and the four test points labeled.

To see if the performance of the device followed predictions, the force was measured at four different starting angles for a flow speed of Mach 0.1. For this to be accomplished, the apparatus was developed to measure the force at four arbitrarily chosen angles. The angles were set by moving the stationary spring connection to one of the four points shown above in Figure 7-6. By moving the stationary point, the starting angle (i.e. no flow) of the wedge was changed. This allowed different amounts of drag and lift forces to be generated based on the angle. Therefore, since the actuation force is dependent on the flow forces, the test apparatus would measure more force as the initial angle was increased (by increasing the number slot the stationary end of the spring was placed).

7.4 Test Results

The tests were performed at the four, previously mentioned spring positions four separate times, for repeatability. These positions correspond to starting angles of 45^{o}, 75^{o}, 77^{o}, and 160^{o}. The four tests were conducted at approximately the same speed, M=0.1 with an Mach number error range of 0.027. Because this was a low-force design, the desired speed chosen was at the higher end of the wind tunnel's operating range. In theory, this higher speed would create larger actuation forces that would be more readily measurable by the test apparatus.

The data in Table 7-1 gives the final angles and forces measured in the testing. It is important to note that during the calculation of the forces, the weight of the wedge and the initial resistance of the spring had to be added to the force calculated from spring movement having values of 0.05 pounds and 0.09 pounds, respectively.

Table 7-1: Angles and forces for tested speeds

Mach Number	Angle (degrees)	Force (lbf)
0.107	30	0.0527
0.107	54	0.0527
0.107	62	0.0652
0.107	Inverted	N/A
0.103	32	0.0527
0.103	59	0.0527
0.103	64	0.0652
0.103	Inverted	N/A
0.100	34	0.0527
0.100	62	0.0527
0.100	65	0.0527
0.100	Inverted	N/A
0.080	36	0.0527
0.080	69	0.0527
0.080	78	0.0527
0.080	Inverted	N/A

As can be seen from these results, the necessary actuation forces are very small. The "Inverted" angles were starting angles in which the flow force aided in opening the wedge. The test apparatus had no stopping mechanism for this direction because it only had a spring attached on one side of the vertical connection rod. Therefore, the wedge continued to open until it turned itself inside out. This was expected to happen at any total angle in excess of 90^o. The test points where the test angle was inverted were discarded in data analysis. This is acceptable because, as described in the "Design Requirements" section, the range of travel is only necessary up to a total angle of 60^o. Further reduction of the data was needed in order to gain insightful knowledge into the system.

For comparison of the measured actuation force to the calculated flow forces, a non-dimensional approach was determined in order to negate the effects of the speed variations. Because the predicted flow forces were all calculated from published lift and

drag coefficients, the tested actuation force was non-dimensionalized in the same manner. The equation is given as

$$C_F = \frac{F}{\frac{1}{2}\rho V^2} \tag{7.2}$$

where, C_F is a generic term referring to any force coefficient, F is the force, ρ is the density and V is the velocity. This graph can be seen in Figure 7-7, with the dimensional graphs given in Appendix E. The non-dimensional graph shows that the measured actuation force is very small, compared to the flow forces. The actuation force is actually lower than all forces, even the viscous forces. This confirms the earlier assumption that the viscous forces can be neglected because of the symmetry of the wedge. It also validates the design in that the actuation forces are not caused by the flow, but by other factors such as weight.

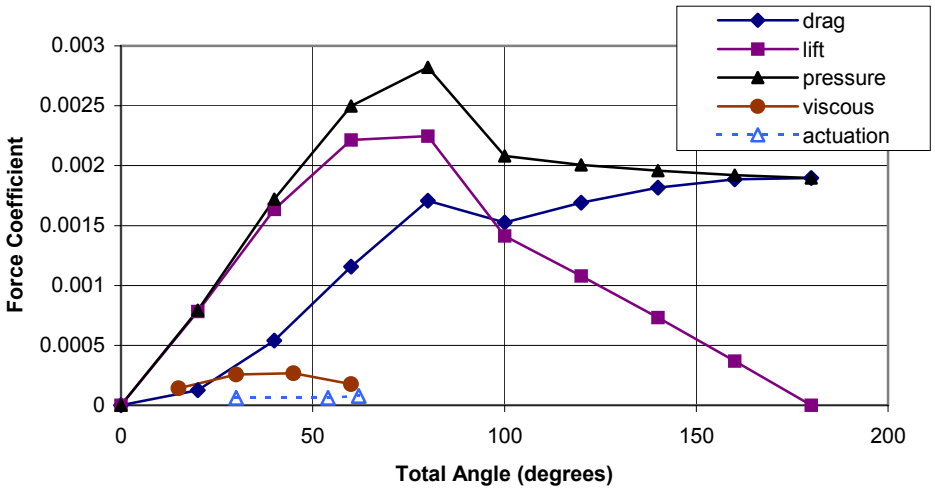

Figure 7-7: Non-dimensional graph of predicted flow forces and measured actuation forces.

7.5 Design Prototype

The next step in verifying that our design was a good choice for future development involved the construction of a prototype distortion generator. This would allow the stepper motor, as well as other components, to be sized. By using the results from the analytical designs and the testing, a prototype was constructed that demonstrated the device's operation.

The first components sized were the lead screw and motor. These had to be determined at the same time because the actuation force is generated by the combination of stepper motor and lead screw. A combination of motor and lead screw had to be found that could generate enough force to move the wedge. After looking at the test results, it was determined that a force of 0.053 pounds would move the wedge under most conditions (i.e. it would only need to overcome the weight and friction). Therefore, the stepper motor could be chosen arbitrarily and the lead screw was chosen to transfer the torque into the required linear actuation force. Throughout the selection process, size relationships to the 4 in^2 wedge were kept in mind so that construction would not be overly complicated and to minimize the weight. The stepper motor chosen was a Nippon Pulse Motor Co., Model PF55-48. This motor generates a maximum holding torque of 1.062 lbf-inch, rotates at a maximum speed of 387.5 RPM, and has a body diameter of 2.7 inches. Controlling the motor involved generating a simple pulse train using a LabVIEW™ program, a National Instruments DAQCard™-AI-16E-4, and an Alltronics™ model 5804-stepper motor driver chip. A lead screw having a diameter of $^3/_8$-inch and a 50 percent efficiency (which is common for a lead screw and plastic nut) generates, in conjunction with the above-mentioned motor, an actuation force of 0.1 pounds. Choosing this lead screw generated more force than was necessary, but was used in order to allow for error in the efficiency. It is common for efficiencies of a lead screw to be as low as 30 percent, which in this case would still generate sufficient force (0.06 pounds). This lead screw was a McMaster-Carr model 99030A303, having 2 revolutions per inch (which when combined with the motor equals 3.23 inches per second, or a minimum of 370.3 degrees per second). This rate was found by using the travel of the lead screw/motor combination and the Law of Cosines to determine the relationship of linear travel to the angle of the wedge. As a side consideration, this rate was checked against that in the "Design Requirements" and found to be well in excess of the 120 degrees per second goal.

The next component selected was the traveling nut that moves linearly along the lead screw. The internal diameter of this nut is set by the size and pitch of the lead screw. But, the material still had to be determined. By looking at various sources, it was determined that a plastic nut would have a higher efficiency than a bronze or steel nut.

Therefore, the nut used was McMaster-Carr model 1349K101. This nut was made of polyethylene terephthalate (PET), had an outer diameter of 1.35 inches and matched the chosen lead screw. As mentioned before, this should provide an efficiency around 50 percent. Selecting the nut completed the power transmission element of the prototype. Other components had to be constructed or altered as well, mostly for connection purposes.

A coupling to connect the lead screw to the stepper motor was needed. It was found that commercial rod connectors were too bulky and heavy for this application. Therefore, a $^{5}/_{32}$-inch hole was drilled in the center of the lead screw, and the shaft of the stepper motor was secured in place with epoxy. Three $^{3}/_{32}$-inch holes were drilled at 120^{o} intervals and $^{3}/_{10}$-inch from the center. Finally, another $^{1}/_{8}$-inch diameter setscrew hole was drilled into the side of the nut, into one of the $^{3}/_{32}$-inch holes, so that the vertical support rod could be locked into the hole. The other three holes had guide rods running through them. A frame was constructed to hold the actuation mechanism in the correct orientation to the distortion generator. A picture of the completed prototype is shown in Figure 7-8. This prototype was placed in a Mach 0.1 flow to prove that the concept would work under operating conditions.

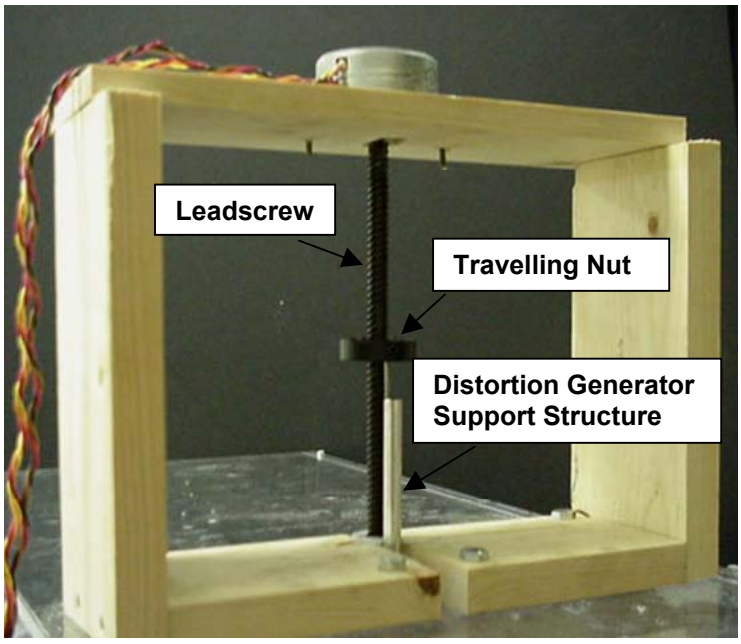

Figure 7-8: Picture of prototype connected to test cell.

8 Conclusions and Recommendations

8.1 Review

For more than forty years, gas turbine manufacturers have perceived a need to test inlet distortion and its effects. The earliest studies concentrated on performance evaluations, while newer studies also focus on structural integrity of the blades and high-cycle fatigue. Some of the more important distortion-creating events include non-uniformities in total temperature and swirl velocities. By far the most widely investigated distortion causing event is the introduction of a total pressure drop. Current research concentrates on steady-state tests to characterize an engine's response to inlet distortion. These tests methods often involve screens to produce the distortion. But current testing is evolving to areas where screens are not applicable. Their usage is becoming too inefficient and they are not testing all of the desired aspects, such as transient responses. A push to replace screens came with the introduction of the Airjet Distortion Generator by Overall (1977). This device used jets of air injected at an opposing direction to the flow. This allowed the distortion patterns to be changed quickly as well as some degree of transient studies to be performed. But, this device had drawbacks that limited its usage. The transient tests could only be performed for short periods of time, because of the short pulses that could be sent to the flow from the airjets. Also, this system introduced blockages to the flow, in the form of support structures, which created distortions in undesirable positions. The inadequacy of the Airjet Distortion Generator and the inefficiency of the screens led to studies on a new design for a total pressure distortion generator.

One idea for a new design that emerged was the concept of using a splitting airfoil to generate patterns of distortion. DiPietro (1996) performed the preliminary studies on this concept, finding it to be a promising idea. Jumel (1999) and Eddy (2001) further studied this idea in order to define its operation and feasibility. They performed studies that evaluated the pressure loss induced by the splitting airfoil design. Their studies determined the concept to have exceptional promise in both the areas of efficiency and transient testing. They also helped in the design of a system by characterizing the

pressure distortion that is created by a variable angle, splitting airfoil. The positive results of all of these studies led the way to the design of an actual splitting airfoil distortion generator.

8.2 Conclusions

In designing the distortion generator, the first aspects looked at were the system requirements. The requirements for the design were set using the conclusions of Eddy, results of previous transient studies, and recommendations from the Arnold Engineering Development Center. The final requirements for the system were a size range of 1 in^2 to 25 in^2, a travel range of 0^o to 60^o, and a rate of 120^o per second. Also, for simplification purposes, a hinged wedge was used to represent a split airfoil. It acted in the same manner an airfoil would, but the flow forces generated were greater. These requirements were kept in mind in designing the system to be used for the distortion generator.

The next step in the design involved selecting the wedge configuration, with respect to its support structure. Four designs were studied, with the result that some designs allowed the support structure to absorb some of the flow forces. This reduced the necessary actuation force for the generator. Also looked at were the actuation directions that were possible for each wedge configuration. This was done in order to define the forces that an actuation device would have to overcome. The design selected was the vertically oriented, center-supported wedge with a vertical-supported actuation direction. This design used the support structure to completely counteract the drag forces generated by the flow, and required actuation at only one point.

By selecting the wedge configuration, the moving parts and in what direction they moved were defined. How this actuation was to be performed was still to be determined. A study of possible motion devices was performed, with a stepper motor chosen because of the variations of force and size available, as well as its ease of control. The most important factor in choosing the stepper motor is the positive placement aspect. This means that no position feedback is necessary to move to specific angles. The method chosen for converting the rotary motion of a motor to a linear motion was a combination of a lead screw and a push/pull rod. This provided a system that has a good mechanical

efficiency (approximately 50%) while being able to operate in any orientation to the test cell. This is important for when an array is implemented, as mentioned later.

Therefore, the final design combined the vertically oriented, center-supported wedge, using a stepper motor in conjunction with a lead screw and a push/pull rod to provide motion. A diagram and picture are shown in Figure 8-1.

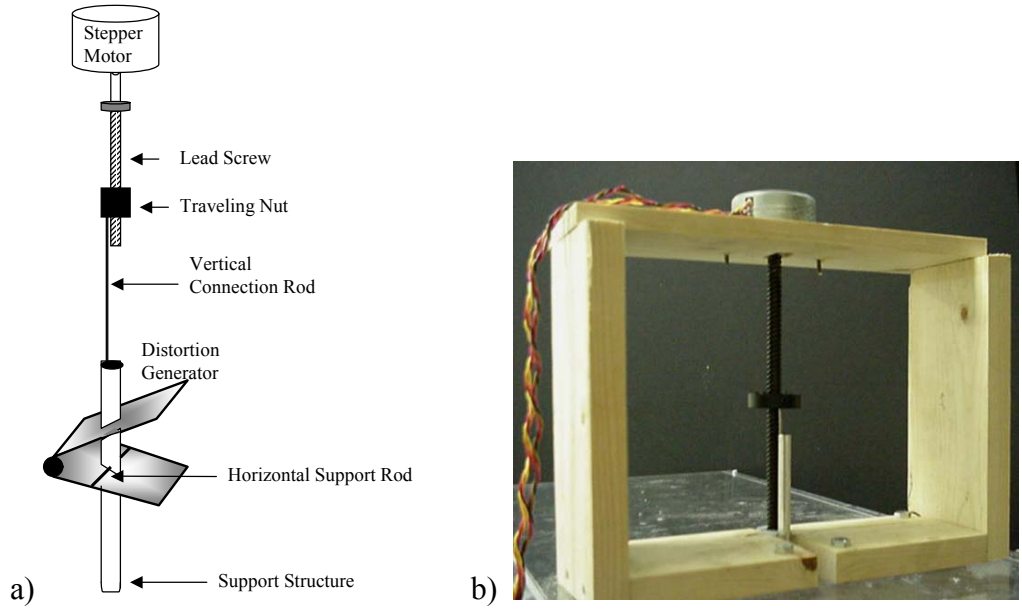

Figure 8-1: a) Diagram of final design and b) Picture of actual distortion generator.

Tests involving the constructed generator confirm our design choices. The actuation force needed was extremely low and was not generated from the flow forces. Also tested was the stepper motor's feasibility in this design. This motor moved the wedge to a fully open position in 0.637 seconds. While this is outside of the design requirements, it is close for the generic motor used. If a better-matched motor was chosen, the time requirements could be met. This time was larger than the predicted time because of unaccounted for system efficiencies. If the travel restriction of a maximum wedge angle equal to 60^{o}, then this distortion generator meets the time requirement.

Therefore, a stepper motor will work as the actuation device for this design, and it should be easy to scale, since large steppers will not be required for subsonic flow. This configuration of the splitting airfoil will be an effective method of replacing screens for distortion testing in aircraft engines. It will increase the efficiency in testing, by allowing multiple conditions to be tested with minimal labor. This design is also very flexible in its implementation because the necessary actuation force is independent of the flow and

allows the same actuation system to be used for various flow speeds. It will also allow a new area of testing to be explored, transient effects, which is becoming more and more important.

8.3 Recommendations

Although the final design was selected as the best choice, many areas of operation still need to be studied. The most important aspect still to be studied is how this design will operate in an array. The distortion patterns that can be created by an array need to be studied in order to make sure they are acceptable. An example, radial array is shown in Figure 8-2. For this configuration, the split airfoils could also be tapered to better fit the circular geometry of an engine intake.

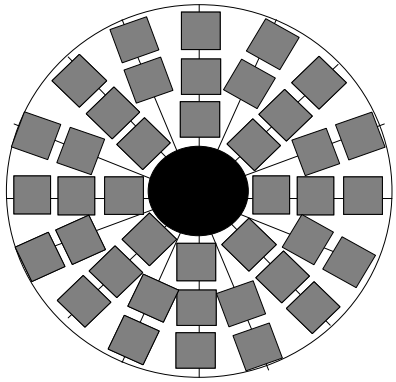

Figure 8-2: Example radial array of split airfoils making up the distortion generator.

The other primary area to be included in future studies is the control system. Most likely, a computer will be used for the controller. But the design's geometry leads to some minor control problems. The wedge angle can be controlled by a simple relationship to the linear distance traveled by the actuation device. But, the center of the wedge will also move linearly with the actuation device. This does not change the relationship of the distortion strength to the angle, but it does change the position of the center of the distortion pattern. This could potentially shift the reduced pressure area, and cause undesired patterns of distortion. Because this is an aspect of the design, the system's control should take into account the possible shifting of the distorted area. As the number of generator elements increases, and the size of each decreases, this problem is minimized. By compensating for this and having a number of airfoils suitable for the necessary precision, predictable distortion patterns can still be created.

Also recommended is using a computational method to define the flow over the wedge. This could provide important information regarding the viscous forces and 3-D effects. It could determine if the actuation forces seen are affected at all by the viscous forces, separations or three-dimensional effects.

Other possible causes of the forces that should be studied include friction and construction imperfections. If the horizontal support rods are not exactly centered on the plates of the wedge, then the moments generated on each side of the rod due to the flow will not cancel each other out. This is one reason as to why the wedge has a tendency to close at lower angles, and open at higher angles. If the larger moment is above the hinge point, the wedge will tend to close. At higher angles, the moment can move below the hinge point, attempting to open the wedge.

A kinematic approach could also be used to study the overall forces on the system. The wedge acts as a four-bar linkage, with the type being classified as a slider-crank mechanism. The mechanism is shown with the individual linkages numbered in Figure 8-3. It is important to note that the design should take into account (if necessary) the dead points located at the extreme extensions of a slider-crank. Kinematics studies of four-bar linkages use the Law of Cosines to accurately predict the position of the linkages, an idea that supports the earlier suggestion of using this law to correlate the wedge angle to the linear travel. Kinematics could also provide a method to optimize the size of the support structure (linkages 3 and 4) with respect to the wedge (linkages 1 and 2) and another method to determine axial forces in all of the members, and therefore the actuation force necessary on linkage 4. It is recommended that in addition to a fluid optimization, a kinematic optimization be performed on the mechanism.

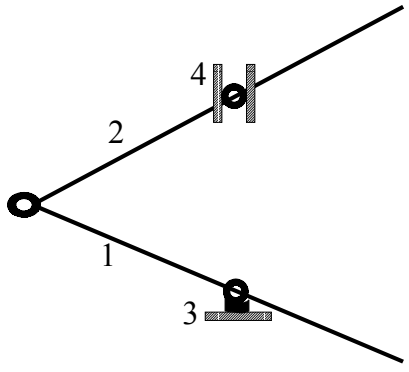

Figure 8-3: Representation of distortion generator as a four-bar linkage. Specifically, a slider-crank mechanism, with 1 being the crank and 4 being the slider.

The final recommendations for continuing the design of this distortion generator include a study into the transient responses created by an array of split airfoils. This could become important in characterizing the generator's usefulness for transient testing.

The new design for the total pressure distortion generator is a design that could easily be accepted for a replacement to screens. This new design retains many of the positive aspects of screens, including the adaptability of distortion patterns and the possible precision to which patterns can be created. But, the split airfoil concept is more efficient in that it requires less labor to conduct many different tests. It is also more versatile in that, unlike screens, it can produce both steady state and transient distortion effects. With more testing and development, the Split Airfoil Total Pressure Distortion Generator could become a very powerful tool for gas turbine engine test and evaluation.

Appendix A: Force Plots for Mach 0.6 Flow

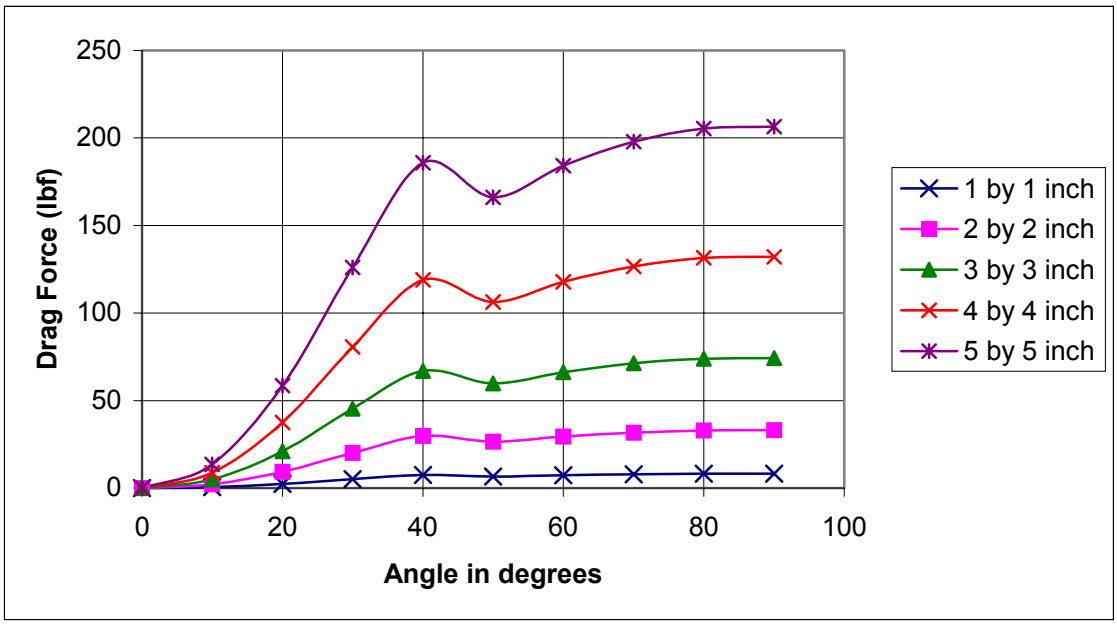

Figure A-1: Drag forces in Mach 0.6 flow for multiple sizes of square wedges.

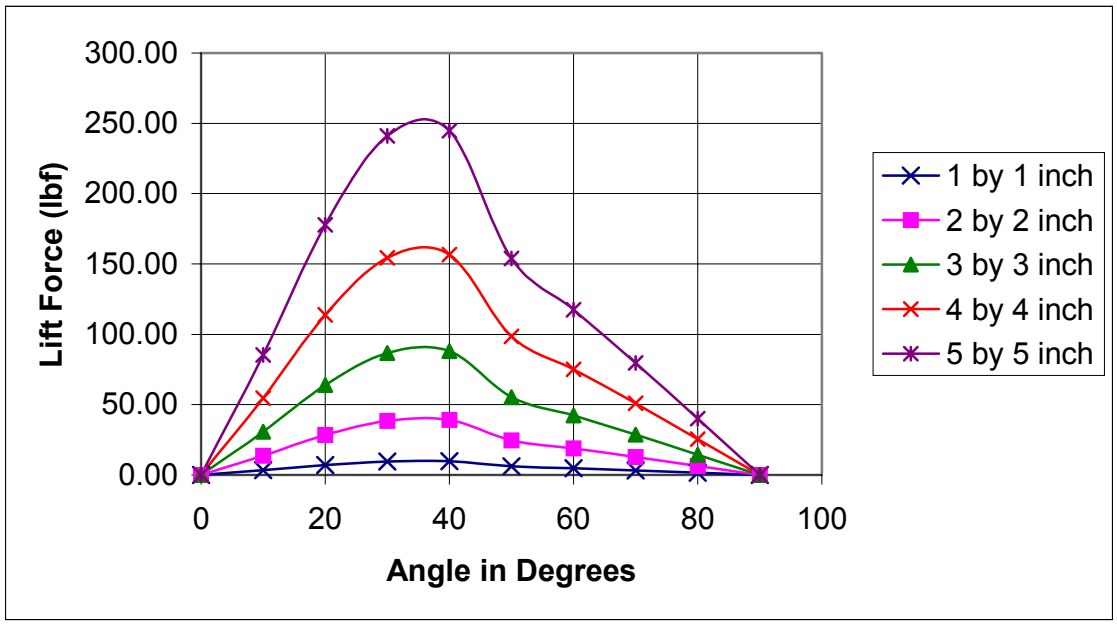

Figure A-2: Lift forces in Mach 0.6 flow for multiples sizes of square wedges.

Appendix B: Force Plots for Mach 0.1 Flow

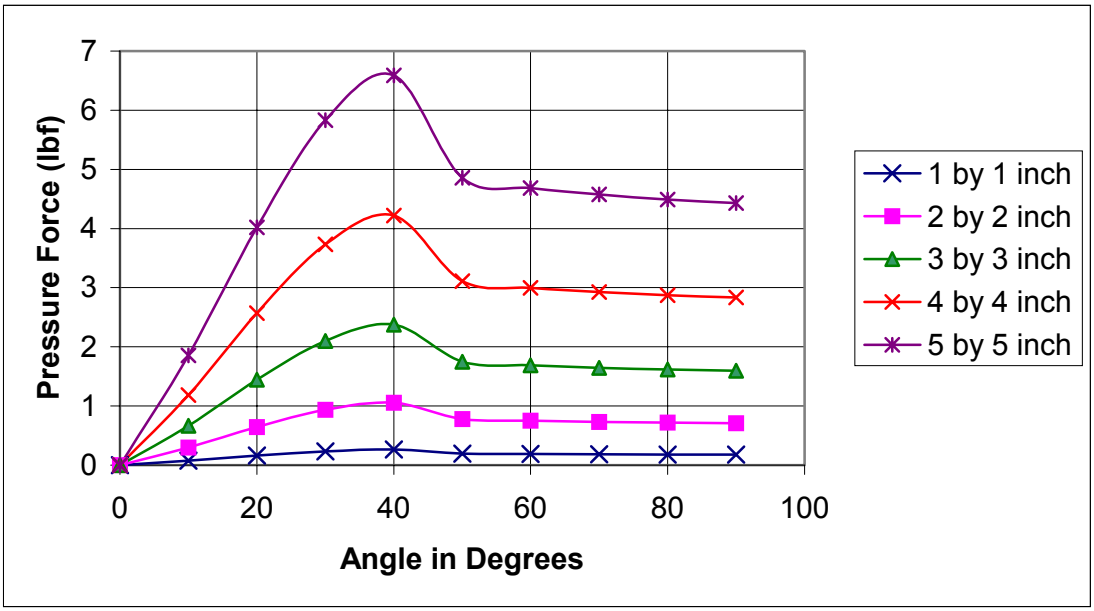

Figure B-1: Pressure forces in Mach 0.1 flow for multiples sizes of square wedges.

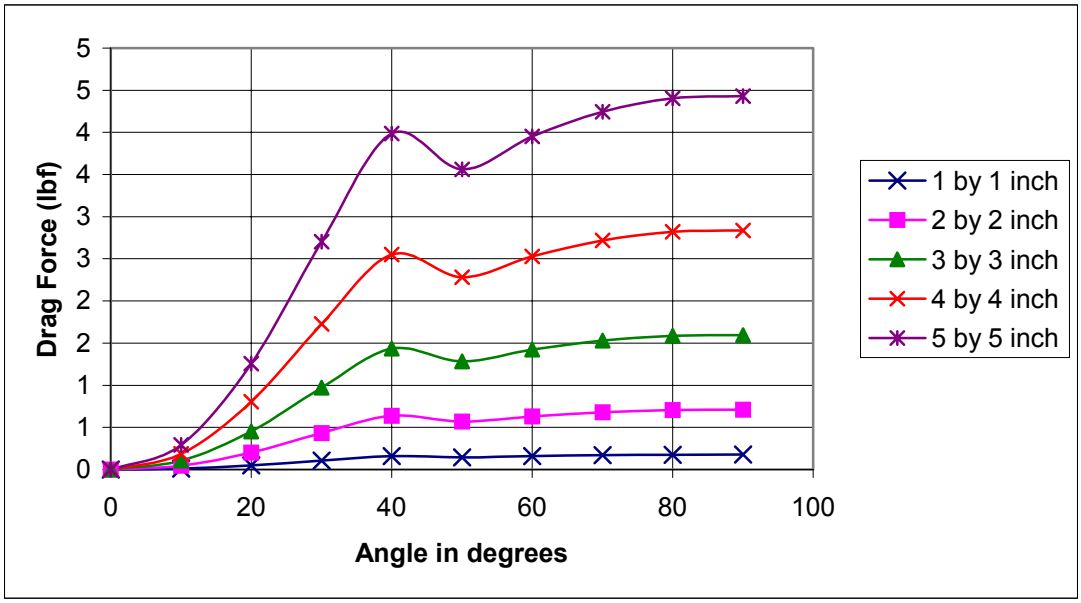

Figure B-2: Drag forces in Mach 0.1 flow for multiple sizes of square wedges.

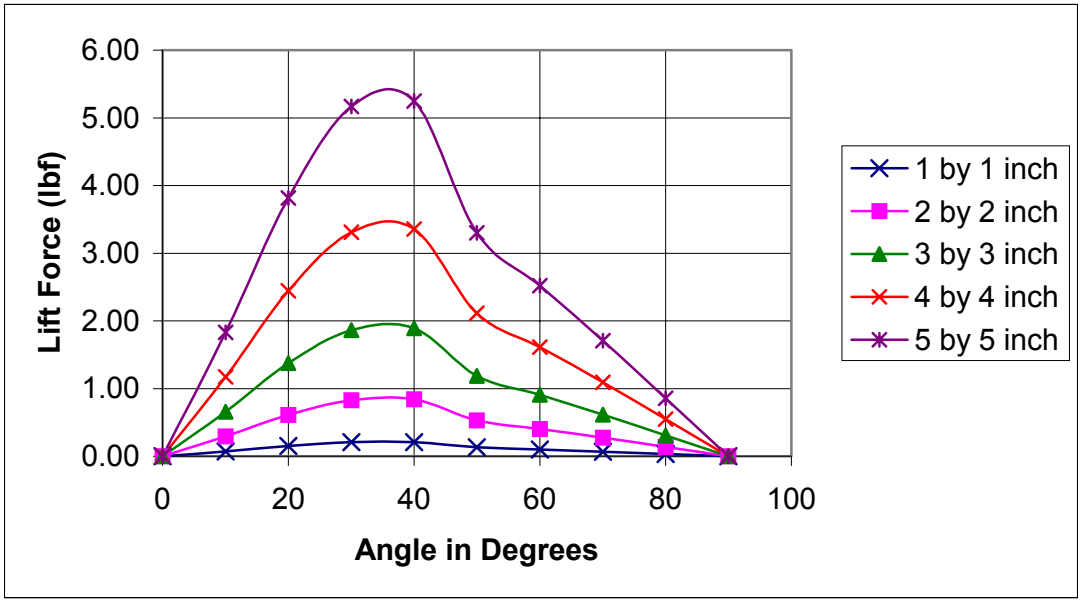

Figure B-3: Lift forces in Mach 0.1 flow for multiples sizes of square wedges.

Appendix C: Free-Body Diagrams for Wedge

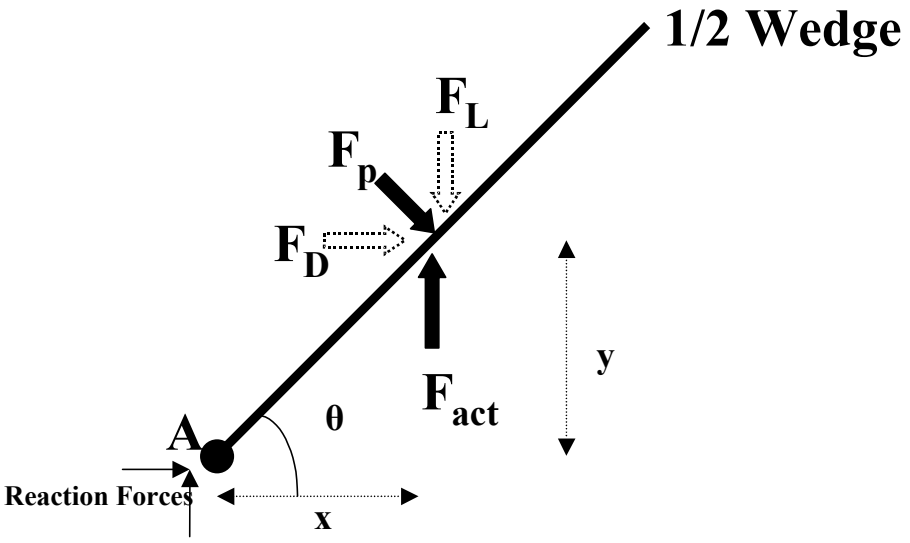

Figure C-1: Free-body diagram for front-supported wedge.

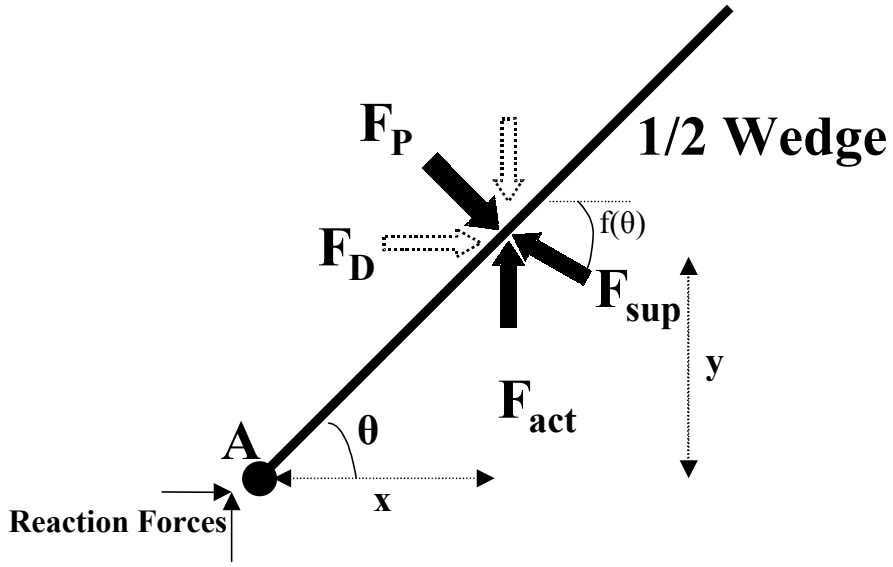

Figure C-2: Free-body diagram for rear-supported wedge.

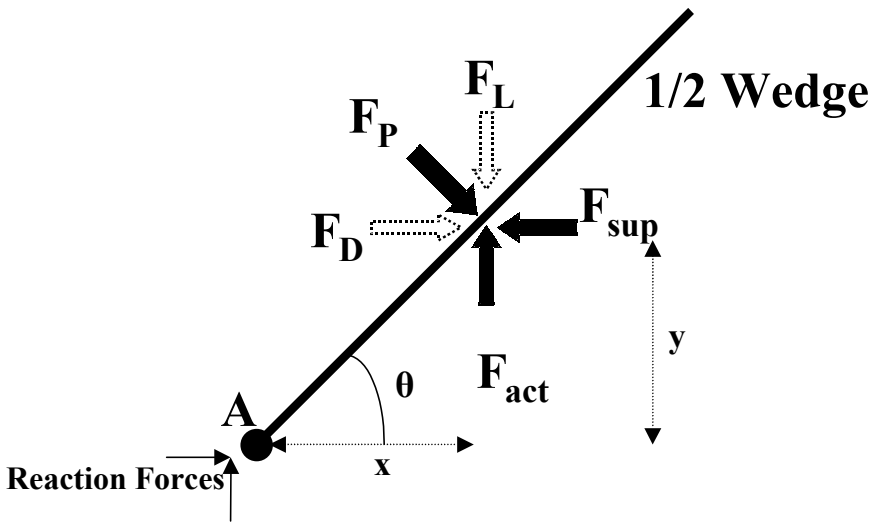

Figure C-3: Free-body diagram for center-supported wedge.

Appendix D: Free-Body Diagrams for Actuation

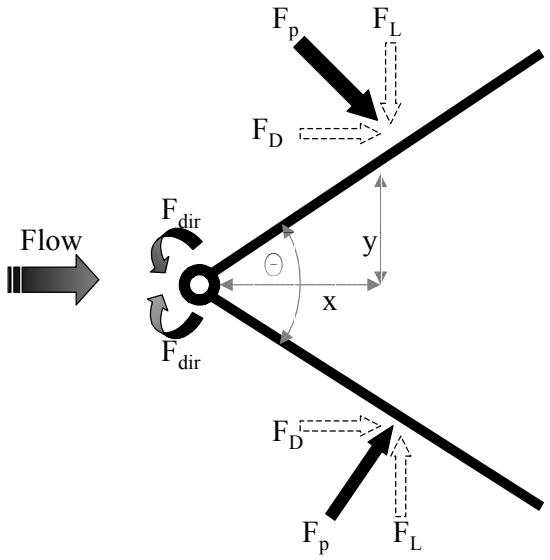

Figure D-1: Free-body diagram for rotationally actuated wedge.

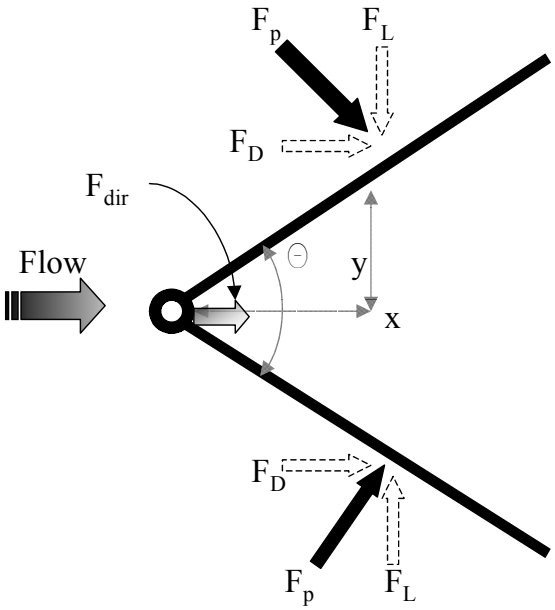

Figure D-2: Free-body diagram for horizontally actuated wedge.

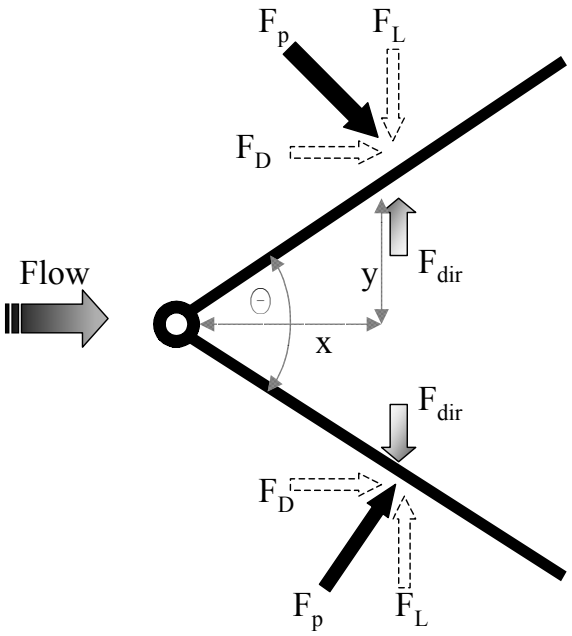

Figure D-3: Free-body diagram for vertically actuated wedge.

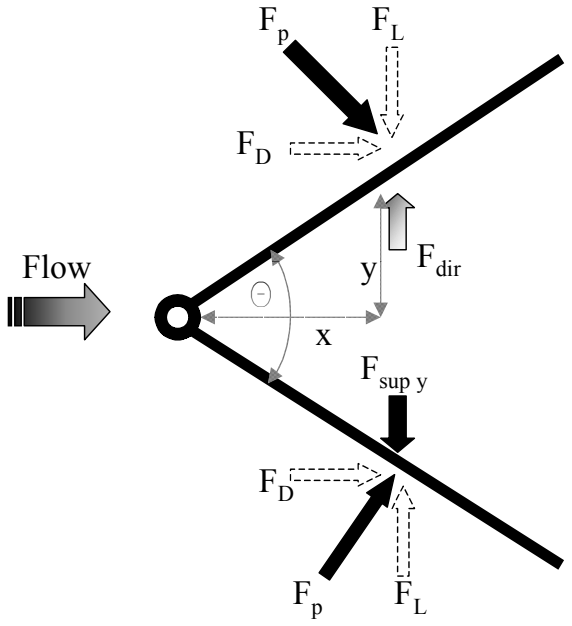

Figure D-4: Free-body diagram for vertically-supported, actuated hinge.

Appendix E: Measured Actuation Forces

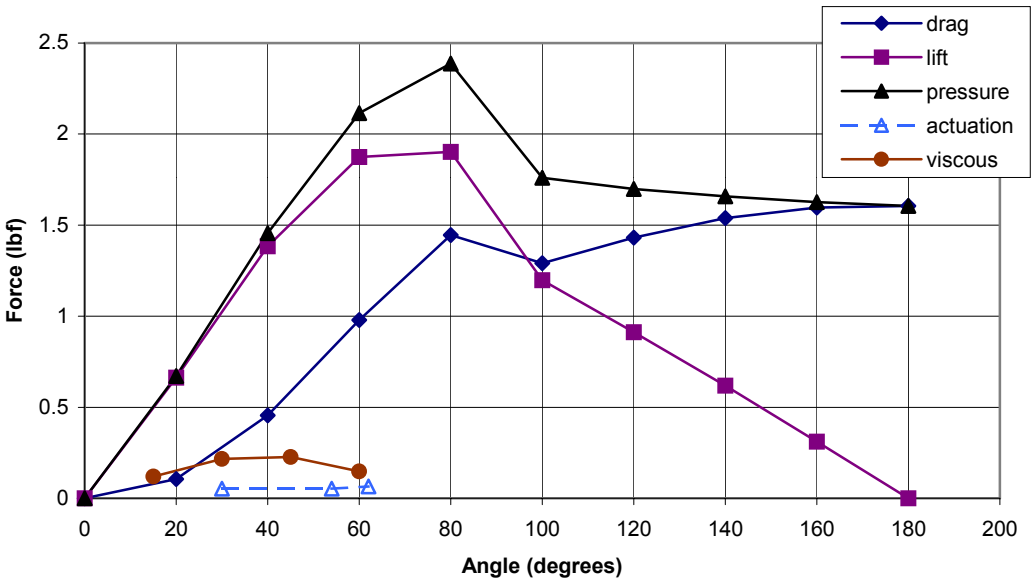

Figure E-1: Force comparison for flow of Mach 0.107.

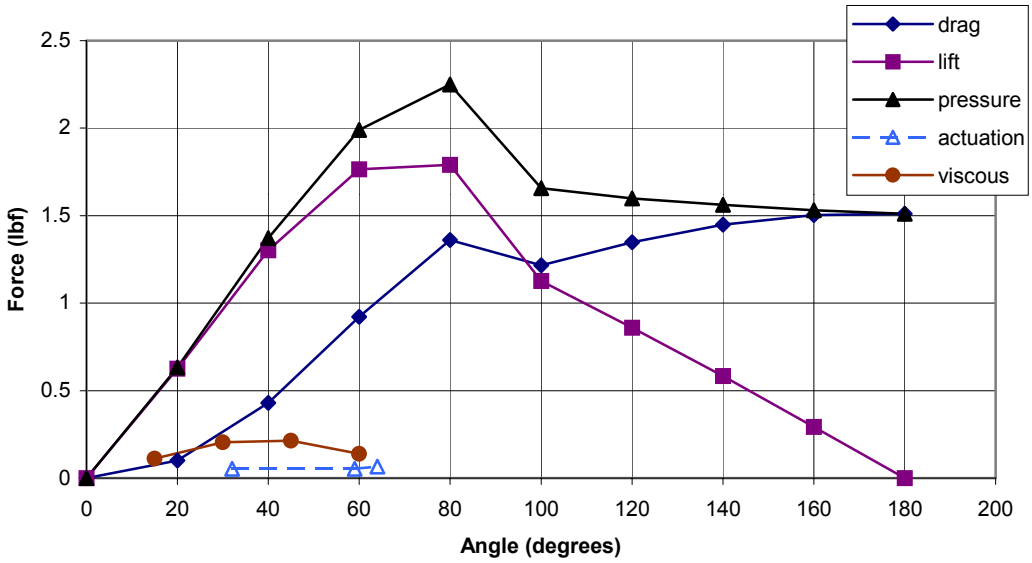

Figure E-2: Force comparison for flow of Mach 0.103.

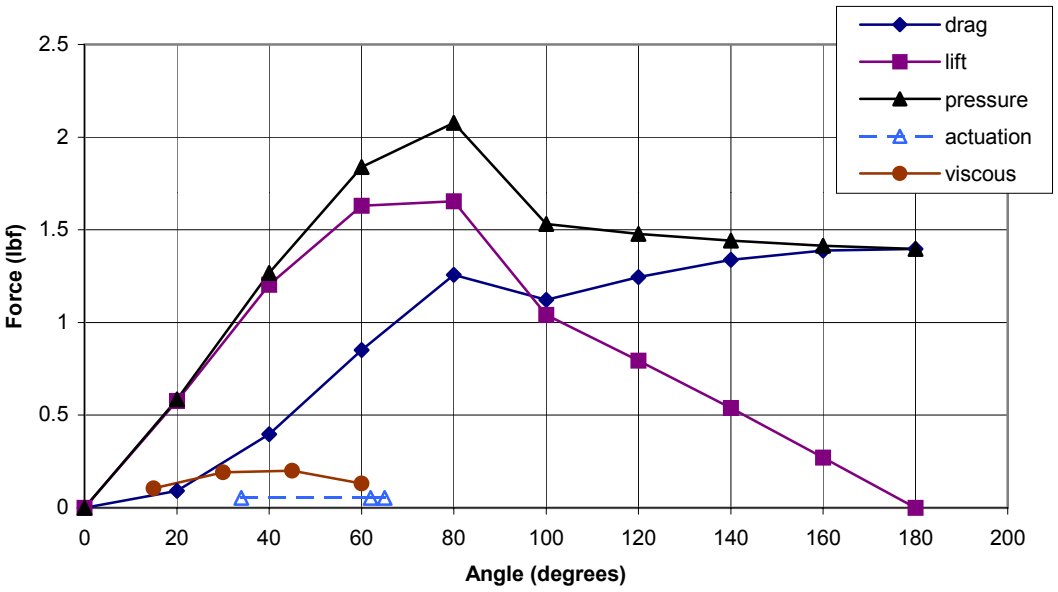

Figure E-3: Force comparison for flow of Mach 0.1.

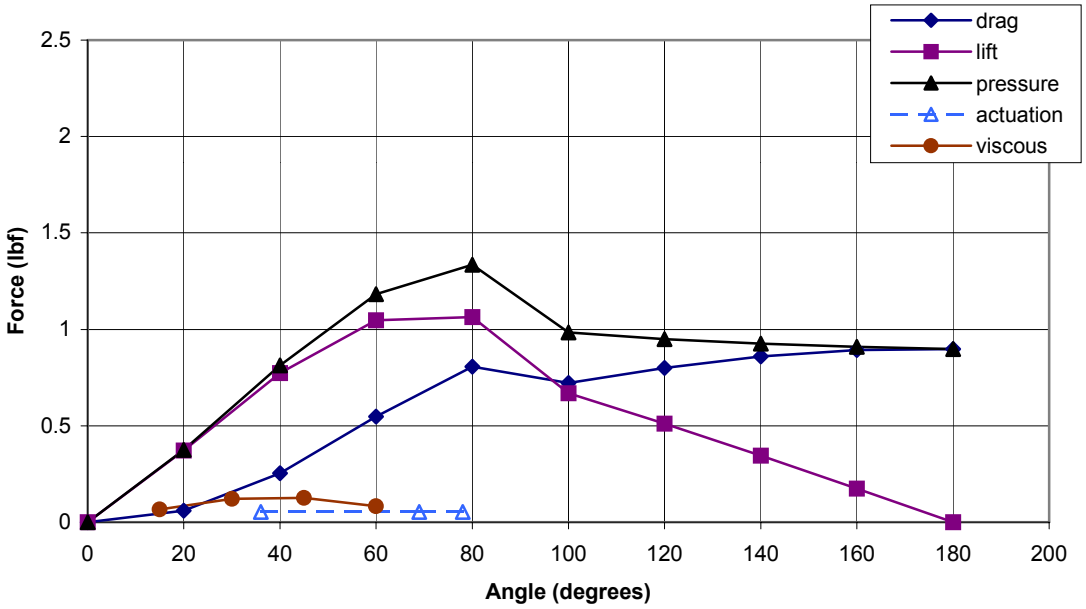

Figure E-4: Force comparison for flow of Mach 0.08.

Appendix F: Uncertainty Analysis

An uncertainty analysis was performed on the Mach number in order to assess the error in the four repetitions of testing. The Mach number was determined from equation F-1, which originates from the Mach number definition of the ratio of velocity to sound speed.

$$M = \frac{\sqrt{\frac{\Delta p}{0.5 * \rho}}}{\sqrt{\gamma * R * T}} \tag{F-1}$$

where: Δp = pressure change
ρ = density of air
γ = specific heat ratio
R = gas constant of air
T= temperature of air

The error of each component propagates through this equation. The error of the manometer reading, Δp, is ± 0.001 in H_2O. The error of the density comes from the error of the barometer reading the pressure, ± 0.0041 in H_2O, and the thermometer, ± 0.05°C. Based on the ideal gas law, this gives a density error of 0.0373 kg/s. Using equation F-2, a Mach number of 0.100, Δp of 3.000 in H_2O, a density of 1.2300 kg/s, and a temperature of 26.0°C, the overall Mach number error was found to be ± 0.015.

$$M + M_{error} = \frac{\sqrt{\frac{\Delta p + \Delta p_{error}}{0.5 * (\rho + \rho_{error})}}}{\sqrt{\gamma * R * (T + T_{error})}} \tag{F-2}$$

This result shows that the first three separate runs were equivalent, within the error of the tests. The fourth run was just outside the error of the tests, and actually acts as a separate test condition. Therefore, non-dimensionalizing the results not only negated the effects of error to the measurements but also allowed comparison between separate test conditions.

References

Adamczyk, J.J., "Unsteady Fluid Dynamic Response of an Isolated Rotor with Distorted Inflow," AIAA Paper No. 74-49, 1974.

Alford, J.S., "Inlet Flow Distortion Index," International Days of Aeronautical Sciences, ONERA, May 1957.

Ashby Jr., G.C., "Investigation of the Effect of Velocity Diagram on Inlet Total-Pressure Distortion Through Single-Stage Subsonic Axial-Flow Compressors," NACA RM L57A03, 1957.

Beale, D., private correspondence, 1997.

Beers, F.P., Johnston Jr., E.R., *Mechanics of Materials*, 2nd Ed., New York, McGraw-Hill, Inc.:1992.

Blevins, Robert D., *Applied Fluid Dynamics Handbook*,
New York, Van Norstrand Reinhold Company: 1984.

Boller, S.M., "One-Dimensional Dynamic Wake Response in an Isolated Rotor Due to Inlet Total Pressure Distortion," M.S. Thesis, Virginia Polytechnic Institute and State University (Blacksburg, Virginia, 1998).

Braithwaite, W.M., Garber Jr., E.J., and Mehalic, C.M., "The Effect of Inlet Temperature and Pressure Distortion on Turbojet Performance," AIAA Paper No. 73-1316, 1973.

Brimlow, B., Collins, T.P., and Pfefferkorn, G.A., "Engine Testing in a Dynamic Environment," AIAA Paper 74-1198, October, 1974.

Campbell, Wilfred, "Protection of Turbine Disk Wheels from Axial Vibration," *Proceedings of the Cleveland Spring Meeting*, ASME, May 1924.

Carta, F.O., "Analysis of Unsteady Aerodynamic Effectos on Axial Flow Compressor Stage with Distorted Inflow." Project Squid—Technical Rep. UARL—A—UP, 1972.

Carta, F.O., "Aeroelasticity and Unsteady Aerodynamics," *Aircraft Propulsion Systems Technology and Design*, Editor: Gordon C. Oates, (Washington D.C.: American Institute of Aeronautics and Astronautics, Inc., 1989.)

Childs, J.H., Kochendorger, F.D., Lubick, R.J., and Friedman, R., "Stall and Flame-Out Resulting from Firing of Armament," NACA RM E55E25, 1955.

Colpin, J., Kool, P., "Experimental Study of an Axial Compressor Rotor Transfer Function with Non-Uniform Inlet Flow," ASME 78-GT-69, April 9-13, (London, England, 1978.)

Cotter, H.N., "Integration of Inlet and Engine—an Engine Man's Point of View," SAE Paper 680286, April-May, 1968.

Cousins, W.T., "Techniques for the Analysis of Unsteady Pressure Measurements in an Axial-Flow Compressor." M.S. Thesis, Virginia Polytechnic Institute & State University, (Blacksburg, Virginia, 1979.)

Cousins, W.T., O'Brien, W.F., "Axial-Flow Compressor Stage Post-Stall Analysis," AIAA Paper No. 85-1349, 1985.

Danforth, C.E., "Distortion-Induced Vibration in Fan and Compressor Blading," *Journal of Aircraft*, vol. 12, no. 4, April 1975, pp. 216-225.

Datko Jr., J.T., O'Hara, J.A., "The Aeromechanical Response of an Advanced Transonic Compressor to Inlet Distortion," ASME 87-GT-189, 1987.

Davis, M., Hale, A., Beale, D., "An argument for Enhancement of the Current Inlet Distortion Ground Test Practice for Aircraft Gas Turbine Engines," ASME 2000-GT-0505, 2000.

DiPietro, Tony, "Fundamental Wind Tunnel Experiments for Total Pressure distortion Generator Concept Selection," Year End Report for Sverdrup Technology, January, 1996.

Eddy, G., "Study of Steady-State Wake Characteristics of Variable Angle Wedges," M.S. Thesis, Virginia Polytechnic Institute & State University, (Blacksburg, Virginia, 2001.)

Fleeter, S., Jay, R.L., Bennett, W.A., "Rotor Wake Generated Unsteady Aerodynamic Response of a Compressor Stator," ASME 78-GT-112, 1978.

Greitzer, E.M., "Surge and Rotating Stall in Axial Flow Compressors; Part I: Theoretical Compression System Model." ASME 75-GT-9, 1975.

Hah, C., Rabe, D.C., Sulliavan, T.J., Wadia, A.R., "Effects of Inlet Distortion on the Flow Fieild in a Transonic Compressor Rotor," *ASME Journal of Turbomachinery*, Vol. 120, April 1998, pp. 233-246.

Hale, A.A., O'Brien, W.F., "A 3-D Turbine Engine Analysis Compressor Code (TEACC) for Steady-State Inlet Distortion." Ph.D. Dissertation, Virginia Polytechnic Institute & State University, (Blacksburg, Virginia, 1996.)

Henderson, R.E., Shen, I.C., "The Influence of Unsteady Rotor Response on a Distorted Flow Field." ASME 81-GT-185, 1981.

Hurad, J., "Determination Experimentale des Lois de Transfert de Perturbations a la Traversee d'un Compresseur Axial," AGARD CP-400, 68th Specialists Meeting, (Munich, Germany, September 8-9, 1986.)

Jumael J., King P.S., O'Brien W.F, "Transient Total Pressure Distortion Generator Development" Final Report for Academic Qualification, (Blacksburg VA, July 1999.)

Kimzey, W.F., "An Analysis of the Influence of Some External Disturbances on the Aerodynamic Stability of Turbine Engine Axial Flow Fans and Compressors." AEDC-TR-77-80, August 1977.

Ladd, J.A., Norby, W.P., "Dynamic Inlet Distortion Predictions Using CFD/Distortion Synthesis Approach," AIAA Paper No. 98-2735, 1998.

Lecht,M., Weyer, H.B., "On the Unsteady Aerodynamic Rotor Blade Loading in a Transonic Axial Flow Compressor with Unsteady Sate Inlet Distortion," IUTAM Symposium on Aeroelasticity in Turbomachines, (Paris, October 18-23, 1976), pp. 1-16.

Lotter, K.W., Jorg, J., "The Effect of Intake Flow Disturbances on APU Compressor Blade High Cycle Fatigue in the Airbus A300," ICAS-82-4.6.2, (Seattle, Aug. 1982.)

Luedke, J., "Use of Nonlinear Volterra Theory in Predicting the Propagation of Non-uniform Flow Through an Axial Compressor," M.S. Thesis, Virginia Polytechnic Institute & State University (Blacksburg, Virginia, 2001.)

Mabie, Hamilton H., Reinholtz, Charles F., *Mechanisms and Dynamics of Machinery*, Fourth Edition (New York: John Wiley & Sons, Inc, 1987.)

Manwaring, S.R., Fleeter, S., "Inlet Distortion Generated Periodic Aerodynamic Rotor Response," ASME 89-GT-299, 1989.

Manwaring, S.R., Rabe, D.C., Lorence, C.B., Wadia, A.R., "Inlet Distortion Generated Forced Response of a Low Aspect-Ratio Transonic Fan," *ASME Journal of Turbomachinery*, Vol. 119, October, 1996, pp. 665-676.

Mazzawy, R.S., "Multiple Segment Parallel Compressor Model for Circumferential Flow Distortion." *ASME Journal of Engineering for Power*, April, 1977.

Mikolajxzak, A.A., Pfeffer, A.M., "Methods to Increase Engine Stability and Tolerance to Distortion," AGARD LS No. 72, September 7, 1974.

Mokelke, H., "Prediction Techniques," AGARD LS No. 72, Sect. 5, 1974.

Munson, Bruce R., Young, Donald F., Okiishi, Theodore H., *Fundamentals of Fluid Mechanics*, Third Edition (New York: John Wiley & Sons, Inc, 1998.)

Nagano, S., Takata, H., "Nonlinear Analysis of Rotating Stall," Institute of Space and Aeronautical Science, University of Tokyo, Report No. 449, 1970.

Newark Electronics Catalog 119, 2001-02.

Overall, B.W., "Evaluation of an Airjet Distortion Generator Used to Produce Steady-State Total-Pressure Distortion at the Inlet of Turbine Engines," AEDC-TR-76-141, December, 1976.

Peacock, R.E., Overli, J., "Dynamic Flows in Compressors with Pressure Maldistributed Inlet Conditions," AGARD CP-177, 1976.

Pearson, H., McKenzie, A., "Wakes in Axial Compressors." *Journal of the Royal Aeronautical Society*), p. 48*,* Vol. 63, July, 1959

Plourde, G.A., and Brimelow, B., "Pressure Fluctuations Cause Compressor Instability," *Proceedings of the Air Force Airframe-Propulsion Compatibility Symposium,* Rept. AFAPL-TR-69-103, (Air Force Aero Propulsion Laboratory*,* Wright-Patterson AFB, OH, June 1970.)

Rabe, D., Bolcs, A. and Russler, P., "Influence of Inlet Distortion on Transonic Compressor Blade Loading,: AIAA Paper No. 95-2461, July 1995.

Rabe, D.C., Williams, C., Hah, C., "Inlet Flow Distortion and Unsteady Blade Response in a Transonic Axial-Compressor Rotor," ASABE 99-7297, 1999.

Reid, C., "The Response of Axial Flow Compressors to Intake Flow Distortion," ASME 69-GT-29, 1969.

Roberts, F., Plourde, G.A., Smakula, F. "Insights into Axial Compressor Response to Distortion.: AIAA Paper No. 68-565, 1968.

SAE Aerospace Information Report -1419, *Inlet Total-Pressure-Distortion Considerations for Gas-Turbine Engines*, (Warrendale, PA, Rev. A, 1999).

SAE Aerospace Recommended Practice -1420, *Gas Turbine Engine Inlet Flow Distortion Guidelines*, (Warrendale, PA, Rev. A, 1998).

SAE Aerospace Resource Document -50015, *A Current Assessment of the Inlet/Engine Temperature Distortion Problem*, (Warrendale, PA, 1991.)

Sexton, M.R., O'Brien, W.F., "A Model for Dynamic Loss Response in Axial-Flow Compressors," ASME 81-GT-154, 1981.

Schwartz, J.R., "An Experimental and Analytical Investigation of Dynamic Flow Response of a Fan Rotor with Distorted Inlet Flow," M.S. Thesis, Virginia Polytechnic Institute & State University, (Blacksburg, Virginia, 1999.)

Slemon, Gordon R., *Magnetoelectric Devices*, John Wiley & Sons, Inc., (New York, 1966.) pp. 73-75.

Small, M., "Improved Methods for Predicting the Effects of Inlet Flow Distortion on the Performance of Axial Flow Compressors," M.S. Thesis, Virginia Polytechnic Institute and State University, (Blacksburg, Virginia, 2001.)

Steenken, W.G., "Engine Operability," *Aircraft Propulsion Systems Technology and Design*, Editor: Gordon C. Oates, (Washington D.C.: American Institute of Aeronautics and Astronautics, Inc., 1989.)

Vuillez, C., Petot, B., "New Methods, New Methodology, Advanced CFD in the SNECMA Turbomachinery Design Process," AGARD LS No. 195, May 1994.

Walter, W.A. and Shaw, M., "Predicted F100 Engine Response to Circumferential Pressure and Temperature Distortion," 1979

Wells, H.S., "A Study of Rocket Exhaust Gas Ingestion Simulation Techniques for the AEDC," ARO ENGR RPT 77-3, March 1977.

www.festo-usa.com/products/allstar.html

www.physikinstrumente.com

Younghans, J.L., Paul, D.L., "Inlets and Inlet/Engine Integration," *Aircraft Propulsion Systems Technology and Design*, Editor: Gordon C. Oates, (Washington D.C.: American Institute of Aeronautics and Astronautics, Inc., 1989.)

Vita

Kevin B. Cramer

The author, son of Richard Jr. and Mary-Catherine Cramer, was born in 1978 in Clearwater, Florida. As a child he moved up the east coast finding his way to Richmond, Virginia. He attended high school at Midlothian High School. His decision to become an engineer led to his enrollment in Mechanical Engineering at Virginia Tech in the fall of 1998. At this time he also enrolled in Air Force Reserve Officers Training Corps. Graduating from Virginia Tech in December of 2000, he was commissioned a Second Lieutenant in the United States Air Force. In the spring of 2001, he began his graduate studies in Mechanical Engineering, again at Virginia Tech. Upon graduation, he will begin his service in the United States Air Force.